Quantum revivals and quantum spin tunneling in effective spin systems

Dem Fachbereich Physik der
Universität Hamburg
zur Erlangung des akademischen Grades eines
Dr. rer. nat.

eingereichte Dissertation

von
Herr Dipl.-Phys. Mario Krizanac
aus
Tomislavgrad

2018

Gutachter der Dissertation:
Herr Prof. Dr. R. Wiesendanger
Herr Prof. Dr. A. Lichtenstein

Gutachter der Disputation:
Herr Prof. Dr. R. Wiesendanger
Herr Prof. Dr. G. Sigl
Herr Prof. Dr. M. Thorwart
Herr Prof. Dr. M. Potthoff
Herr Prof. Dr. W. Hansen

Vorsitzender des Prüfungsausschusses:
Herr Prof. Dr. W. Hansen

Vorsitzender des Promotionsausschusses:
Prof. Dr. Wolfgang Hansen

Dekan der MIN-Fakultät:
Prof. Dr. Heinrich Graener

Abstract

This work uses theoretical models first to analyse the recurrence behaviour of effective single spins and their connection to magnetic tunneling, secondly to study the magnetic tunneling dynamics of individual magnetic molecules, and thirdly to investigate the magnetization behaviour of open and closed exchange-coupled effective quantum spin chains. Regarding the recurrence behaviour, we analyse, with the help of the time-dependent Schrödinger equation, the precession behaviour of effective single spins under the influence of a uniaxial anisotropy. With regard to magnetic tunneling of single molecular magnets, the tunneling behaviour of effective two-level systems, where the Hamiltonian contains a transversal anisotropy and a transversal magnetic field, is investigated with the aid of the time-dependent perturbation calculation. Finally, this work deals with the magnetization behaviour of open and closed exchange-coupled effective quantum spin chains with the aim of reproducing experimental results that have so far avoided a theoretical description (open chain) and secondly with the search of stable configurations for ring-like closed spin chains, for systems which are subject to a uniaxial anisotropy, an exchange interaction and a dipolar interaction.

Zusammenfassung

Diese Arbeit untersucht mithilfe von theoretischen Modellen das Wiederkehrverhalten von effektiven Einzelspins und deren Verbindung zum magnetischen Tunneln, die magnetische Tunneldynamik von einzelnen magnetischen Molekülen und das Magnetisierungsverhalten von offenen und geschlossenen austauschgekoppelten effektiven Quantenspinketten. Bezüglich des Wiederkehrverhaltens wird, unter Zuhilfenahme der zeitabhängigen Schrödingergleichung, das Präzessionsverhalten von effektiven Einzelspins, unter der Einwirkung einer uniaxialen Anisotropie, untersucht. Bezüglich des magnetischen Tunnelns von Einzel-Molekül-Magneten wird, mit Zuhilfenahme der zeitabhängigen Störungsrechnung, das Tunnelverhalten von beliebigen effektiven zwei Niveau Systemen, welche sich unter dem Einfluss einer transversalen Anisotropie und einem transversalen Magnetfeld befinden, untersucht. Schlussendlich behandelt diese Arbeit das Magnetisierungsverhalten von offenen und geschlossenen austauschgekoppelten effektiven Quantenspinketten mit dem Ziel erstens experimentelle Befunde zu reproduzieren, welche sich bisher einer theoretischen Beschreibung entzogen haben (offene Ketten) und zweitens stabile Konfigurationen für ringartige geschlossene Spinketten, für Systeme die einer uniaxialen Anisotropie, einer Austschauschwechselwirkung sowie einer dipolaren Wechselwirkung unterliegen, zu ermitteln.

Contents

Chapter 1

Introduction

The importance of information storage was never so relevant as in today's modern times. Our information based societies needs vast capacities to conserve all the different kind of data, like texts, books, video and audio information. In the past this information classes were conserved on different platforms, like on paper for books or on vinyl records for audio related content. The introduction of digital computers and thus the invention of digital information based storage like magnetic hard drives led to a unification of the storage platforms. Nowadays, books, videos and audio information are digitalized and conserved through bits on various storage media. This transition from different platforms to one unified digitalized platform is still in progress since more and more societies adapt this concept. Especially the info/entertainment centric aspect of video data storage consumes in our modern societies, due to the trend of higher definition qualities, a lot of the available storage resources. The concept of the magnetic hard drive is that it records data by magnetizing a thin film of ferromagnetic material. Sequential changes in the direction of magnetization represent binary data bits. The data extraction from the disk is done by the detection of the transitions in magnetization. This means that the magnetization of thin films of ferromagnetic materials leads to discrete areas of a specific magnetization direction which differs from the magnetization direction of areas which are in between. The principle is similar to the patterns of a vinyl record, with the difference that instead of different modulated spiral grooves now different magnetic direction areas are responsible for the information storage. The density of such magnetic direction areas is responsible for the

storage capacity. The research endeavoured to increase the memory density, but with the problem of reading these increasingly fine magnetic structures, it had reached its limits. Here, the GMR effect turned out to be the solution to this problem. Through the read construction, which consists of two magnetic layers, which are separated by a non-magnetic one, flows current. If the variable layer changes its magnetization direction, then the resistance of the read head changes. If the two magnetic layers have a different magnetization direction, the resistance is higher, which results in a decrease in the current strength than if both point in the same direction. This phenomenon, changing the current resistance depending on the direction of magnetization, is the giant magneto-resistance effect (GMR). Even very weak magnetic fields can cause the magnetization directions to change and trigger the change in the current intensity. Because of this, the size of the storage units (and thus their magnetic field) on a hard drive could be massively reduced. Since the areas of storage bits could consist of several hundred atoms, there is plenty of room to improve the storage density further. The purpose of this thesis is to investigate possibilities in order to store bits in single magnetic atoms or single magnetic molecules from a quantum mechanical perspective. These quantum dynamical phenomena become increasingly important also in solid state physics. Particularly, quantum mechanical tunneling has been reported for nanomagnets [20], molecules [21, 22] and single atoms [23].
Our first investigation is on the quantum revival, which is defined by the quantum recurrence theorem [15, 16, 17, 18, 19], where the system return arbitrarily close to the initial state. Here we analyse the correlation between the spin precession and the magnetization tunneling. Particular attention is given to the non-linear character of the uniaxial anisotropy, which leads to non-harmonic dynamics, when combined with a linear energy. Our second investigation is related to single molecular magnets (SMM). This field is an actual topic in today's research [37, 38, 49, 50, 51, 52, 53] on magnetic molecules for storage purpose. These single molecule magnets are treated as effective two level systems (ground doublets). The investigations concentrate on techniques to switch the magnetization of those SMM controlled and hold them in a requested magnetization orientation. This would allow us to store bits in form of up and down oriented magnetic moments of the single molecule magnets and

would increase the density of information storage extremely, relative to today's standards. Our approach is to analyse the switching behaviour of SMM, from a time dependent perturbative theory point of view. Further we analyse if there is a switching correlation between single molecule magnets with different degrees of freedom, by studying SMM for arbitrary quantum numbers s.
The third and last investigation, documented in this thesis, is about the magnetization behaviour of exchange coupled open [57, 59] and closed spin chains. For the case of open spin chains we analyse the magnetic behaviour of anti-ferromagnetically coupled Fe spins on a Cu(111) substrate. These systems are of interest, because the magnetization behaviour of the spin chains, from the experimental data [57], can not be reproduced by theoretical models, like the Ising model, for parameters given from the experiment. Here we investigate if the Landau-Zener scenario is able to reproduce the data from the experiment and further we analyse if a magnetic field dependence of the magnetic moments of the edge spins can generate the magnetisation behaviour from the experiment. For the case of closed spin chains we studied stationary equilibrium magnetic configurations of effective magnetic moments of closed magnetic chains with uniaxial anisotropy coupled with anti-ferromagnetic exchange. The main objective is to identify which kind of magnetic states, different from the collinear ground states, can be stabilized. Further we investigate at finite temperatures non-frustrated rings or other closed shapes with an even number of sites, if they can be stabilized without the Dzyaloshinskii-Moriya interaction. Again, we try to find ways to identify magnetic structures, consisting of a few spins in the form of rings, which can be stabilized, regarding their magnetic structure, in order to use them as a way to store data.

Chapter 2

Theory

In this chapter we present theoretical models, which we used in our research work, to obtain results on quantum revival in single spin systems, magnetization tunneling in single magnetic molecules and on the magnetization behaviour of open and closed exchange coupled spin chains.

2.1 Equation of motion and equation of energy

2.1.1 Spin wave function

The complete wave function of magnetic systems, can be written as a product of the wave function in position space and the spin wave function:

$$\Psi(\vec{r},t) = \phi(\vec{r},t) \cdot \psi(t). \tag{2.1}$$

Equation (2.1) is valid, because the spatial behaviour of the electrons is independent of their spin behaviour. Within this work we focus solely on the spin wave function $\psi(t)$. The equation of motion, which is used here is the time dependent Schrödinger equation [72]:

$$i\hbar\frac{\partial}{\partial t}\big|\psi(t)\big\rangle = \hat{H}_{eff}\big|\psi(t)\big\rangle, \tag{2.2}$$

which is a linear ordinary differential equation of first order. The wave function $\big|\psi(t)\big\rangle$ in Eq.(2.2) defines the eigenstates of the spin system:

$$\big|\psi(t)\big\rangle = \sum_{i=0}^{2s} \varphi_{s-i}(t)\big|\hat{e}_{i+1}\big\rangle = \begin{pmatrix} \varphi_{+s}(t) \\ \vdots \\ \varphi_{-s}(t) \end{pmatrix}, \tag{2.3}$$

where s defines the spin quantum number [73, 74]. The normalization condition is given by the expression

$$\sum_{i=0}^{2s} \left|\left\langle \varphi_{s-i}(t)\middle|\varphi_{s-i}(t)\right\rangle\right|^2 = 1, \tag{2.4}$$

and $\left|\left\langle \varphi_n(t)\middle|\varphi_n(t)\right\rangle\right|^2$ is the probability to measure the system in the n'th state.

2.1.2 Effective Hamiltonian

The effective Hamiltonian $\hat{H}_{eff}$ in Eq.(2.2) describes the energy landscape of the spin systems and contains solely effective interactions between the spins among themselves and with the environment [73, 74]:

$$\hat{H}_{eff} = \begin{pmatrix} \left\langle \varphi_s(t)\middle|\hat{H}_{eff}\middle|\varphi_s(t)\right\rangle & \cdots & \left\langle \varphi_s(t)\middle|\hat{H}_{eff}\middle|\varphi_{-s}(t)\right\rangle \\ \vdots & \ddots & \vdots \\ \left\langle \varphi_{-s}(t)\middle|\hat{H}_{eff}\middle|\varphi_s(t)\right\rangle & \cdots & \left\langle \varphi_{-s}(t)\middle|\hat{H}_{eff}\middle|\varphi_{-s}(t)\right\rangle \end{pmatrix}. \tag{2.5}$$

The advantage of an effective Hamiltonian is the simplicity to model atomic systems, because all interactions are defined in a reduced Hilbert space and thus only a part of the eigenvalue spectrum of the complete Hamiltonian is described. An example system could be a single spin on a substrate within an external magnetic field:

$$\hat{H} = -\hat{\vec{S}}\vec{B} - K\hat{S}_z^2. \tag{2.6}$$

The Hamiltonian in Eq.(2.6) describes such a situation. The first term defines the Zeeman energy (through the external magnetic field $\vec{B}$) and the second term in Eq.(2.6) defines the uniaxial anisotropy with the anisotropy constant K, which describes the effective interaction between the substrate and the quantum spin. The $\hat{\vec{S}}$ in Eq.(2.6) stands for the spin operator vector and $\hat{S}_z$ is an element of it. The spin operator vector is defined by

$$\hat{\vec{S}} = \begin{pmatrix} \hat{S}_x \\ \hat{S}_y \\ \hat{S}_z \end{pmatrix}, \tag{2.7}$$

and obeys the commutation relations $[\hat{S}_i, \hat{S}_j] = i\hbar\epsilon_{ijl}\hat{S}_l$, analogous to those of the orbital angular momentum. For the special case of a spin 1/2 system, $\hat{S}_x$,

$\hat{S}_y$ and $\hat{S}_z$ are the three Pauli matrices [73, 74], given by

$$\hat{S}_x = \begin{pmatrix} 0 & \frac{1}{2} \\ \frac{1}{2} & 0 \end{pmatrix}, \quad \hat{S}_y = \begin{pmatrix} 0 & -\frac{i}{2} \\ \frac{i}{2} & 0 \end{pmatrix}, \quad \hat{S}_z = \begin{pmatrix} \frac{1}{2} & 0 \\ 0 & -\frac{1}{2} \end{pmatrix}, \tag{2.8}$$

which are hermitian and unitary. This means that the Pauli matrices span the space of observables of the 2-dimensional complex Hilbert space. The generalized form of the spin operators $\hat{S}_i$, with $i \in [x, y, z]$, for arbitrary spin quantum numbers s is given by [74]

$$\begin{aligned} (S_{x_{a,b}}) &= \frac{\hbar}{2}(\delta_{a,b+1} + \delta_{a+1,b})\sqrt{(s+1)(a+b-1) - ab} \\ (S_{y_{a,b}}) &= \frac{i\hbar}{2}(\delta_{a,b+1} - \delta_{a+1,b})\sqrt{(s+1)(a+b-1) - ab} \\ (S_{z_{a,b}}) &= \hbar(s-(a-1))\delta_{a,b} = \hbar(s-(b-1))\delta_{a,b} \end{aligned} \tag{2.9}$$

$$1 \leq a, b \leq 2s+1,$$

where a and b are indices which define positions of the matrix elements of the spin operator $\hat{S}_i$. The $\delta_{a,b}$ in Eq.(2.9) represent the Kronecker delta:

$$\delta_{a,b} = \begin{cases} 1 & \text{if } a = b \\ 0 & \text{if } a \neq b \end{cases}$$

2.1.3 Many-spin systems

In order to model many-quantum-spin systems it is necessary to expand the Hilbert space of the single spin systems:

$$\hat{H} = \hat{H}_1 \otimes ... \otimes \hat{H}_n. \tag{2.10}$$

This is done by the Kronecker product $\otimes$, which is defined by

$$\hat{A} \otimes \hat{B} = \begin{pmatrix} a_{11} \cdot \hat{B} & \cdots & a_{1n} \cdot \hat{B} \\ \vdots & \ddots & \vdots \\ a_{m1} \cdot \hat{B} & \cdots & a_{mn} \cdot \hat{B} \end{pmatrix}. \tag{2.11}$$

$\hat{A}$ is an $m \times n$ matrix and $\hat{B}$ is a $p \times q$ matrix in Eq.(2.11), then the Kronecker product $\hat{A} \otimes \hat{B}$, which is in general non-commutative, is a $mp \times nq$ block matrix.

The dimension of the spin operators $\hat{S}_i$ is equal to the dimension of the entire many-spin Hilbert space:

$$\dim(\hat{S}_x, \hat{S}_y, \hat{S}_z) = \dim(\hat{H}_1 \otimes ... \otimes \hat{H}_n). \tag{2.12}$$

An example of a two spin system without interaction, based on the Hamiltonian in Eq.(2.6), is

$$\hat{H}_1 \otimes \hat{H}_2 = -\begin{pmatrix} \hat{S}_x \otimes \mathbb{I}_2 \\ \hat{S}_y \otimes \mathbb{I}_2 \\ \hat{S}_z \otimes \mathbb{I}_2 \end{pmatrix} \cdot \vec{B} - \begin{pmatrix} \mathbb{I}_1 \otimes \hat{S}_x \\ \mathbb{I}_1 \otimes \hat{S}_y \\ \mathbb{I}_1 \otimes \hat{S}_z \end{pmatrix} \cdot \vec{B} - K(\hat{S}_z \otimes \mathbb{I}_2)^2 - K(\mathbb{I}_1 \otimes \hat{S}_z)^2, \tag{2.13}$$

where $\mathbb{I}_1$ and $\mathbb{I}_2$ in Eq.(2.13) are the identity matrices of their respective spin operators $\hat{S}_i$ and may possess different dimensions. In order to measure the subsystem $\hat{H}_1$ of a composite system with density matrix $\rho_{S_1S_2}$ on the tensor-product space $\hat{H}_1 \otimes \hat{H}_2$ it is necessary to use the reduced density operator ρ_{S1}. This means that in order to estimate the expectation values from the two spin system, described by Eq.(2.13), separately for each spin it is required to use the reduced density matrix

$$\rho_{S_1} = \mathrm{Tr}_{S_2}(\rho_{S_1S_2}). \tag{2.14}$$

This leads to the following expression for the expectation values:

$$\mathrm{Tr}(\rho_{S_1}\hat{S}_1) = \big\langle \psi(t) \big| \hat{S}_{i_1} \otimes \mathbb{I}_2 \big| \psi(t) \big\rangle. \tag{2.15}$$

The order of $\mathbb{I}$ and $\hat{S}_i$ in Eq.(2.15) is responsible for which spin is measured.

2.2 Quantum revival

The quantum revival is a periodic recurrence of the quantum wave function towards its initial state

$$\big|\Psi(t)\big\rangle = \big|\Psi(t + \alpha\Delta t)\big\rangle \quad \alpha \in \mathbb{N}. \tag{2.16}$$

The most important term here is the periodicity, because for a given phase space with a finite volume, the recurrence is not necessarily a periodic re-currency. This means that a return to a state arbitrary close to the initial state, without a periodicity, is possible (even in systems with periodic orbits).

The general principle for periodic and non-periodic recurrence is defined by Poincaré's recurrence theorem, which states that if H is a Hamiltonian on a phase space Ω, with finite volume, then a trajectory exists for every open set $U \subset \Omega$ which pass U an infinite number of times. Due to the Liouville's theorem all Hamiltonian systems are volume-preserving.
Beside the quantum revival of the wave function, the periodic recurrence of the expectation values $\langle S_x \rangle, \langle S_y \rangle$ and $\langle S_z \rangle$, and the relation to the recurrence of the quantum wave function is the main focus of the chapter: "Quantum revivals and magnetization tunneling in effective spin systems". Especially the revival of the expectation values $\langle S_x \rangle$ and $\langle S_y \rangle$, which together defines the spin precession, are a primary topic.

2.2.1 Larmor precession

A special case of spin precession is the Larmor precession, which is defined as the precession of the magnetic moment of an object (atom or molecule) around an external magnetic field. This means that the external magnetic field exerts a torque on the magnetic moment,

$$\tau = \gamma \vec{J} \times \vec{B}. \tag{2.17}$$

The τ in Eq.(2.17) represents the torque, whereby γ is the gyromagnetic ratio, $\vec{J}$ is the angular momentum vector and $\vec{B}$ is the external magnetic field. This precession has a specific recurrence frequency, known as the Larmor frequency

$$\omega = -\gamma \cdot B. \tag{2.18}$$

The recurrence frequency ω in Eq.(2.18) solely depends on the external magnetic field and thus belongs to the harmonic oscillations. The situation changes drastically, if the magnetic moment is on a substrate with a uniaxial anisotropy. Because then the precession is not harmonic anymore, but instead non-harmonic, which is one of the results of the chapter: "Quantum revivals and magnetization tunneling in effective spin systems".

2.2.2 Non-harmonic oscillation

A non-harmonic oscillation is a superposition of several harmonic oscillations with different frequencies $\omega_i \neq \omega_j$. The resulting frequency which describes a non-harmonic oscillation is the fundamental frequency

$$\omega_f = \gcd(\omega_1, ..., \omega_m), \tag{2.19}$$

where "gcd" is the greatest common divider. The consequence of the "gcd" is that the fundamental frequency ω_f is always equal or lower than the lowest ω_i in Eq.(2.19), which can be expressed by an infimum: $\omega_f \leq \inf(\omega_1, ..., \omega_m)$.
The non-harmonic precession of a magnetic moment originates from the combination of a linear term and a term with an even exponent $\hat{S}^{2n}$ ($n \in \mathbb{N} \setminus \{0\}$), like a quadratic one, in the Hamiltonian:

$$\hat{H} = -B_z \hat{S}_z - K\hat{S}_z^2. \tag{2.20}$$

The linear term in Eq.(2.20) is the Zeeman term and the quadratic term is the uniaxial anisotropy.

2.3 Quantum spin tunneling

Quantum spin tunneling [75, 76] is an effect, which occurs because of symmetry breaking of an unperturbed system by perturbations which leads to a loss of degeneracy of energy levels. It is a well known effect, with many experiments especially on single-molecular magnets (SMM) [37, 38, 49, 50, 51, 52, 53, 76]. In order to understand this in more detail, an example of a single atomic spin on a substrate, with no external magnetic field, will be introduced. The simplest Hamiltonian of such a system is a spin 1/2 atomic system with a uniaxial anisotropy:

$$\hat{H}_0 = -K\hat{S}_z^2. \tag{2.21}$$

By writing the Hamiltonian $\hat{H}_0$ out, which is done in Eq.(2.22) it is obvious that the system solely contains diagonal elements and thus the time dependent Schrödinger equation with the Hamiltonian $\hat{H}_0$ in Eq.(2.21) is a system of uncoupled linear differential equations.

$$\hat{H}_0 = \begin{pmatrix} -\frac{1}{4}K & 0 \\ 0 & -\frac{1}{4}K \end{pmatrix} \tag{2.22}$$

The consequence of a such an Hamiltonian is that the eigenstates are time invariant. In order to enable the system in Eq.(2.21) to change the eigenstates a transversal perturbation is necessary:

$$\hat{H} = \hat{H}_0 + \hat{H}_p = -K\hat{S}_z^2 - \widetilde{B}_x\hat{S}_x. \tag{2.23}$$

The transversal perturbation in Eq.(2.23) is realised by a transversal magnetic field. This leads to a system of coupled linear differential equations

$$i\hbar\frac{\partial}{\partial t}\psi(t) = \begin{pmatrix} -\frac{1}{4}K & -\frac{1}{2}\widetilde{B}_x \\ -\frac{1}{2}\widetilde{B}_x & -\frac{1}{4}K \end{pmatrix} \cdot \begin{pmatrix} \varphi_{+1/2}(t) \\ \varphi_{-1/2}(t) \end{pmatrix}. \tag{2.24}$$

Calculating the expectation value $\langle S_z \rangle$ using Eq.(2.24) leads to an oscillation between the two eigenstates, shown in figure 2.1. The ability of a system to

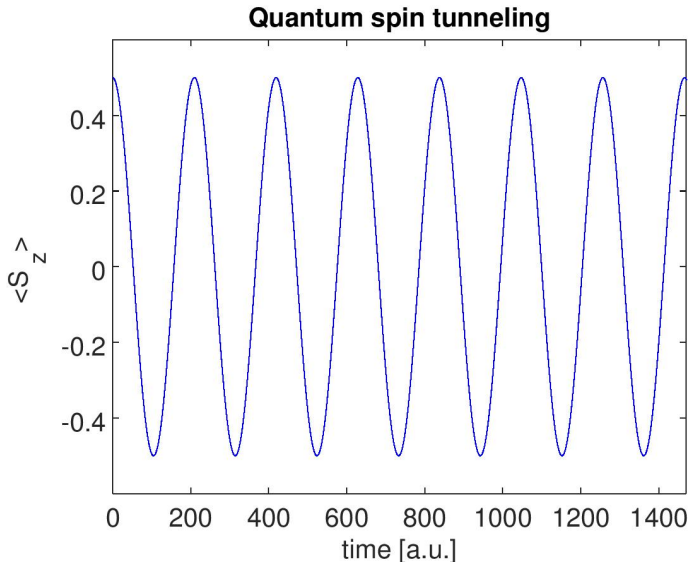

Figure 2.1: Oscillations between two eigenstates of a spin 1/2 system

execute such state transition, without the necessity of a thermal activation, in order to overcome the energy barrier, is defined as quantum spin tunneling. The energy landscape of the Hamiltonian in Eq.(2.23), extended by a Zeeman term $B_z\hat{S}_z$, reveals an energy gap between the eigenvalues, shown in figure 2.2. This avoided level crossing, caused by the transversal perturbation $\hat{H}_p = -\widetilde{B}_x\hat{S}_x$, is known as the energy splitting of the ground doublet ΔE_{split}. The magnitude of the ground doublet energy splitting correlates with the frequency of the eigenstate transitions, shown in figure 2.1, in the way that a larger

energy splitting $\Delta E_{\text{split}} = 2\hbar\omega$, caused by stronger transversal perturbations, leads to higher frequencies within the eigenstate oscillations. The zero-field

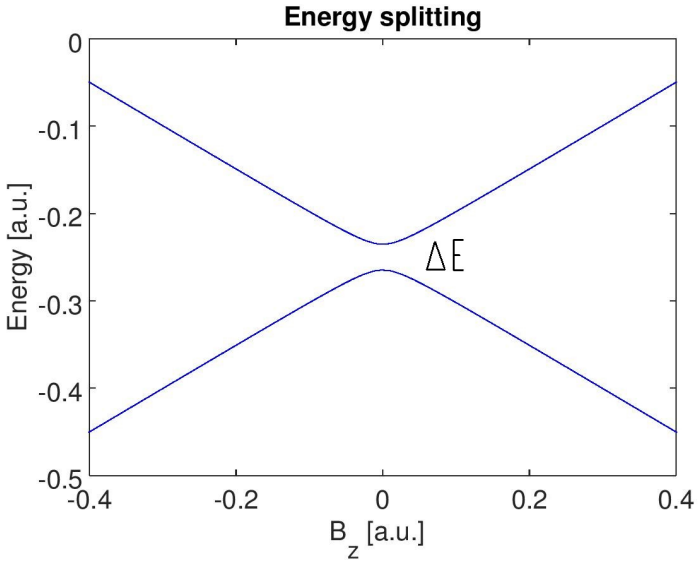

Figure 2.2: The zero-field energy splitting ΔE_{split} at an avoided level crossing.

energy splitting ΔE_{split} for arbitrary spin quantum numbers s, which fulfil the Hamiltonian in Eq.(2.23), is given by

$$\Delta E_{\text{split}} = 8|K|s^2\Big(\frac{\widetilde{B}_x}{2|K|}\Big)^{2s}\frac{1}{(2s)!}. \tag{2.25}$$

Perturbations, which lead to a loss of degeneracy of energy levels, are often caused by small transversal anisotropies, especially in single-molecular magnets (SMM):

$$\hat{H} = \hat{H}_0 + \hat{H}_p = -K\hat{S}_z^2 - \widetilde{K}(\hat{S}_x^2 - \hat{S}_y^2). \tag{2.26}$$

Energy contributions with operators of the form $\hat{S}_x^{2n}$, $\hat{S}_y^{2n}$ $(n \in \mathbb{N} \setminus \{0\})$ in the Hamiltonian, leads to the circumstance that, due to Kramers degeneracy theorem, only integer quantum spins show quantum spin tunneling effects. The zero-field energy splitting ΔE_{split}, for arbitrary integer spin quantum numbers s, defined by the Hamiltonian in Eq.(2.26), is given by

$$\Delta E_{\text{split}} = 8|K|s^2\Big(\frac{\widetilde{K}}{4|K|}\Big)^{s}\frac{(2s)!}{(s!)^2}. \tag{2.27}$$

2.3.1 Kramers degeneracy theorem

For every energy eigenstate of a time-reversal symmetric system with half-integer spin, the Kramers degeneracy theorem states that each energy level is at least doubly degenerated. This is only valid for electric fields and does not apply to magnetic fields. From a matrix operator perspective, Kramers degeneracy theorem means that, because of symmetry reasons, the ground doublet states of half-integer spins can not be coupled directly or indirectly by transversal perturbations with spin operators of the form $\hat{S}_x^{2n}$ and $\hat{S}_y^{2n}$ ($n \in \mathbb{N}\backslash\{0\}$). Solely linear spin operators and operators of the form $\hat{S}_i^{2n-1}$ ($n \in \mathbb{N}\backslash\{0\}$) can couple the ground doublet states of a half-integer spin system.

2.3.2 Quenched tunnel splitting

Quenched tunnel splitting describes an effect where the energy splitting ΔE_{split}, for the ground doublet is vanishing $\Delta E_{\text{split}} = 0$ for certain parameters of the parameter space. This phenomenon occurs because of destructive interferences between the tunneling paths. Tunneling paths are direct and indirect couplings of ground doublet states, like of $\left|+1/2\right\rangle$ and $\left|-1/2\right\rangle$ by off-diagonal elements in the Hamilton operator. The first condition for destructive interferences of the tunneling paths is the presence of at least two operators $\hat{S}_{x,y}^n$, with a different power of n, in the Hamiltonian. The second condition is that the signs of the spin operators $\hat{S}_{x,y}^n$ have to be opposite relative to each other. This means, for example, that it is necessary to model a system with a hard-axis transversal anisotropy (negative $\widetilde{K}$) and a transversal magnetic field with an opposite sign relative to $\widetilde{K}$.

2.4 Heisenberg model

Magnetism is a pure quantum mechanical effect, which appears on a macroscopic scale. Werner Heisenberg explained the phenomenon of ferromagnetism by a combination of the Coulomb interaction and the Pauli-principle, which led to the model Hamiltonian

$$\hat{H} = -\sum_{<i,j>}^{n} J_{ij}\hat{S}_i \otimes \hat{S}_j, \tag{2.28}$$

where J_{ij} is the exchange integral of the Coulomb interaction. The spin operators $\hat{S}_i$ represent the spins on the grid position i. For the case of $J_{ij} > 0$ in Eq.(2.28) there is a ferromagnetic coupling, while an anti-ferromagnetic coupling is present for the case of $J_{ij} < 0$. The brackets $< i, j >$, under the sum symbol in Eq.(2.28), indicate that the sum is only valid for next neighbour spins. The Heisenberg model describes a class of solid state systems, in which magnetism occurs because of permanent local moments with direct or indirect exchange interactions. This case can be found in insulator materials and in some metals.

2.4.1 Exchange interaction

The question of the underlying principle of the spontaneous collective magnetic order, below the Curie temperature, can be answered by taking into account the Coulomb interaction in combination with the Pauli principle. In order to understand how a spin-independent Coulomb interaction can be the reason for collective magnetic order, an example of a two electron system will be introduced[74]. Since the spatial behaviour of the electrons is independent of their spin behaviour it is valid to state $\Psi(\vec{r}_1, \vec{r}_2, S_{z1}, S_{z2}) = \phi(\vec{r}_1, \vec{r}_2) \cdot \psi(S_{z1}, S_{z2})$, where $S_z = \pm 1/2$. Since electrons are fermions their wave function has to be anti-symmetric under exchange $\Psi(\vec{r}_1, \vec{r}_2) = -\Psi(\vec{r}_2, \vec{r}_1)$. This leads to the following form of the wave function in position space

$$\Psi(\vec{r}_1, \vec{r}_2) = \theta_A(\vec{r}_1)\theta_B(\vec{r}_2) \pm \theta_B(\vec{r}_1)\theta_A(\vec{r}_2). \tag{2.29}$$

The interaction between the electrons is defined by the Coulomb potential $\hat{H}_C = e^2/(4\pi\varepsilon_0|\vec{r}_1 - \vec{r}_2|)$. Thus the energy of the system is given by $\left\langle \Psi(t) \middle| \hat{H}_C \middle| \Psi(t) \right\rangle = D \pm A$, with

$$D = \left\langle \theta_A(\vec{r}_1)\theta_B(\vec{r}_2) \middle| \hat{H}_C \middle| \theta_A(\vec{r}_1)\theta_B(\vec{r}_2) \right\rangle = \iint \mathrm{d}^3 r_1 \mathrm{d}^3 r_2 \frac{e^2}{4\pi\varepsilon_0} \frac{|\theta_A(\vec{r}_1)|^2 |\theta_B(\vec{r}_2)|^2}{|\vec{r}_1 - \vec{r}_2|} \tag{2.30}$$

and

$$A = \left\langle \theta_B(\vec{r}_1)\theta_A(\vec{r}_2) \middle| \hat{H}_C \middle| \theta_A(\vec{r}_1)\theta_B(\vec{r}_2) \right\rangle = \iint \mathrm{d}^3 r_1 \mathrm{d}^3 r_2 \frac{e^2}{4\pi\varepsilon_0} \frac{\theta_A(\vec{r}_1)\theta_B^*(\vec{r}_1)\theta_B(\vec{r}_2)\theta_A^*(\vec{r}_2)}{|\vec{r}_1 - \vec{r}_2|}, \tag{2.31}$$

where D is the direct Coulomb integral, which can be interpreted as the classical Coulomb repulsion force of two cloud charges with spatial densities

$|\theta_A(\vec{r}_1)|^2$, $|\theta_B(\vec{r}_2)|^2$, and where A is the exchange term, which occurs because electrons are indistinguishable particles and because of the overlap of the orbitals $\theta_A(\vec{r})$ and $\theta_B(\vec{r})$. The consequence of the exchange term A is that the degenerated energy level splits into two different levels, although the two occupied orbitals of the electrons in both levels stay the same. The lower energy level $D - A$ belongs to the anti-symmetric wave function in position space and the higher one $D + A$ belongs to the symmetric case. Within the anti-symmetric case the energy is lower, because the Coulomb repulsion is lower ($\Psi(\vec{r}_1, \vec{r}_2) = -\Psi(\vec{r}_2, \vec{r}_1) \implies \Psi(\vec{r}, \vec{r}) = 0$). The connection to the spin is given by the condition that in case of an anti-symmetric wave function in position space a symmetric spin wave function is mandatory and vice versa. The consequence for the two spin 1/2 system is that the energy level is split into a singlet level $S = 0$ and a triplet level $S = 1$. The triplet level, which is energetically the lower one, occurs by a symmetric spin wave function and an anti-symmetric wave function in position space and vice versa for the singlet level. By summarizing, the exchange interaction causes, in this case, an effective reduction of the potential energy (anti-symmetric wave function in position space). On the other hand, according to the Pauli principle, the parallel spin electrons (symmetric spin wave function) can not be in the same spatial state and must occupy successively higher levels, and consequently increasing their kinetic energy ($(\Psi(\vec{r}_1, \vec{r}_2) = -\Psi(\vec{r}_2, \vec{r}_1) \implies \Psi(\vec{r}, \vec{r}) = 0)$). The spontaneous parallel position of the spins and thus a ferromagnetic order will only come about if the lowering of the potential energy overcompensates the increase of the kinetic energy.

2.5 Landau-Zener scenario

Transition dynamics of a 2-level quantum mechanical system, subject to an external magnetic field with time-independent coupling elements in the off-diagonals of the system's Hamiltonian are described within the Landau-Zener scenario. Assuming the magnetic-field dependence is linear, the simplest Hamiltonian, which enables Landau-Zener scenarios, is given by

$$\hat{H} = \begin{pmatrix} \frac{\mu_B B_z(t)}{2} & \alpha \\ \alpha & -\frac{\mu_B B_z(t)}{2} \end{pmatrix}, \tag{2.32}$$

where α is some time-independent coupling between the two states. The diagonal elements in Eq.(2.32) represent the energies (E_1, E_2) of the diabatic states (energies where α is virtually zero) with the corresponding diabatic states $\big|1\big\rangle$ and $\big|2\big\rangle$. However, as $\hat{H}$ is not a diagonal matrix, it follows that these energies and states are not eigenvalues and eigenstates of the Hamiltonian. The eigenstates will be defined as $\big|\varphi_1(t)\big\rangle$ and $\big|\varphi_2(t)\big\rangle$ with the respective eigenvalues

$$\widetilde{E}_{1,2}(t) = \pm\sqrt{\alpha^2 + (\mu_B B_z(t))^2}. \tag{2.33}$$

If a system is initially in state $\big|\varphi_1(t)\big\rangle$ in zero magnetic field, shown in figure

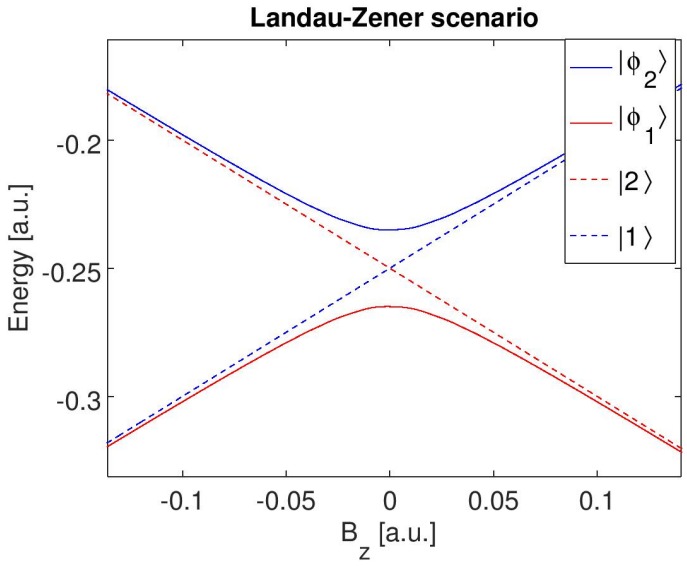

Figure 2.3: Adiabatic (curves) and diabatic (dotted lines) energy paths.

2.3 (on the red curve, from left), then an adiabatic increase in magnetic field $\frac{dB}{dt} \to 0$ will ensure that the system remains in an eigenstate $\big|\varphi_1(t)\big\rangle$ of the Hamiltonian $\hat{H}$. In contrast, an adiabatic increase in magnetic field $\frac{dB}{dt} \to \infty$ will ensure that the system follows the diabatic path (the dotted blue line in figure 2.3), thus the system undergoes a transition to state $\big|\varphi_2(t)\big\rangle$. For finite magnetic field sweep rates ($0 < \frac{dB}{dt} < \infty$) there will be a finite probability of finding the system in either of the two eigenstates, which is given by the probability function:

$$P_D = e^{-\pi\Gamma}, \tag{2.34}$$

where $\Gamma = \frac{\alpha^2/\hbar}{\frac{\partial}{\partial t}(\widetilde{E}_2 - \widetilde{E}_1)}$.

Chapter 3

Simulation methods

3.1 Exact diagonalization

In order to estimate the eigenvalues of a n-dimensional Hamiltonian, it is necessary to find the roots to the characteristic polynomial of degree n, for which in general no exact solution can be found for $n > 4$. A strategy to solve this is to find a unitary, or orthogonal, transformation that makes the Hamiltonian diagonal

$$\hat{H} \rightarrow \hat{U}^{\dagger}\hat{H}\hat{U}. \tag{3.1}$$

The purpose is to construct the matrix U in an iterative way,

$$\hat{H} \rightarrow \hat{U}_1^{\dagger}\hat{H}\hat{U}_1 \rightarrow \hat{U}_2^{\dagger}\hat{U}_1^{\dagger}\hat{H}\hat{U}_1\hat{U}_2 \rightarrow \cdots, \tag{3.2}$$

until the matrix becomes diagonal. The columns of $\hat{U} = \hat{U}_1\hat{U}_2 \cdots$ contains the eigenvectors of $\hat{H}$. Here we used the c++ library "Eigen" in order to find the eigenstates and eigenvalues of exchange coupled spin systems.

3.2 Classical Runge-Kutta-method

In order to solve the time dependent Schrödinger equation of motion, which is given by

$$i\hbar\frac{\partial}{\partial t}|\psi(t)\rangle = \hat{H}_{eff}|\psi(t)\rangle, \tag{3.3}$$

for single spin systems as well as exchange coupled spin chains we used the classical Runge-Kutta-method. The benefit of the Runge-Kutta approximation,

here, is the ability to use non-linear, non-hermitian Hamiltonians, for example in order to study damping effects. The classical Runge-Kutta-method is an approximation, which includes the principles of the Euler method, albeit in contrast to the Euler method it is using four increments instead of one, which leads to greater accuracy. The general procedure of the classical Runge-Kutta-method is: For $\dot{y} = f(t, y)$, with the initial condition $y(t_0) = y_0$ it follows

$$\begin{aligned} y_{n+1} &= y_n + \frac{h}{6}(k_1 + 2k_2 + 2k_3 + k_4), \\ k_1 &= f(t_n, y_n), \\ k_2 &= f(t_n + \frac{h}{2}, y_n + h\frac{k_1}{2}), \\ k_3 &= f(t_n + \frac{h}{2}, y_n + h\frac{k_2}{2}), \\ k_4 &= f(t_n + h, y_n + hk_3), \end{aligned} \tag{3.4}$$

where h $(h > 0)$ is the step size.

Chapter 4

Quantum revivals and magnetization tunneling in effective spin systems

This chapter is an extract from the publication:

M. Krizanac, D. Altwein, E. Y. Vedmedenko, and R. Wiesendanger, New J. Phys. **18** 033029 (2016).

4.1 Introduction

The wave-function of a quantum particle can decay over time, but its initial state is not lost and can reappear in certain time windows. This phenomenon of the wave-function reincarnation is known as the quantum revival [1, 2, 3, 4]. The analysis of the quantum revival reveals two types of systems. First, systems of excited localized wave packets in which the recovering of the complete wave-function destroyed by the decay processes has been studied in the context of two-level quantum systems [5, 6, 7], quantum wells [8, 9, 10, 11, 12] and Bose-Einstein condensates [13, 14]. The second type discusses systems with discrete energy eigenvalues in which, due to the quantum recurrence theorem, the systems return arbitrarily close to the initial state [15, 16, 17, 18, 19]. Meanwhile, the quantum dynamical phenomena become increasingly important also in solid state physics. Particularly, quantum mechanical tunneling

or the non-classical field dependence of magnetization has been reported for nanomagnets [20], molecules [21, 22] and single atoms [23]. Therefore, instead of studies of time-averaged properties like, e.g., magnetization curves [23, 24], nowadays the emphasis is put on the time-dependent behavior of magnetization [25, 26, 27, 28, 29]. This trend is promoted further by the development of novel pump-probe techniques [30] allowing for sub-femto-second time resolution of magnetization dynamics, which might shed light on the revival phenomena in nano-magnetic systems. Hence, theoretical predictions are urgently required. Until now, however, the systematic theoretical description of quantum revival in magnetic systems is lacking, while existing investigations come to controversial conclusions. Particularly, an increase as well as a decrease of the quantum revival time (QRT) with increasing spin s have been reported [25, 26].

Here, we studied the second type of the quantum revival analysis where an exact expression for the time evolution of an effective quantum magnetic moment has been derived analytically using the Schrödinger formalism. In contrast to previous investigations, which do not differentiate between the revival of the total wave function (state) and that of the expectation values of the wave-function, we distinguish the quantum revival time of the total wave-function (QRT) and the revival time of expectation values (EVRT) and show that they are not identical. We concentrate on EVRT as only this quantity can be measured experimentally. The analysis of the expression, which we obtain for EVRT, shows that the time-dependent behaviour of spin operators can be represented via the Fourier series of characteristic frequencies ω_i. These frequencies, in turn, define the non-harmonic precession of expectation values of spin components. Surprisingly, it doesn't depend on the angular momentum as previously predicted, but rather is defined via the ratio of the anisotropy constant K and the external magnetic field B. The shortest EVRT can be found for $\widetilde{B}_z = N \cdot K$ with any integer N. For any other $\widetilde{B}_z/K$ ratio the EVRT is larger or even infinite for an irrational ratio. Furthermore, our analysis reveals that the quantum tunneling of magnetization occurs at $\widetilde{B}_z = N \cdot K$, where $N \leq 2s$, in the regime of small transversal fields. Hence, the QRT and the magnetization tunneling are closely related to one another.

4.2 Time evolution of expectation values

The Quantum Recurrence Theorem [15] defines the QRT as the shortest time interval Δt after which the full wave-function $\left|\Psi(t)\right\rangle$ of a system periodically repeats $\left|\Psi(t)\right\rangle = \left|\Psi(t+\alpha\Delta t)\right\rangle$ $\alpha \in \mathbb{N}$. In experiment, however, only measurements of expectation values of the magnetization components $\left\langle S_j\right\rangle_t$ ($j := x, y, z$) are possible. Consequently, the periodicity of $\left|\Psi(t)\right\rangle$ recurrence is inaccessible, while that of the expectation values can be measured. The periodicity of expectation values may be different from the standard QRT as has been shown for a particle in a quantum well [12]. However, systematic comparison of these two quantities in quantum magnetic systems is still lacking.
For the sake of a systematic analysis of the dynamics of expectation values the time-dependent equation of motion

$$i\hbar\frac{\partial}{\partial t}\Psi(t) = \hat{H}\Psi(t) \tag{4.1}$$

has been solved analytically. The Hamilton operator in (6.3) includes the standard spin operators $\hat{S}_i$, uniaxial on-site anisotropy K and a magnetic field $\vec{B} = (0, 0, B_z)$. This Hamiltonian models an effective quantum spin representing a nanoparticle, a molecule, or an atomic cluster [31, 24, 20].

$$\hat{H} = -\hat{S}_z\widetilde{B}_z - K\hat{S}_z^2 \quad , \tag{4.2}$$

where

$$\widetilde{B}_z = \mu_B B_z. \tag{4.3}$$

The equations (6.3) and (4.2) define a system of uncoupled linear ordinary differential equations of first order

$$i\hbar\frac{\partial}{\partial t}\Psi(t) = \begin{pmatrix} -s\widetilde{B}_z - s^2K & \cdots & 0 \\ \vdots & \ddots & \\ 0 & & s\widetilde{B}_z - s^2K \end{pmatrix} \cdot \begin{pmatrix} \varphi_{+s}(t) \\ \vdots \\ \varphi_{-s}(t) \end{pmatrix} \tag{4.4}$$

with the following solutions for the eigenstates

$$\left|\Psi(t)\right\rangle = \begin{pmatrix} \varphi_{+s}(t) = \varphi_{+s}(t_0)\cdot e^{-i(-s\widetilde{B}_z - s^2K)t/\hbar} \\ \vdots \\ \varphi_{-s}(t) = \varphi_{-s}(t_0)\cdot e^{-i(s\widetilde{B}_z - s^2K)t/\hbar} \end{pmatrix} \tag{4.5}$$

where s is the spin quantum number and the initial conditions are

$$\varphi_{+s}(t_0), ..., \varphi_{-s}(t_0) \in \mathbb{C}. \tag{4.6}$$

The normalization condition is given by the expression

$$\sum_{i=0}^{2s} |\varphi_{s-i}(t)|^2 = |\varphi_{+s}(t)|^2 + \ldots + |\varphi_{-s}(t)|^2 = 1. \tag{4.7}$$

With the knowledge of eigenstates, the time-dependent expectation values of spin operators can be obtained as

$$\langle \hat{S}_i \rangle_t = \langle \Psi(t) | \hat{S}_i | \Psi(t) \rangle \qquad i := x, y, z. \tag{4.8}$$

An example of a real part of the expectation value for the spin operator $\hat{S}_x$ with $s = 1\hbar$ is given by (4.9).

$$\begin{aligned} \left\langle S_{x_{real}} \right\rangle_t = \frac{2\hbar}{\sqrt{2}} \cdot \Big[& (\underset{real}{\varphi_{+1}}(t_0)\, \underset{real}{\varphi_0}(t_0)) \cdot \cos\big((-\widetilde{B}_z - K)\frac{t}{\hbar}\big) \\ & + (\underset{real}{\varphi_{-1}}(t_0)\, \underset{real}{\varphi_0}(t_0)) \cdot \cos\big((\widetilde{B}_z - K)\frac{t}{\hbar}\big)\Big]. \end{aligned} \tag{4.9}$$

The complete solutions of the expectation values $\langle S_x \rangle, \langle S_y \rangle$ and $\langle S_z \rangle$ for an effective quantum spin $s = 1\hbar$ defined by the Hamilton operator $\hat{H} = -\hat{S}_z \widetilde{B}_z -$

$K\hat{S}_z^2$ are:

$$
\begin{aligned}
\langle S_x \rangle &= \frac{2\hbar}{\sqrt{2}} \\
&\cdot \Big[(\underset{real}{\varphi_{+1}}(t_0)\,\underset{real}{\varphi_0}(t_0) + \underset{imag}{\varphi_{+1}}(t_0)\,\underset{imag}{\varphi_0}\,(t_0)) \cdot \cos[(-B_z - \hbar K)t] \\
&+ (\underset{real}{\varphi_{-1}}(t_0)\,\underset{real}{\varphi_0}(t_0) + \underset{imag}{\varphi_{-1}}(t_0)\,\underset{imag}{\varphi_0}\,(t_0)) \cdot \cos[(B_z - \hbar K)t] \\
&+ (-\underset{real}{\varphi_{+1}}(t_0)\,\underset{imag}{\varphi_0}\,(t_0) + \underset{imag}{\varphi_{+1}}(t_0)\,\underset{real}{\varphi_0}(t_0)) \cdot \sin[(-B_z - \hbar K)t] \\
&+ (\underset{imag}{\varphi_{-1}}(t_0)\,\underset{real}{\varphi_0}(t_0) - \underset{real}{\varphi_{-1}}(t_0)\,\underset{imag}{\varphi_0}\,(t_0)) \cdot \sin[(B_z - \hbar K)t] \Big]
\end{aligned}
$$

$$
\begin{aligned}
\langle S_y \rangle &= \frac{2\hbar}{\sqrt{2}} \\
&\cdot \Big[(\underset{real}{\varphi_{+1}}(t_0)\,\underset{real}{\varphi_0}(t_0) + \underset{imag}{\varphi_{+1}}(t_0)\,\underset{imag}{\varphi_0}\,(t_0)) \cdot \sin[(-B_z - \hbar K)t] \\
&+ (-\underset{real}{\varphi_{-1}}(t_0)\,\underset{real}{\varphi_0}(t_0) - \underset{imag}{\varphi_{-1}}(t_0)\,\underset{imag}{\varphi_0}\,(t_0)) \cdot \sin[(B_z - \hbar K)t] \\
&+ (-\underset{real}{\varphi_{+1}}(t_0)\,\underset{imag}{\varphi_0}\,(t_0) - \underset{imag}{\varphi_{+1}}(t_0)\,\underset{real}{\varphi_0}(t_0)) \cdot \cos[(-B_z - \hbar K)t] \\
&+ (\underset{imag}{\varphi_{-1}}(t_0)\,\underset{real}{\varphi_0}(t_0) - \underset{real}{\varphi_{-1}}(t_0)\,\underset{imag}{\varphi_0}\,(t_0)) \cdot \cos[(B_z - \hbar K)t] \Big]
\end{aligned}
\tag{4.10}
$$

$$
\langle S_z \rangle = \frac{\hbar}{2}\Big[|\underset{real}{\varphi_{+1}}(t_0)|^2 - |\underset{real}{\varphi_{-1}}(t_0)|^2 + |\underset{imag}{\varphi_{+1}}(t_0)|^2 - |\underset{imag}{\varphi_{-1}}(t_0)|^2 \Big]
$$

These expressions have been obtained using $\langle \Psi(t)|\hat{S}_i|\Psi(t)\rangle$ $(i := x, y, z)$ where

$$
|\Psi(t)\rangle = \begin{pmatrix} \varphi_{+s}(t) = \varphi_{+1}(t_0) \cdot e^{-i(-\widetilde{B}_z - K)t/\hbar} \\ \varphi_0(t) = \varphi_0(t_0) \\ \varphi_{-1}(t) = \varphi_{-1}(t_0) \cdot e^{-i(\widetilde{B}_z - K)t/\hbar} \end{pmatrix}. \tag{4.11}
$$

A remarkable peculiarity of the expression (4.9) is the superposition of two characteristic frequencies $\omega_1 = (-\widetilde{B}_z - K)/\hbar$ and $\omega_2 = (\widetilde{B}_z - K)/\hbar$, which appear due to the quadratic nature of the uniaxial anisotropy term in the Hamilton operator of (4.2). The presence of two harmonics in (4.9) defines a non-harmonic oscillation [34], which is characterized by time-dependent amplitudes. It reveals that for a Hamilton operator including anisotropy terms

with an even exponent, for example, $K \cdot \hat{S}_\alpha^{2n}$ ($\alpha = x, y, z$ and $n \in \mathbb{N} \setminus \{0\}$), the expectation values $\langle S_j \rangle_t$ ($j := x, y$) can be represented in the form of Fourier series, while $\langle S_z \rangle_t$ is a constant. A solution of $\langle S_x \rangle_t$ for an arbitrary value of a quantum spin number is given by (4.12):

$$\langle S_x \rangle_t = \sum_{i=1}^{2s} \big(\alpha_i \cdot \cos(\omega_i t) + \beta_i \cdot \sin(\omega_i t)\big) \tag{4.12}$$

where

$$\begin{aligned} \alpha_i &= 2(S_x)_{i,i+1}\Big(\varphi(t_0)^{real}_{s-(i-1)} \cdot \varphi(t_0)^{real}_{s-i} + \varphi(t_0)^{imag}_{s-(i-1)} \cdot \varphi(t_0)^{imag}_{s-i}\Big) \\ \beta_i &= 2(S_x)_{i,i+1}\Big(- \varphi(t_0)^{real}_{s-(i-1)} \cdot \varphi(t_0)^{imag}_{s-i} + \varphi(t_0)^{imag}_{s-(i-1)} \cdot \varphi(t_0)^{real}_{s-i}\Big) \end{aligned} \tag{4.13}$$

and

$$(S_x)_{i,i+1} = \frac{\hbar}{2}\sqrt{(s+1)2i - (i^2+i)} \tag{4.14}$$

$$\omega_i = \frac{\big(- \widetilde{B}_z - (2s - (2i-1))K\big)}{\hbar}. \tag{4.15}$$

The derivation of expressions (4.12) can be found in the following sub-chapter "Fourier series form".

Hence, the time evolution of the magnetization components of an arbitrary quantum spin subject to quadratic terms in the Hamilton operator can be represented by a superposition of $2s$ characteristic frequencies ω_i. Clearly, these frequencies define a general non-harmonic oscillation. An exception is given by a spin $\hbar/2$ particle as in this case only one frequency $\widetilde{B}_z/\hbar$ survives. The spectrum of a general non-harmonic oscillation is discrete and is characterized by its fundamental frequency ω_f. The fundamental frequency ω_f corresponds to the greatest common divisor (gcd) of all harmonics $\gcd(\omega_1, ..., \omega_i)$. In our case all these frequencies depend on the magnitudes of K and $\widetilde{B}_z$. In the simplest case of spin $1\hbar$ there are only two of them, namely $\omega_1 = (-\widetilde{B}_z - K)/\hbar$ and $\omega_2 = (\widetilde{B}_z - K)/\hbar$. Quite generally, the shortest period of any oscillation

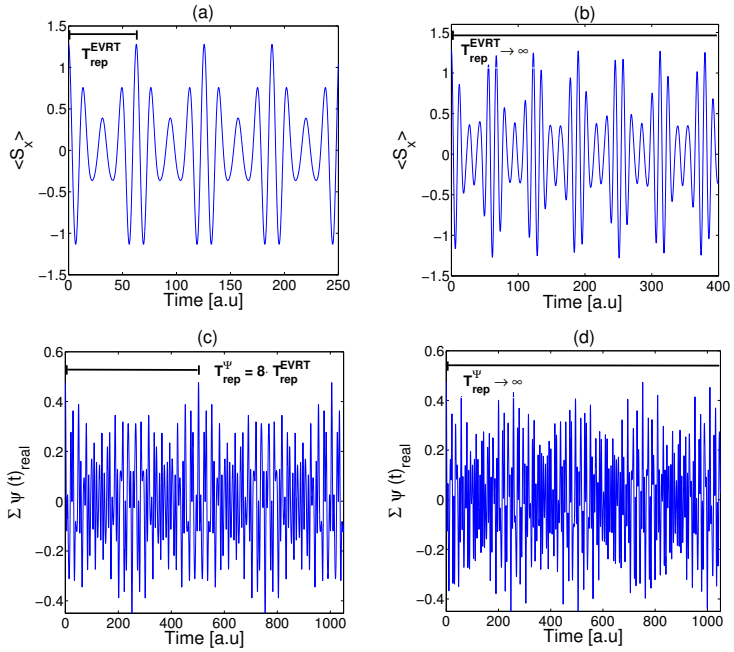

Figure 4.1: Example of the time-evolution for an effective quantum spin $3\hbar/2$: **a)** The time evolution of the expectation value $\langle S_x \rangle_t$ for $\widetilde{B}_z = 0.5$ [a.u] and $K = 0.05$ [a.u] ($\widetilde{B}_z/K = 10$). The lowest possible periodicity of the expectation value corresponds to $T_{rep} \approx 62$ [a.u]; **b)** The same $\langle S_x \rangle_t$ for $\widetilde{B}_z = 0.18 \cdot \pi$ [a.u] and $K = 0.05$ [a.u], with $\widetilde{B}_z/K \in \mathbb{I} = \mathbb{R} \backslash \mathbb{Q}$ leads to $T_{rep} \to \infty$; **c)** Time evolution of the total wave-function $|\Psi(t)\rangle$. The $\Sigma\psi(t)_{real}$ represents the real part of the total wave-function components. For the same magnitude of $\widetilde{B}_z$ and K as in (a), much larger values of $T_{rep} \approx 500$ [a.u] compared to (a) have been obtained; **d)** $\Sigma\psi(t)_{real}$ for parameters used in (b) with $T_{rep} \to \infty$.

corresponds to a reciprocal of the fundamental frequency defined above and is known as the repetitive time $T_{rep} = \frac{2\pi}{\omega_f}$

$$T_{rep} = \frac{2\pi}{\gcd(\omega_1, ..., \omega_i)} \quad , \ \omega_i \in \mathbb{Z} \tag{4.16}$$

In figure 4.1(a, c) a portion of the time-dependent evolution of $\langle S_x \rangle$ and the total wave-function with integer $\widetilde{B}_z/K$ value are shown, while in Fig. 4.1 (b, d) the signal for the case of an irrational $\widetilde{B}_z/K$ ratio is presented. While both cases represent the non-harmonic oscillation, their behaviour shows significant differences. Most importantly, $\langle S_x \rangle_t$ for $\widetilde{B}_z/K = 10$ of Fig. 4.1 (a) shows much smaller periodicity T_{rep}, than that of irrational $\widetilde{B}_z/K$ (Fig. 4.1 (b)). In figures

4.1(c) and 4.1(d), which represent the time evolution of the sum $\Sigma\psi(t)$ of the wave-function $|\Psi(t)\rangle = (\psi_s(t), ..., \psi_{-s}(t))^T$, the same values of $\widetilde{B}_z$ and K have been used. Nevertheless, much longer repetition periods of expectation values have been obtained. For irrational $\widetilde{B}_z/K$ ratio the periodicity of the total wave-function is infinite. In the next step, the relation between the repetitive time, the QRT and the EVRT for a given Hamilton operator will be revealed.

4.2.1 Fourier series form

Here we present the derivation of Eq.(4.12). The expectation values $\langle S_x\rangle, \langle S_y\rangle$ and $\langle S_z\rangle$ for a general effective quantum spin s, defined by a Hamilton operator without off-diagonal elements, can be generalized as:

$$\langle S_m\rangle = \langle \Psi(t)|S_m|\Psi(t)\rangle \qquad m \in [x, y, z] \tag{4.17}$$

where $|\Psi(t)\rangle$ is

$$\begin{pmatrix} \varphi_{+s}(t) = \varphi_{+s}(t_0) \cdot e^{-i(-s\widetilde{B}_z - s^2K)t/\hbar} \\ \vdots \\ \varphi_{-s}(t) = \varphi_{-s}(t_0) \cdot e^{-i(s\widetilde{B}_z - s^2K)t/\hbar} \end{pmatrix} \tag{4.18}$$

The generalized spin matrices S_m are defined by

$$\begin{aligned} (S_{x_{a,b}}) &= \frac{\hbar}{2}(\delta_{a,b+1} + \delta_{a+1,b})\sqrt{(s+1)(a+b-1) - ab} \\ (S_{y_{a,b}}) &= \frac{i\hbar}{2}(\delta_{a,b+1} - \delta_{a+1,b})\sqrt{(s+1)(a+b-1) - ab} \\ (S_{z_{a,b}}) &= \hbar(s-(a-1))\delta_{a,b} = \hbar(s-(b-1))\delta_{a,b} \end{aligned} \tag{4.19}$$

$$1 \leq a, b \leq 2s+1,$$

The generalized components of the time dependent spin eigenstate vector $\big|\Psi_s(t)\big\rangle$ are

$$\begin{aligned} &\varphi_{s-j}(t) = \varphi_{s-j}(t_0) \cdot e^{-i(-(s-j)\widetilde{B}_z - (s-j)^2 K)\frac{t}{\hbar}} \\ &0 \leq j \leq 2s \end{aligned} \tag{4.20}$$

The generalized form of $\big|\Psi_s(t)\big\rangle$ in (4.20) is a consequence of the fact that the Hamilton operator $\hat{H} = -\hat{S}_z\widetilde{B}_z - K\hat{S}_z^2$ does not contain off-diagonal elements. Hence, it represents a system of uncoupled linear ordinary differential equations of first order. Inserting (4.20) and (4.19) in (4.17) leads to

$$\begin{aligned} \big\langle S_m \big\rangle &= \varphi_s^*(t)(S_{m_{1,2}})\varphi_{s-1}(t) \\ &+ \varphi_{s-1}^*(t)\Big((S_{m_{2,1}})\varphi_s(t) + (S_{m_{2,3}})\varphi_{s-2}(t)\Big) \\ &+ \varphi_{s-2}^*(t)\Big((S_{m_{3,2}})\varphi_{s-1}(t) + (S_{m_{3,4}})\varphi_{s-3}(t)\Big) \\ &+ \varphi_{s-3}^*(t)\Big((S_{m_{4,3}})\varphi_{s-2}(t) + (S_{m_{4,5}})\varphi_{s-4}(t)\Big) \\ &\vdots \\ &+ \varphi_{-s}^*(t)(S_{m_{a,a-1}})\varphi_{-s+1}(t) \end{aligned} \tag{4.21}$$

We remark that the eigenstates and components $(S_{m_{a,a-1}})$ of the spin matrices S_m in (4.21) have a systematic structure, which can be extracted in the following form:

$$\begin{aligned} \big\langle S_m \big\rangle &= \varphi_s^*(t)(S_{m_{1,2}})\varphi_{s-1}(t) + \varphi_{-s}^*(t)(S_{m_{a,a-1}})\varphi_{-s+1}(t) \\ &+ \sum_{j=1}^{2s-1} \Big(\varphi_{s-j}^*(t)\Big((S_{m_{j+1,j}})\varphi_{s-(j-1)}(t) + (S_{m_{j+1,j+2}})\varphi_{s-(j+1)}(t)\Big)\Big) \\ &m \in [x, y] \end{aligned} \tag{4.22}$$

Repeating and sorting of the equation (4.22) leads to

$$\langle S_z \rangle = \sum_{j=0}^{2s-1} \Big((S_{z_{j+1,j+1}}) \varphi^*_{s-j}(t) \cdot \varphi_{s-j}(t) \Big) \tag{4.23}$$

and

$$\begin{aligned}
&\langle S_x \rangle_t = \sum_{j=1}^{2s} \big(\alpha_j \cdot \cos(\omega_j t) + \beta_j \cdot \sin(\omega_j t) \big) \\
&\alpha_j = 2(S_x)_{j,j+1} \Big(\varphi(t_0)^{real}_{s-(j-1)} \cdot \varphi(t_0)^{real}_{s-j} + \varphi(t_0)^{imag}_{s-(j-1)} \cdot \varphi(t_0)^{imag}_{s-j} \Big) \\
&\beta_j = 2(S_x)_{j,j+1} \Big(- \varphi(t_0)^{real}_{s-(j-1)} \cdot \varphi(t_0)^{imag}_{s-j} + \varphi(t_0)^{imag}_{s-(j-1)} \cdot \varphi(t_0)^{real}_{s-j} \Big)
\end{aligned}$$

$$\begin{aligned}
&\langle S_y \rangle_t = \sum_{j=1}^{2s} \big(\alpha_j \cdot \sin(\omega_j t) + \beta_j \cdot \cos(\omega_j t) \big) \\
&\alpha_j = 2(S_y)_{j,j+1} \Big(- \varphi(t_0)^{real}_{s-(j-1)} \cdot \varphi(t_0)^{real}_{s-j} - \varphi(t_0)^{imag}_{s-(j-1)} \cdot \varphi(t_0)^{imag}_{s-j} \Big) \\
&\beta_j = 2(S_y)_{j,j+1} \Big(\varphi(t_0)^{real}_{s-(j-1)} \cdot \varphi(t_0)^{imag}_{s-j} - \varphi(t_0)^{imag}_{s-(j-1)} \cdot \varphi(t_0)^{real}_{s-j} \Big)
\end{aligned} \tag{4.24}$$

$$\omega_j = -\widetilde{B}_z - (2s - (2j-1))K$$

Equation (4.24) is particularly interesting because it has a Fourier series form. This form occurs if the Hamilton operator contains terms with an even exponent $\hat{S}^{2n} (n \in \mathbb{N} \setminus \{0\})$. It means the presented approach applies to all terms which are quadratic in the spin operators, for example, different kinds of anisotropy.

4.3 Non-harmonic revival of expectation values

As the repetitive time gives the shortest period of oscillation it corresponds to the revival time. Figure 4.1 demonstrates that the T_{rep} for the time evolution of wave-functions (Figure 4.1(c,d)) and that of expectation values (Figure 4.1(a,b)) may be quite different even for the same Hamiltonian. Additionally, the frequencies ω_i, which determine the T_{rep}, depend on the ratio of the

external magnetic field and the anisotropy. In the next step the reasons for differences between QRT and EVRT as well as the role of the $\widetilde{B}_z/K$ ratio for T_{rep} will be analyzed.

While expectation values are always real, the wave-functions and coefficients α_i in (4.12) may be complex. For the sake of comparison between EVRT and QRT analytically we first explore the real solution for T_{rep} only. However, the generalization to complex variables is straightforward and doesn't change our conclusions. For that purpose we use the Bézout's identity [33] stating:

$$\gcd(\omega_1, ..., \omega_m) = \sum_{i=1}^{m} a_i \cdot \omega_i \tag{4.25}$$

where $a_i, \omega_i \in \mathbb{Z}$. With (4.25) T_{rep} becomes

$$T_{rep} = \frac{2\pi}{\gcd(\omega_1, ..., \omega_m)} = \frac{2\pi}{a_1\omega_1 + ... + a_m\omega_m}. \tag{4.26}$$

The numerator and denominator of this expression can be expanded as

$$T_{rep} = \frac{2\pi \cdot 10^n}{a_1\omega_1 10^n + ... + a_m\omega_m 10^n} = \frac{2\pi \cdot 10^n}{\gcd(\omega_1 \cdot 10^n, ..., \omega_m \cdot 10^n)}, \tag{4.27}$$

where $\omega_i \in \mathbb{R}$, $n \in \mathbb{N}$ and $\omega_i \cdot 10^n \in \mathbb{Z}$. The expansion of (4.27) leaves the period T_{rep} unchanged and Bézout's identity unaffected. It means that the initial greatest common divider can be replaced by an equivalent expression using simple multiplication of the characteristic frequencies and the numerator by 10^n. For any irrational number $\widetilde{B}_z/K \in \mathbb{R}\backslash\mathbb{Q}$ the sequence in the denominator of (4.27) and, hence, T_{rep} is infinite. This fact explains why we were not able to find the quantum revival in figure 4.1(b,d). For any integer or rational $\widetilde{B}_z/K \in \mathbb{Q}$, the T_{rep} is finite. Hence, the interesting question arises how the revival time of expectation values is connected to the $\widetilde{B}_z/K$ ratio in this case. This question is addressed in detail in sub-section "Derivation of critical B_z/K ratios for EVRT".

The fundamental frequency $\omega_f = \gcd(\omega_1 \cdot 10^n, ..., \omega_m \cdot 10^n)$ of EVRT is always equal or lower than the lowest ω_i in (4.12), which can be expressed by an infimum (inf) :

$$\omega_f \leq \inf(\omega_1 \cdot 10^n, ..., \omega_m \cdot 10^n). \tag{4.28}$$

For a given spin value s the allowed frequencies of individual harmonics ω_i given in (4.15) depend on the magnitude of $\widetilde{B}_z$ and K only. Defining $\widetilde{B}_z/K = N$ for a given s and replacing $\widetilde{B}_z$ by $N \cdot K$ in (4.15) we end up with the following expression:

$$\omega_i = \frac{\big[-N - (2s - (2i-1))\big] \cdot K}{\hbar} \tag{4.29}$$

which leads to:

$$\omega_i = \begin{cases} (-N-1)K, (-N-3)K, ..., (-N-(2n+1))K & \text{for integer } s \\ (-N)K, (-N-2)K, (-N-4)K, ..., (-N-2n)K & \text{for half-integer } s \end{cases} \tag{4.30}$$

with n-number of harmonics. Hence, the spin value s is not at all present in the analytical expression (4.30). As i is an integer and s is an integer or half-integer in (4.29) the fundamental frequency corresponds to the very specific choices of $\widetilde{B}_z/K = N$. All possible values of the fundamental frequency ω_f for integer, rational or irrational N and different spin numbers are derived in subsection "Derivation of critical B_z/K ratios for EVRT". The most important results are summarized in the following.

Most importantly, the T_{rep} corresponding to the fundamental frequency ω_f is different for different combinations of spin statistics (integer or half-integer) and N ratios. The lowest possible T_{rep} and, hence, the lowest EVRT among all possible combinations of N and the spin statistics appears for any

$$\frac{\widetilde{B}_z}{K} = N \in \mathbb{Z}. \tag{4.31}$$

Particularly,

$$T_{rep} = \begin{cases} \dfrac{2\pi\hbar}{K} & \text{, (integer } s \text{ and even } N \text{ or } N=0) \text{ or (half-integer } s \text{ and odd } N) \\ \dfrac{\pi\hbar}{K} & \text{, (integer } s \text{ and odd } N) \text{ or (half-integer } s \text{ and even } N \text{ or } N=0) \end{cases} \tag{4.32}$$

Thus, there are only two possible values of the revival time for the expectation values $T_{rep}^{\mathrm{EVRT}} = \frac{2\pi\hbar}{K} \vee \frac{\pi\hbar}{K}$ for any $N \in \mathbb{Z}$. These EVRT do not depend on the spin values as predicted before[25, 26], but only on the spin statistics. Because of our analytical findings it becomes clear why it happens. As the

spin dynamics is described by the superposition of harmonic frequencies there is only one fundamental frequency for the given set of parameters.
If N is rational $\widetilde{B}_z/K = N \in \mathbb{Q}\backslash\mathbb{Z}$, for example $N = 3/5$, the revival times are still finite but always somewhat larger than those in case of $N \in \mathbb{Z}$,

$$T_{rep} = \begin{cases} \dfrac{\pi b}{K} & , b > 2 \\ \dfrac{2\pi b}{K} & , b > 1 \end{cases} \tag{4.33}$$

where b is the denominator from the definition of $N = a/b \in \mathbb{Q}$ in sub-section "Derivation of critical B_z/K ratios for EVRT". In summary,

$$T^{\mathrm{EVRT}}_{N\in\mathbb{R}\backslash\mathbb{Q}} > T^{\mathrm{EVRT}}_{N\in\mathbb{Q}\backslash\mathbb{Z}} > T^{\mathrm{EVRT}}_{N\in\mathbb{Z}} \tag{4.34}$$

where $\mathbb{R}\backslash\mathbb{Q}$ are irrational numbers. The derivation of (4.56) and (4.34) can be found in sub-section "Derivation of critical B_z/K ratios for EVRT". An external field can easily be tuned experimentally. Therefore one can use the time-dependent measurement of EVRT to determine the anisotropy of the system. It can be done by experimental measurements of the revival times. Knowing the value of the field at the shortest revival the anisotropy value can be derived using (4.41).
Up to this point only the EVRT has been considered. The QRT have been addressed in detail in sub-section "Derivation of critical field-anisotropy ratios for QRT" using the procedure similar to that of sub-section "Derivation of critical B_z/K ratios for EVRT". We find that EVRT and QRT are identical for all effective quantum spins with integer spin number, while they are different for half-integer s. Particularly,

$$\begin{aligned} T^{\mathrm{EVRT}}_{rep} &= T^{\mathrm{QRT}}_{rep}, && \text{for integer } s \\ T^{\mathrm{EVRT}}_{rep} &= \frac{1}{\alpha}\cdot T^{\mathrm{QRT}}_{rep}, \quad \alpha \in [1,2,4,8], && \text{for half-integer } s \end{aligned} \tag{4.35}$$

In contrast to EVRT for half-integer spins, T^{QRT}_{rep} is shortest for $\widetilde{B}_z/K = (2\beta - 1)/2 \in \mathbb{Q}\backslash\mathbb{Z}$ with $\beta \in \mathbb{Z}$. This means, that while the expectation values of magnetization repeat fastest for any $\widetilde{B}_z/K \in \mathbb{Z}$ it is not the case for the wave-functions as $(2\beta - 1)/2 \notin \mathbb{Z}$.

In summary, the standard QRT and the EVRT of an effective spin are identical for even spin numbers but very different for half-integer spins. The EVRT depends on the ratio N only but is independent of the magnitude of the spin quantum number. The shortest revivals can be observed for $N \in \mathbb{Z}$.

4.3.1 Derivation of critical B_z/K ratios for EVRT

In this section we want to present a proof for the statement that the relation $\widetilde{B}_z/K = N \in \mathbb{Z}$ for constant K always leads to a lower time T_{rep} than that for $N \in \mathbb{Q} \setminus \mathbb{Z}$. We investigate the set of rational numbers $\mathbb{Q}$ only, because the "gcd(...)" used for the definition of quantum revival of expectation values (EVRT) given in the main text is only defined for integers. Due to the fact that the irrational numbers (subset of $\mathbb{R}$) can not be extended to become integers we can not use them for the "gcd(...)". First we formulate two Lemma's, which are necessary for our proof.

Lemma 1:
If $\gamma_1 + \gamma_2 = G$, in which $\gamma_1, \gamma_2, G \in \mathbb{Z}$, $\gamma_1/x \in \mathbb{Z}$, $G/x \in \mathbb{Z}$ and $x \in \mathbb{Q}$, then $\gamma_2/x \in \mathbb{Z}$. Otherwise it would lead to a contradiction. If only $G/x \in \mathbb{Z}$ is given, then γ_1/x and γ_2/x are not necessarily an element of $\mathbb{Z}$.

Proof 1. (Lemma 1):

$$\begin{aligned} & G/x \in \mathbb{Z} \ \wedge \ \gamma_2/x \in \mathbb{Z} \\ & \frac{\gamma_1 + \gamma_2}{x} = \frac{G}{x} \\ & \Rightarrow \frac{\gamma_1}{x} = \frac{G}{x} - \frac{\gamma_2}{x} \\ & \Rightarrow \frac{G}{x} - \frac{\gamma_2}{x} \in \mathbb{Z} \ \Rightarrow \frac{\gamma_1}{x} \in \mathbb{Z} \end{aligned} \tag{4.36}$$

Proof 2. (Lemma 1):

$$\begin{aligned} & G = 6 \ \wedge \ \gamma_1 = 2 \ \wedge \ \gamma_2 = 4 \wedge \ x = 3 \\ & \gamma_1 + \gamma_2 = G \ \Rightarrow 6 = 2 + 4 \\ & \Rightarrow \frac{G}{x} = 2 \ \in \mathbb{Z} \\ & \Rightarrow \frac{\gamma_1}{x} = \frac{2}{3} \notin \mathbb{Z} \\ & \Rightarrow \frac{\gamma_2}{x} = \frac{4}{3} \notin \mathbb{Z} \end{aligned} \tag{4.37}$$

Lemma 2:
If $\omega_1 + \Delta_{\omega_1,\omega_2} = \omega_2$, in which $\omega_1, \omega_2, \Delta_{\omega_1,\omega_2} \in \mathbb{Z}$ then it follows for $\omega_2/x \in \mathbb{Z}$, $\omega_1/x \notin \mathbb{Z}$ and $\Delta_{\omega_1,\omega_2}/x \notin \mathbb{Z}$ that $\gcd(\omega_1, \omega_2) \neq x$.

Proof (Lemma 2):

$$\begin{aligned} & \gcd(\omega_1, \omega_2) \leq \inf(\omega_1, \omega_2) \\ & \omega_1 < \omega_2 \\ & x \leq \omega_1 \\ & \omega_i/x \in \mathbb{Z} \ \ (\text{condition for } \gcd(\omega_1, ..., \omega_i)) \\ & \text{if } \frac{\omega_2}{x} \in \mathbb{Z} \ \wedge \ \frac{\omega_1}{x} \notin \mathbb{Z} \\ & \Rightarrow \gcd(\omega_1, \omega_2) \neq x \end{aligned} \tag{4.38}$$

Lemma 1 and Lemma 2 enable us to use the structure of (4.43) to find all possible greatest common divisors.

$$\widetilde{B}_z = NK \tag{4.39}$$

$$\omega_j = -\widetilde{B}_z - (2s - (2j - 1))K \tag{4.40}$$

$$\omega_j = \begin{cases} (-N-1)K, (-N-3)K, ..., (-N-(2n+1))K & \text{for integer } s \\ (-N)K, (-N-2)K, (-N-4)K, ..., (-N-2n)K & \text{for half-integer } s \end{cases} \tag{4.41}$$

$$n \in \mathbb{N}_0$$

Equation (4.41) demonstrates that the frequencies ω_j defined by (4.40) have the form of series.

Based on (4.41) we substitute N via $N = a/b$, where $a, b \in \mathbb{Z}$. This substitution enables us to create any element of $\mathbb{Q}$. Further, we use the conclusion of the series form of (4.41) and exchange the numbers through a variable Γ_n, which contains all properties of (4.40) for $N = 0$.

$$N := \frac{a}{b}, \qquad N \in \mathbb{Q} \Rightarrow a, b \in \mathbb{Z} \tag{4.42}$$

$$\omega_j := \xi_n := \Big(\frac{a}{b} + \Gamma_n\Big)K, \qquad \Gamma_n = \begin{cases} 2n+1 & \text{for integer } s \\ 2n & \text{for half-integer } s \end{cases} \tag{4.43}$$

$$n \in \mathbb{N}_0 \tag{4.44}$$

Next, we expand the numerator and denominator of T_{rep} with b in order to obtain the necessary integer frequency condition for the greatest common divisor:

$$T_{rep} = \frac{2\pi}{\gcd(\xi_0, ..., \xi_j)} \quad \Rightarrow \quad T_{rep} = \frac{2\pi \cdot b}{\gcd(\xi_0 b, ..., \xi_j b)} \tag{4.45}$$

The expanded frequencies $\xi_n b$ in (4.45) are defined by

$$\xi_n b = \Big(a + \Gamma_n \cdot b\Big)K \tag{4.46}$$

Next, we substitute the first multiplier of (4.46) via $\Omega = 2m$ or $\Omega = 2m+1$ to distinguish between the even or odd solution for each frequency series $\xi_n b$:

$$\begin{aligned} &\xi_0 b = \Big(a + \Gamma_0 \cdot b\Big)K = \Omega K \\ &\vdots \\ &\xi_n b = \Big(a + \Gamma_n \cdot b\Big)K = (\Omega + n \cdot 2b)K \end{aligned} \qquad \Omega := \begin{cases} 2m \\ 2m+1 \end{cases} \tag{4.47}$$

$$\xi_n b - \xi_0 b = n \cdot 2b, \qquad m \in \mathbb{Z} \tag{4.48}$$

Equation (4.47) provides us with an expression which permits to use Lemma 1 and Lemma 2 in order to estimate the greatest common divisor.

As $\xi_0 b$ corresponds to the lowest frequency it follows that

$$\begin{aligned} &\gcd(\xi_0 b, ..., \xi_j b) \leq \xi_0 \cdot b \\ &\Rightarrow \gcd(\xi_0 b, ..., \xi_j b) \leq \Omega K \end{aligned} \tag{4.49}$$

In order to estimate if ΩK is a common divisor of all $\xi_n b$ we divide (4.47) by ΩK, which leads to

$$\frac{\xi_n \cdot b}{\Omega K} = \Big(\frac{a}{\Omega} + \frac{\Gamma_n \cdot b}{\Omega}\Big) = \Big(1 + \frac{n \cdot 2b}{\Omega}\Big). \tag{4.50}$$

The ΩK in (4.50) is a common divisor of (4.47) for $\Omega \in [b, 2b, 1, 2]$. Next, we have to distinguish in which cases $\Omega K = bK$, $\Omega K = 2bK$, $\Omega K = 1K$ and $\Omega K = 2K$ is the greatest common divisor of (4.47). The case $\Omega = b$ leads to

$$\frac{\xi_n \cdot b}{\Omega K} = \Big(\frac{a}{b} + \Gamma_n\Big) \tag{4.51}$$

Because of $\Gamma_n \in \mathbb{Z}$ and Lemma 1 it follows from (4.51) that if $\xi_n \cdot b/\Omega K \in \mathbb{Z}$ then a/b has to be an element of $\mathbb{Z}$. The case $\Omega = 2b$ leads to

$$\frac{\xi_n \cdot b}{\Omega K} = \Big(\frac{a}{2b} + \frac{\Gamma_n}{2}\Big), \tag{4.52}$$

and it follows that

$$\begin{aligned} &\Big(\frac{a}{2b} + \frac{\Gamma_n}{2}\Big) = \sigma \in \mathbb{Z} \\ &\Rightarrow \frac{a}{b} = 2\sigma - \Gamma_n \end{aligned} \tag{4.53}$$

Because of $\sigma,\ \Gamma_n \in \mathbb{Z}$ from (4.53) and Lemma 1 it follows that $a/b \in \mathbb{Z}$. The conclusion from (4.51) and (4.52) is that

$$\gcd(\xi_1 \cdot b, ..., \xi_n \cdot b) = \begin{cases} 2bK \\ bK \end{cases} \tag{4.54}$$

for $a/b \in \mathbb{Z}$, which leads to

$$T_{rep} = \begin{cases} \frac{2\pi}{K} \\ \frac{\pi}{K} \end{cases} \tag{4.55}$$

Because of the result from (4.55) and Lemma 2 it follows by inserting $\Omega = 1$ and $\Omega = 2$ in (4.50) that the greatest common divisor of (4.47) has to be

$\Omega K = 1K$ or $\Omega K = 2K$ for $a/b \notin \mathbb{Z}$, which leads to:

$$T_{rep} = \begin{cases} \dfrac{\pi b}{K} & , \ b > 2 \\ \dfrac{2\pi b}{K} & , \ b > 1 \end{cases} \tag{4.56}$$

The estimation of the lower bound for the b in (4.56) is done using (4.47) by permutation of even and odd Ω.
The consequence of (4.56) and (4.55) is that

$$T_{rep}^{N\in\mathbb{Z}} < T_{rep}^{N\notin\mathbb{Z}}. \tag{4.57}$$

q.e.d.

Figure 4.2 represents a visualization of the result of (4.57).

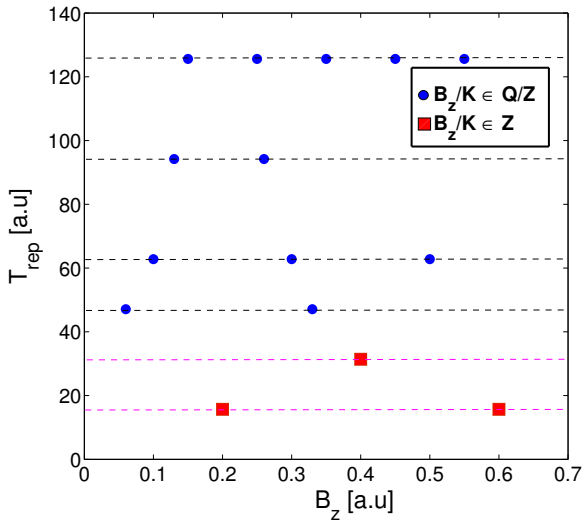

Figure 4.2: Revival times of expectation values (EVRT) of a spin $1\hbar$ for different B_z values and $K = 0.2$ [a.u] = const. Because the EVRT is not continuous for any B_z we choose to give an example for discrete B_z values. This demonstrates the result $T_{rep}^{N\in\mathbb{Z}} < T_{rep}^{N\notin\mathbb{Z}}$.

4.3.2 Derivation of critical field-anisotropy ratios for QRT

In this section we derive the QRT for two scenarios: $\widetilde{B}_z/K = N \in \mathbb{Z}$ and $\widetilde{B}_z/K = N \notin \mathbb{Z}$ with $K = const$. We start with the wave functions from

equation (4.5)

$$\begin{aligned}\varphi_{+s}(t) &= \varphi_{+s}(t_0)\cdot e^{-i(-s\widetilde{B}_z - s^2K)\frac{t}{\hbar}}\\ &\vdots\\ \varphi_{-s}(t) &= \varphi_{-s}(t_0)\cdot e^{-i(s\widetilde{B}_z - s^2K)\frac{t}{\hbar}}\end{aligned} \tag{4.58}$$

where

$$\omega_j = \frac{(-s-j)\widetilde{B}_z - (s-j)^2K}{\hbar}, \quad \text{for} \quad j \in \mathbb{N}_0 \tag{4.59}$$

$$\omega_j = \begin{cases}(-N-1)K, (-2N-4)K, (-3N-9)K, ..., (-nN-n^2)K & \text{for integer } s\\ (-2N-1)K, (-6N-9)K, ..., (-(4n+2)N-(2n+1)^2)K & \text{for half-integer } s\end{cases} \tag{4.60}$$

$$n \in \mathbb{N}_0$$

The derivation follows the same principles like in sub-section "Derivation of critical B_z/K ratios for EVRT". Lemma 1 and Lemma 2 are guidelines for the following derivation.

Integer s case:

$$\begin{aligned}&\xi_0 b = (a+b)K = \Omega K\\ &\xi_1 b = \Big(2(a+b)+2b\Big)K = (2\Omega + 2b)K\\ &\vdots\\ &\xi_n b = \Big((n+1)(a+b) + b\sum_{i=0}^{n} 2n\Big)K = \Big((n+1)\Omega + b\sum_{i=0}^{n} 2n\Big)K\end{aligned} \qquad \Omega := \begin{cases}2m\\ 2m+1\end{cases} \tag{4.61}$$

$$\frac{\xi_1 b}{\Omega} = (2 + \frac{2b}{\Omega})K \tag{4.62}$$

For $a/b = N \in \mathbb{Z}$ it follows that:

$$T_{rep} = \begin{cases}\dfrac{2\pi}{K}\\ \dfrac{\pi}{K}\end{cases} \tag{4.63}$$

For $a/b = N \notin \mathbb{Z}$ equation (4.61) leads for the greatest common divisor

$$\gcd(\xi_0 b, ..., \xi_j b) = \begin{cases} 2K \\ K \end{cases} \tag{4.64}$$

$$\Rightarrow T_{rep} = \begin{cases} \dfrac{\pi b}{K} & , b > 2 \\ \dfrac{2\pi b}{K} & , b > 1 \end{cases} \tag{4.65}$$

Half-Integer s case:

$$\begin{aligned} &\xi_0 b = (2a+b)K = \Omega K \\ &\xi_1 b = \Big(3(2a+b)+6b\Big)K = (3\Omega + 6b)K \\ &\vdots \\ &\xi_n b = \Big((2n+1)(2a+b) - 2nb + b\sum_{i=0}^{n} 8n\Big)K \qquad \Omega := \begin{cases} 2m \\ 2m+1 \end{cases} \\ &= \Big((2n+1)\Omega - 2nb + b\sum_{i=0}^{n} 8n\Big)K \end{aligned} \tag{4.66}$$

For $N \in \mathbb{Z}$ it follows

$$\begin{aligned} \frac{\xi_1 b}{\Omega} &= \Big(3 + \frac{6b}{\Omega}\Big)K \\ \frac{\xi_2 b}{\Omega} &= \Big(5 + \frac{20b}{\Omega}\Big)K \end{aligned} \tag{4.67}$$

The result of (4.67) is that

$$\begin{aligned} &\gcd(\xi_0 b, ..., \xi_j b) = bK \\ &\Rightarrow T_{rep} = 4 \cdot \frac{2\pi}{K} \qquad \text{for} \quad N \in \mathbb{Z} \end{aligned} \tag{4.68}$$

For $N \notin \mathbb{Z}$ one can write

$$\begin{aligned} \frac{\xi_1 b}{\Omega} &= \Big(3 + \frac{6b}{\Omega}\Big)K = \Big(3 + \frac{6b}{2a+b}\Big)K \\ \frac{\xi_2 b}{\Omega} &= \Big(5 + \frac{20b}{\Omega}\Big)K = \Big(5 + \frac{20b}{2a+b}\Big)K \end{aligned} \tag{4.69}$$

$$\begin{aligned} \frac{6b}{2a+b} = \beta \in \mathbb{Z} \quad &\Rightarrow \frac{a}{b} = \frac{(6-\beta)}{2\beta} \\ \frac{20b}{2a+b} = \beta \in \mathbb{Z} \quad &\Rightarrow \frac{a}{b} = \frac{(20-\beta)}{2\beta} \end{aligned} \tag{4.70}$$

$$\begin{aligned} &\frac{(6-\beta)}{2\beta} = \frac{(20-\beta)}{2\beta} \\ &\Rightarrow 14 = 0 \quad \Rightarrow \quad \gcd(\xi_0 b, ..., \xi_j b) \neq \Omega K \end{aligned} \tag{4.71}$$

The next step is to estimate which of the values $2bK$ or bK is the greatest common divisor. Because of the condition $(2a+b)/2b \in \mathbb{Z}$ for $a = \frac{b(2\gamma-1)}{2}$ it follows that

$$\begin{aligned} &\gcd(\xi_0 b, ..., \xi_j b) = 2K \\ &\Rightarrow T_{rep} = 4 \cdot \frac{\pi}{K} \qquad \text{for} \quad N = \frac{(2\gamma-1)}{2} \notin \mathbb{Z} \end{aligned} \tag{4.72}$$

For $N \neq (2a+b)/2b$ and $N \notin \mathbb{Z}$ it follows

$$\Rightarrow \gcd(\xi_0 b, ..., \xi_j b) = \begin{cases} 2K \\ K \end{cases} \tag{4.73}$$

$$\Rightarrow T_{rep} = \begin{cases} 4 \cdot \frac{2\pi b}{K} & , \ b > 2 \\ 4 \cdot \frac{\pi b}{K} & , \ b > 3 \end{cases} \tag{4.74}$$

We can summarize the results for the half-integer s case as:

$$T_{rep} = \begin{cases} 4 \cdot \frac{2\pi}{K} & , \ N \in \mathbb{Z} \\ 4 \cdot \frac{\pi}{K} & , \ N = \frac{(2\gamma-1)}{2} \notin \mathbb{Z} \\ 4 \cdot \frac{2\pi b}{K} & , \ b > 2 \quad N \notin \mathbb{Z} \\ 4 \cdot \frac{\pi b}{K} & , \ b > 3 \quad N \notin \mathbb{Z} \end{cases} \tag{4.75}$$

By comparing (4.75) with (4.56) and (4.55) from sub-section "Derivation of critical B_z/K ratios for EVRT" for the same values of K, a, and b it follows:

$$T_{rep}^{\text{EVRT}} = \frac{1}{\alpha} \cdot T_{rep}^{\text{QRT}}, \quad \alpha \in [1, 2, 4, 8], \qquad \text{for half-integer } s \tag{4.76}$$

We use this expression in the main text.

4.4 Quasi-quantum revival and magnetization tunneling

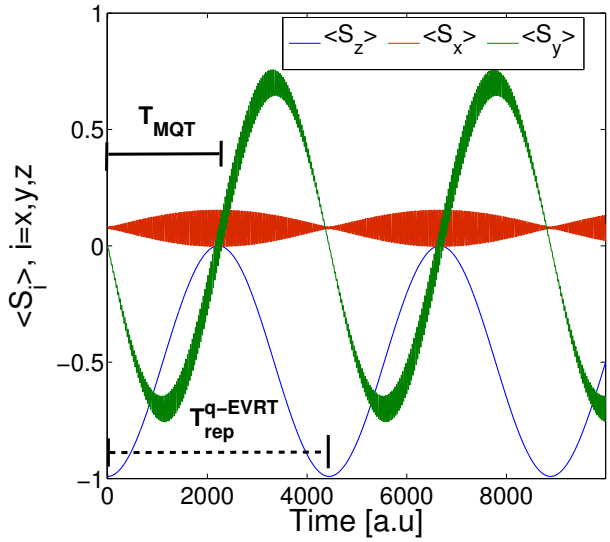

Figure 4.3: Behaviour of expectation values within the tunneling regime obtained using the numerical solution of the Schrödinger equation. For $\widetilde{B}_z/K = N \in \mathbb{Z}$ with $\widetilde{B}_z = 0.1$ [a.u], $K = 0.1$ [a.u] and a small transversal field $\widetilde{B}_x = 0.001$ [a.u]. The repetitive time T_{rep} is equal for the expectation values $\langle S_j \rangle_t$ ($j := x, y, z$) and it is two times the magnetization tunneling time $T_{rep}^{\text{q-EVRT}} \approx 2 \cdot T_{MQT}$.

Previous considerations of quantum spin dynamics in the literature have been performed for uncoupled and unperturbed systems [25, 26]. In the following we want to analyze the behaviour of the EVRT under the influence of a small time-independent perturbation. Such an investigation is important, because

small perturbations like a transversal field or anisotropy break the rotational symmetry about the z-axis and make the $\hat{S}_z$ spin operator and the energy non-commuting. This symmetry breaking promotes the spontaneous transition of magnetization from one energy well (expectation value of magnetization) to another one under the energy barrier, known as the resonant quantum tunneling of magnetization (MQT). The MQT have been measured in many solid state and molecular magnetic systems and is of considerable technological importance [22, 29, 23, 31, 27], because it is directly connected to the life-times of the information bits. In zero external magnetic field $\vec{B}_z = 0$, the quantum mechanical levels $m = \pm s$ have the lowest energy. When a non-zero $\vec{B} = (0, 0, B_z)$ is applied, the levels with $m > 0$ decrease in energy, while those with $m < 0$ increase. At certain B values the crossing of positive and negative levels occurs. When a transversal field is added the avoided level crossing appears [22, 31, 35]. This avoided level crossing promotes the MQT. However, the probability of the MQT depends strongly on the velocity at which the field $B(t)$ is swept [35, 36]. Hence, it is reasonable to anticipate that some connection between the EVRT and the probability of MQT exists. In the following this connection will be explored.

The interplay between EVRT and QRT has been studied by the numerical solution of (6.3). We used Simpson's rule, which is similar to the Runge-Kutta procedure of third order for the numerical approximation of the solution of (6.3). The Hamiltonian (4.2) has been modified to

$$\hat{H} = -\hat{S}_z \widetilde{B}_z - K\hat{S}_z^2 - \hat{S}_x \lambda \widetilde{B}_x \tag{4.77}$$

with $\lambda\widetilde{B}_x \ll \widetilde{B}_z$. Figure 4.3 gives the time evolution values of $\langle S_z \rangle$, $\langle S_x \rangle$ and $\langle S_y \rangle$ for $s = 1\hbar$ and for $\widetilde{B}_z/K = 1$. In contrast to figure 4.1, where $\langle S_z \rangle$ was always constant, the vertical component of magnetization in the present case oscillates between $\langle S_z \rangle = -1$ and $\langle S_z \rangle = 0$ values, while the y-component of magnetization switches (tunnels) between $\langle S_y \rangle \approx -0.7$ and $\langle S_y \rangle \approx 0.7$. This behaviour is typical for the MQT. The time, which is needed to switch the magnetization $\langle S_z \rangle$ from the $|-1\rangle$ to the $|0\rangle$ state is denoted in the following as magnetization tunneling time T_{MQT}.

The numerical analysis of the results obtained for several N-ratios has shown that for $\widetilde{B}_x \ll \widetilde{B}_z$ the T_{rep}^{EVRT} is of the order of $2 \cdot T_{MQT}$. This definition is

not mathematically exact, because, strictly speaking, the EVRT cannot be described analytically for perturbed arbitrary quantum spin systems. However, the numerical data indicates that the MQT oscillation (see $\langle S_z \rangle_t$ in figure 4.2), with small $\widetilde{B}_x$, is similar to an harmonic oscillation. This means we describe for small values of $\widetilde{B}_x$ a non-harmonic oscillation as a harmonic oscillation, because the differences $\Delta_{<S_z>} = \langle S_z \rangle_{\text{minima}_1} - \langle S_z \rangle_{\text{minima}_2}$ between two successive minima of $\langle S_z \rangle_t$ decrease for decreasing $\widetilde{B}_x$ and the non-harmonic behaviour is not immediately obvious.

$$\lim_{\widetilde{B}_x \to 0} \Delta_{<S_z>} = \lim_{\widetilde{B}_x \to 0} \left(\langle S_z \rangle_{\text{minima}_1} - \langle S_z \rangle_{\text{minima}_2} \right) = 0 \tag{4.78}$$

The consequence of (4.78) for the experiment is that for small transversal $\widetilde{B}_x$-fields the non-harmonic dynamics is beyond the experimental resolution, but it could be useful to define a quasi-expectation value revival time (q-EVRT), which treats the MQT oscillation as an harmonic oscillation and defines the revival time $T_{rep}^{\text{q-EVRT}}$ as the time between two successive minima of $\langle S_z \rangle_t$ (see figure 4.2). To estimate the quasi-EVRT in the tunneling regime with reasonable accuracy the standard ansatz of the time-dependent perturbation theory can be used. Defining

$$|\Psi(t)\rangle = \sum_{n=0}^{2s} \sigma(t)_{s-n} e^{-iE_{(s-n)}t/\hbar} |\psi_{s-n}\rangle, \tag{4.79}$$

where $\sigma(t)$ are the time-dependent coefficients and E are the energy eigenvalues, and substituting (4.79), (4.77) in (6.3) we utilize the standard perturbation theory power series ansatz:

$$\sigma(t)_{s-n} = \sigma(t)_{s-n}^{(0)} + \lambda \sigma(t)_{s-n}^{(1)} + ... = \sum_{i=0}^{\infty} \lambda^i \sigma(t)_{s-n}^{(i)}. \tag{4.80}$$

Using coefficient comparison in first order perturbation theory, we obtain

$$\begin{aligned}
\sigma_s(t)^{(1)} &= \frac{\sigma_{s-1}(t_0)\widetilde{B}_x(S_x)_{1,2}}{E_{s-1}-E_s}\cdot(-e^{i(E_{s-1}-E_s)t/\hbar}+1)\\
&\vdots\\
\sigma_{s-n}(t)^{(1)} &= \widetilde{B}_x\Big(\frac{\sigma_{s-(n-1)}(t_0)(S_x)_{a,b}}{E_{s-(n-1)}-E_{s-n}}\cdot(-e^{i(E_{s-(n-1)}-E_{s-n})t/\hbar}+1)\\
&\quad+\frac{\sigma_{s-(n+1)}(t_0)(S_x)_{a,c}}{E_{s-(n+1)}-E_{s-n}}\cdot(-e^{i(E_{s-(n+1)}-E_{s-n})t/\hbar}+1)\Big),
\end{aligned} \tag{4.81}$$

where $(S_x)_{1,2}$ is an element of the $\hat{S}_x$ matrix from (4.14). The square of the absolute value of $\sigma_s(t)^{(1)}$ leads to the well known Fermi's golden rule which reads:

$$|\sigma(t)_s^{(1)}|^2 = \left|\sigma_{s-1}(t_0)\widetilde{B}_x(S_x)_{1,2}\right|^2\cdot\left|\frac{\sin\left(\frac{E_{s-1}-E_s}{2\hbar}t\right)}{(E_{s-1}-E_s)/2}\right|^2, \qquad |\sigma_{s-1}(t_0)|=1 \tag{4.82}$$

Equation (4.82) describes the probability of quantum transitions between neighbouring states $|\psi_{\sigma(t)_s}\rangle$ and $|\psi_{\sigma(t)_{s-1}}\rangle$, and has a maximum for $E_s = E_{s-1}$, which is only valid for times t

$$|\sigma(t)_s^{(1)}|^2 \leq 1 \quad\Longrightarrow\quad t < \frac{\hbar}{\left|\widetilde{B}_x(S_x)_{1,2}\right|}. \tag{4.83}$$

Comparing t of (4.83) with T_{MQT}, obtained in numerical simulations, leads to a proportionality constant of $T_{MQT}/t \approx \pi/2$ within the tunneling regime, which can be expressed as

$$\lim_{\widetilde{B}_x\to 0}\frac{T_{MQT}}{t} = \frac{\pi}{2} \tag{4.84}$$

Furthermore, the analysis of the numerical data leads to

$$T_{MQT} \approx \frac{T_{rep}^{\text{q-EVRT}}}{2} \approx \frac{\pi\hbar}{2\left|\widetilde{B}_x(S_x)_{1,2}\right|}, \tag{4.85}$$

which occurs for a $\widetilde{B}_z/K = N \in \mathbb{Z}$ ratio with $N \leq 2s$. Hence, the magnetization tunneling time T_{MQR} at the avoided level crossing points is unambiguously related to the repetitive time $T_{rep}^{\text{q-EVRT}}$ if nonegligible transversal perturbations are present. In the limit of vanishing perturbations $T_{MQR} \to \infty$, that is, no tunneling occurs and (4.41) for $T_{rep}^{\text{q-EVRT}}$ can be applied. The conditions for magnetization tunneling $\widetilde{B}_z/K = 2s$ for the Hamiltonian of (4.77) is a subset of the condition $\widetilde{B}_z/K \in \mathbb{Z}$ defined in (4.31).

4.5 Conclusion

Analytical and numerical studies of the quantum dynamics of effective quantum spins have revealed that the quantum revival of expectation values and the total wave-function is identical for integer spin values, but very different for half-integer spins. This finding permitted to resolve the contradicting conclusions in the literature on the dependence of the revival time on the spin value. It has been concluded that the QRT doesn't depend on the spin number but only on the spin statistics (integer or half-integer). According to the derived analytical expressions the EVRT is shortest for integer field-anisotropy ratios. As the field can easily be tuned experimentally, and time-dependent measurements have become available in the last years, we hope that this finding will permit a highly precise measurement of magnetic anisotropies. For that purpose one should measure the EVRT as a function of external magnetic field and define the shortest one among all measured values.

An applied transverse field promotes the MQT. Our analysis shows that the EVRT is strongly correlated with the MQT. By increasing the revival time using specific combinations of material parameters and fields one can increase the life-times of the quantum states, which may be used as bits of information in future data storage technologies.

Chapter 5

Perturbative calculations of quantum spin tunneling in effective spin systems with a transversal magnetic field and transversal anisotropy

This chapter is an extract from the publications:

M. Krizanac, E. Y. Vedmedenko, and R. Wiesendanger, New J. Phys. **19** 013032 (2017).
M. Krizanac, E. Y. Vedmedenko, and R. Wiesendanger, New J. Phys. **19** 078001 (2017).

5.1 Introduction

Quantum tunneling in spin systems is the consequence of symmetry breaking of an unperturbed system by perturbations which leads to a loss of degeneracy of energy levels. At a mesoscopic scale the quantum tunneling has been extensively studied experimentally [37, 38, 49, 50, 51, 52, 53] by using single-molecular magnets (SMM) and theoretically by path-integral methods [39, 40, 41, 48] and perturbative approaches [42, 43, 44, 45, 46, 47]. Especially,

the influence of a transversal magnetic field in combination with transversal anisotropies on the tunnel splitting energy has been studied experimentally [37, 38] and theoretically [39, 41]. The appearance of a transversal magnetic field for a system which already contains a transversal anisotropy can be important, because for half-integer spin systems with a transversal anisotropy the appearance of a transversal magnetic field enables tunneling effects which otherwise would not be possible due to Kramers degeneracy theorem, which states that every energy level is at least doubly degenerate if it is a half-integer spin. This phenomenon is known as the spin parity effect [37, 38, 48], where a sole transversal anisotropy enables spin tunneling for integer spin systems but is not enough to enable tunneling in half-integer systems. It has also been shown that half-integer spin systems are much more sensitive to transversal magnetic fields than integer spin systems [38].

A further important effect is the quenched tunnel splitting, which describes the destructive interference of two quantum spin paths of opposite windings [39, 54] (instantons). These destructive interferences lead to a vanishing of the energy splitting for certain values of the transversal magnetic field and are not related to the Kramers degeneracy theorem. So far, quenched tunnel splitting has been described through spin-coherent-state path integrals which leads to the two instanton path picture. Instantons, for example in a double well potential, can be interpreted as solutions of the path integral which occurs by minimizing the Euclidean action of the path integral. The potential energy described within the Euclidean action change sign under the Wick rotation and the minima of the double well potential transform into maxima which enables a classical approach by minimizing the action. Regarding this, the perturbative approach has the potential to reveal a more detailed quantum mechanical understanding of the quenched tunnel splitting, beyond the two instanton path picture. In order to understand the spin parity effect and the quenched tunnel splitting from a perturbative point of view a perturbative approach with two or more perturbations is necessary, which is still missing. In this paper, we close this description gap by deriving a tunnel splitting energy formula for a system which contains two perturbations, a transversal magnetic field and a transversal anisotropy. The goal is to give a detailed theoretical description of the quenched tunnel splitting and in general a description of the influence

of the transversal magnetic field and the transversal anisotropy on the energy splitting from a perturbation theory point of view.

5.2 Perturbative approach

In order to describe the influence of a transversal magnetic field and a transversal anisotropy on the ground doublet energy splitting by a time-dependent perturbative approach it is necessary to use two perturbations simultaneously [46]. The simplest effective Hamiltonian which is capable of describing quantum tunneling at a mesoscopic scale with two perturbations is

$$\hat{H} = -K_z\hat{S}_z^2 - \hat{S}_x\widetilde{B}_x + \widetilde{K}(\hat{S}_x^2 - \hat{S}_y^2), \tag{5.1}$$

where $\widetilde{B}_x$ and $\widetilde{K}$ represents the two perturbations. In order to perform a perturbative calculation with two perturbations it is necessary to define a shared coefficient for $\widetilde{B}_x$ and $\widetilde{K}$, otherwise it would not be possible to use the coefficient comparison.

$$\begin{aligned} \widetilde{B}_x &= \lambda B_x = \lambda \mu_B H_x \\ \widetilde{K} &= \lambda K. \end{aligned} \tag{5.2}$$

The λ in Eq.(5.2) represent the shared coefficient. It is worth mentioning that the concept of the shared coefficient is not limited to two perturbations. From now on we performed the standard time-dependent perturbative approach to obtain a formula for the energy splitting. The difficulty was to master the sheer complexity, which arises when two or more perturbations occur. A short introduction of the construction of a perturbative series with two perturbations is shown in Appendix A. Due to the parity effect we obtained two formulas for the energy splitting of the ground doublet energy splitting, one for the integer spins and one for the half-integer ones. For the integer spin case the formula

has the following structure

$$
\begin{aligned}
\Delta E_{\text{split}} &= \left| \frac{2 \prod_{j=1}^{2s} (S_x)_{j,j+1} \cdot (\Delta_{B_x} + \Delta_K + \Delta_{B_x K})}{\prod_{j=1}^{2s-1} |(E_{s-j} - E_{-s})|} \right| \\
\Delta_{B_x} &= B_x^{2s} \\
\Delta_K &= (-1)^s 2^s K^s \prod_{j=1}^{s} |(E_{s-(2j-1)} - E_{-s})| \\
\Delta_{B_x K} &= \sum_{n=1}^{s-1} B_x^{\beta=2n} \cdot K^{\gamma=s-n} \cdot (-1)^\gamma 2^\gamma \sum_{j_1=1}^{\beta+1} \ldots \sum_{j_\gamma=j_{\gamma-1}+2}^{\beta+2\gamma-1} \prod_{i=1}^{\gamma} |(E_{s-j_i} - E_{-s})| \\
(S_{x_{j,j+1}}) &= \frac{1}{2} \sqrt{(s+1)2j - j(j+1)} \\
|(E_{s-j} - E_{-s})| &= |j^2 - 2s \cdot j| K_z,
\end{aligned}
\tag{5.3}
$$

where B_x represents the transversal magnetic field energy, K the transversal anisotropy and $\Delta_{B_x K}$ the mixed paths which occur when a transversal magnetic field interacts with a transversal anisotropy. $(S_{x_{j,j+1}})$ in Eq.(5.3) and Eq.(5.4) define matrix elements of the operator $\hat{S}_x$, and $|(E_{s-j} - E_{-s})|$ represents the absolute value of the difference of energy levels.

The formula for the half-integer spin case, which is defined by Eq.(5.4) differs mainly from the integer spin formula by the absence of the transverse anisotropy term Δ_K, which is forbidden due to the Kramers degeneracy theorem.

$$
\begin{aligned}
\Delta E_{\text{split}} &= \left| \frac{2 \prod_{j=1}^{2s} (S_x)_{j,j+1} \cdot (\Delta_{B_x} + \Delta_{B_x K})}{\prod_{j=1}^{2s-1} |(E_{s-j} - E_{-s})|} \right| \\
\Delta_{B_x} &= B_x^{2s} \\
\Delta_{B_x K} &= \sum_{n=0}^{s-\frac{3}{2}} B_x^{\beta=2n+1} \cdot K^{\gamma=s-\frac{1}{2}-n} \cdot (-1)^\gamma 2^\gamma \sum_{j_1=1}^{\beta+1} \ldots \sum_{j_\gamma=j_{\gamma-1}+2}^{\beta+2\gamma-1} \prod_{i=1}^{\gamma} |(E_{s-j_i} - E_{-s})|
\end{aligned}
\tag{5.4}
$$

To confirm the accuracy of our derivations we have performed exact diagonalizations, where we estimated the energy splitting ΔE_{Diag} of the ground doublet by the difference between the two highest eigenvalues and compared them with the results of the formulas of Eq.(5.3) and Eq.(5.4). The results, which are listed in table I, show a very good agreement.

Table 5.1: Comparison between the energy splitting ΔE obtained by the formulas and by exact diagonalizations. Parameters for spin $s = 2$ and $s = 5/2$: $B_x = 0.002$[meV] ($H_x = 0.035$[T]), $K = 0,001$[meV], $K_z = 1.0$[meV]. Parameters for spin $s = 5$: $B_x = 0.02$[meV] ($H_x = 0.35$[T]), $K = 0,01$[meV], $K_z = 1.0$[meV].

Spin s	$\Delta E_{\text{Formula}}$	ΔE_{Diag}
2	$2.99333 \cdot 10^{-6}$	$2.99334 \cdot 10^{-6}$
5/2	$6.65625 \cdot 10^{-9}$	$6.65917 \cdot 10^{-9}$
5	$1.50179 \cdot 10^{-10}$	$1.50223 \cdot 10^{-10}$

5.2.1 Perturbative series derivation

Here we would like to introduce in a short form the construction of a perturbative series with two perturbations:

$$\hat{H} = -K_z \hat{S}_z^2 - \hat{S}_x \widetilde{B}_x + \widetilde{K}(\hat{S}_x^2 - \hat{S}_y^2), \tag{5.5}$$

We start with a Hamiltonian which contains two perturbations $\widetilde{B}_x$ and $\widetilde{K}$.

$$i\hbar \frac{\partial}{\partial t} \big|\Psi(t)\big\rangle = \hat{H} \big|\Psi(t)\big\rangle \tag{5.6}$$

$$\big|\Psi(t)\big\rangle = \sum_{n=0}^{2s} a(t)_{s-n} e^{-iE_{s-n}t/\hbar} \big|\psi_{s-n}\big\rangle \tag{5.7}$$

We define the coefficient a from a general definition of a wave-function as time-dependent $a(t)$.

$$\begin{aligned} \widetilde{B}_x &= \lambda B_x = \lambda \mu_B H_x \\ \widetilde{K} &= \lambda K. \end{aligned} \tag{5.8}$$

By inserting the wave-function with the time-dependent coefficient (Eq.(5.7)) in the Schrödinger equation Eq.(5.6),

$$i\hbar\frac{\partial}{\partial t}\Big(\sum_{n=0}^{2s} a(t)_{s-n}e^{-iE_{s-n}t/\hbar}|\psi_{s-n}\rangle\Big) = \hat{H}\Big(\sum_{n=0}^{2s} a(t)_{s-n}e^{-iE_{s-n}t/\hbar}|\psi_{s-n}\rangle\Big) \quad (5.9)$$

we obtain Eq.(5.9).

$$\begin{aligned} &i\hbar\cdot e^{-iE_st/\hbar}\frac{\partial}{\partial t}a(t)_s = E_sa(t)_se^{-iE_st/\hbar} - (S_x)_{1,2}\widetilde{B}_xa(t)_{s-1}e^{-iE_{s-1}t/\hbar} \\ &i\hbar\cdot e^{-iE_{s-1}t/\hbar}\frac{\partial}{\partial t}a(t)_{s-1} = ... \\ &\quad\vdots \end{aligned} \quad (5.10)$$

By expanding Eq.(5.9) we obtain a system of ordinary differential equations, demonstrated through Eq.(5.10).

$$\begin{aligned} &i\hbar\frac{\partial}{\partial t}a(t)_s = -(S_x)_{1,2}\lambda B_xa(t)_{s-1}e^{i(E_s-E_{s-1})t/\hbar} + 2(S_x)_{1,2}(S_x)_{2,3}\lambda Ka(t)_{s-2}e^{i(E_s-E_{s-2}t/\hbar)} \\ &i\hbar\frac{\partial}{\partial t}a(t)_{s-1} = ... \\ &\quad\vdots \end{aligned} \quad (5.11)$$

After rearranging Eq.(5.10) and using the definition of Eq.(5.8) we obtain a system of differential equations with an expansion of the time-dependent coefficient $a(t)$, demonstrated through Eq.(5.11).

$$a(t)_{s-n} = a(t)^{(0)}_{s-n} + \lambda a(t)^{(1)}_{s-n} + ... = \sum_{i=0}^{\infty}\lambda^i a(t)^{(i)}_{s-n}. \quad (5.12)$$

Now we utilize the standard perturbation theory power series ansatz (Eq.(5.12)) by inserting it in Eq.(5.11) and rearranging the λ's.

$$\begin{aligned}
&\frac{\partial}{\partial t}a(t)_s^{(0)} = 0 \\
&\frac{\partial}{\partial t}a(t)_s^{(1)} = \frac{i}{\hbar}\Big((S_x)_{1,2}B_x a_{s-1}^{(0)} e^{i(E_s-E_{s-1})t/\hbar} - 2(S_x)_{1,2}(S_x)_{2,3}K a_{s-2}^{(0)} e^{i(E_s-E_{s-2}t/\hbar)}\Big) \\
&\quad\vdots \\
&\frac{\partial}{\partial t}a(t)_{s-1}^{(0)} = 0 \\
&\quad\vdots
\end{aligned} \tag{5.13}$$

The next step is to use the coefficient comparison to obtain systems of differential equations for every order of the time-dependent coefficients $a(t)^{(i)}$ from the power series ansatz in Eq.(5.12). This is implied through Eq.(5.13.).
From here onwards we expand the series in the same way as we would do for the Fermi's golden rule, by repeating the integration and the inserting of the coefficients $a(t)^{(i)}$ in Eq.(5.13) until the resonant case. The only difference from the situation with only one perturbation is that we now have much more direct paths which generate a resonant case.

5.2.2 Alternative formula

Here we want to introduce a more compact version of our formulas in Eq.(5.2) and Eq.(5.3), derived by A.Garg [77]:

$$\begin{aligned}
\Delta E &= \frac{4s}{2^{2s}(2s-1)!{K_z}^{2s-1}} \prod_{n=1}^{2s}(B_x - (2s+1-2n)B_a) \\
B_a &= \sqrt{2KK_z},
\end{aligned} \tag{5.14}$$

which agrees very well with our equations (see table 5.2). The more compact formula in Eq.(5.14) has the advantage that it enables a simpler and faster calculation of the energy splitting ΔE, but on the other hand has the disadvantage that it can not distinguish between the tunneling paths which contribute to the energy splitting ΔE, without further transformations. These

Table 5.2: Comparison between the energy splitting ΔE obtained by the formula in Eq.(5.14) from A.Garg (ΔE_{Garg}) and by our formulas (ΔE_{ours}). Parameters for spin $s = 3$: $B_x = 0.05$[meV], $K = 0,002$[meV], $K_z = 1.0$[meV]. Parameters for spin $s = 4$: $B_x = 0.002$[meV], $K = 0,01$[meV], $K_z = 1.0$[meV]. Parameters for spin $s = 5$: $B_x = 0.01$[meV], $K = 0,06$[meV], $K_z = 1.0$[meV].

Spin s	ΔE_{ours}	ΔE_{Garg}	$\lvert\Delta E_{\text{ours}} - \Delta E_{\text{Garg}}\rvert$
3	$7.65527 \cdot 10^{-9}$	$7.65527 \cdot 10^{-9}$	$4.96308 \cdot 10^{-24}$
4	$2.18699 \cdot 10^{-8}$	$2.18699 \cdot 10^{-8}$	$6.61744 \cdot 10^{-24}$
5	$1.19484 \cdot 10^{-6}$	$1.19484 \cdot 10^{-6}$	$2.11758 \cdot 10^{-22}$

transformations would lead to a much more complicated form, similar to our expressions in Eq.(5.2) and Eq.(5.3).

5.3 Tunneling paths

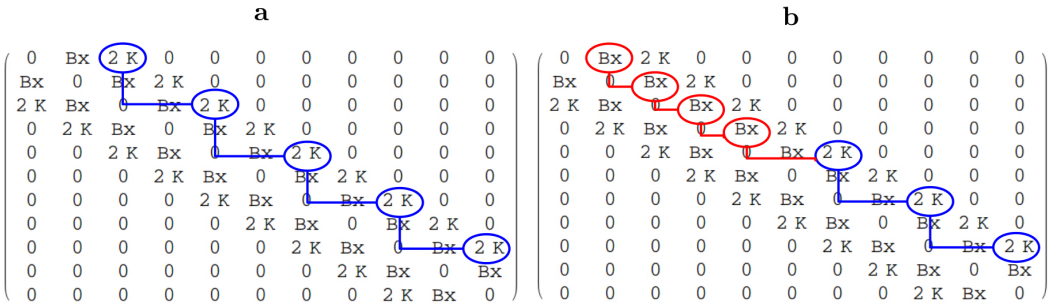

Figure 5.1: Illustration of tunneling paths from a perturbative point of view: **a.)** Here we demonstrate a pure path where we only used energy contributions from the transversal anisotropy to obtain a resonant case. **b.)** Here we show a mixed path were we used energy contributions from the transversal magnetic field energy B_x and the transversal anisotropy K.

Before we begin with the analysis of Eq.(5.3) and Eq.(5.4), we want to define first what we mean by paths. In Figure 5.1a and 5.1b we illustrate a matrix which only contains the off-diagonal elements of the Hamiltonian in Eq.(5.1) in a simplified form. In order to obtain an energy splitting of the ground doublet through a perturbative calculation it is necessary to expand the perturbative series to the order where we obtain a resonant case. The resonant case is a

situation within the perturbative series where we obtain a perturbative term with the energy difference between the highest state $|s\rangle$ and its symmetric opposite state $|-s\rangle$. This series expansion has a specific iterative structure where we can choose a path to obtain a resonant case. A path which only contains energy contributions of the transversal anisotropy K is shown in figure 5.1a, where we expand the perturbative series only with transversal anisotropy energies to obtain a resonant situation. Such a path is called a pure path because it contains only energies from one term of the Hamiltonian in Eq.(5.1). In contrast to a pure path a so-called mixed path is shown in figure 5.1b where we used two energy contributions from different sources to obtain a resonant case (one source is from the magnetic transversal field energy B_x and the other is from the transversal anisotropy K). It should be mentioned at this point that a spin system will always take all possible paths, but as we will show it is useful to distinguish between those. With these definitions of the paths we are now in a position to explain the properties of Eq.(5.3) and Eq.(5.4).

5.4 Quenched tunnel splitting from a perturbative point of view

The perturbative approach enables us to make conclusions complementary to a path integral formalism [55]. Through Eq.(5.3) and Eq.(5.4) we are able to distinguish separately between the energy splitting contributions from the transversal magnetic field and the transversal anisotropy, represented by Δ_{B_x}, Δ_K, and Δ_{B_xK}. With the ability to distinguish separately between the energy splitting contributions we want to analyze here the quenched tunnel splitting from a perturbative theory point of view. Figure 5.2a shows the well known effect of the quenched tunnel splitting [54], where under certain values of the transversal magnetic field the energy splitting of the ground doublet is vanishing. This is already explained through a two instanton paths model with destructive interference [39, 54]. The perturbative approach we used here enables us to analyze this effect from a more detailed perspective. Through Eq.(5.3) and Eq.(5.4) we can identify the mixed path Δ_{B_xK} as the trigger for the quenched tunnel splitting for half integer spins and even integer spins.

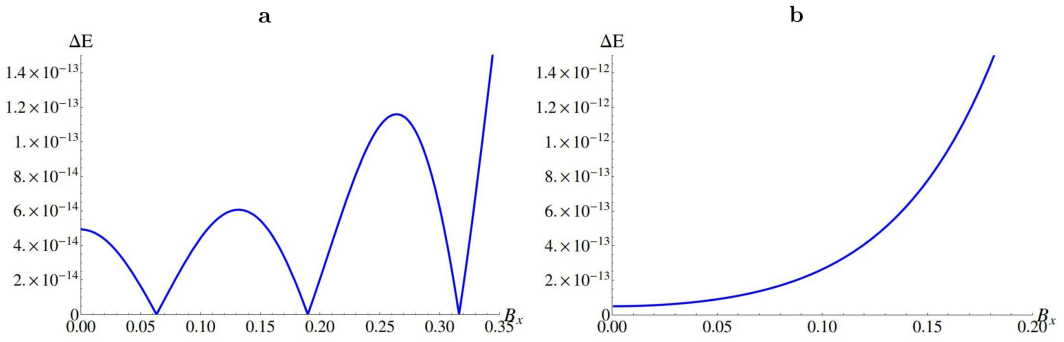

Figure 5.2: Quenched tunnel splitting. **a.)** Here we show the well known quenched tunnel splitting, where the energy splitting ΔE is vanishing for certain values of B_x[meV] ($B_x = \mu_B$[meV/T] $\cdot\, H_x$[T]) for a spin $s = 5$ system. Used parameters: $K = 0.01$ [meV] and $K_z = 1$ [meV]. **b.)** In contrast to figure 2a, here we demonstrate the absence of the quenched tunnel splitting for negative K. Used parameters: spin $s = 5$: $K = -0.01$ [meV] and $K_z = 1$ [meV].

This can be seen through the property that Δ_{B_xK} is an alternating series for a positive K. Since Δ_K in Eq.(4.14) is positive for even spin quantum numbers the only term which can cause negative contributions is consequently Δ_{B_xK}. The scenario of odd integer spins leads to a combined cause of Δ_{B_xK} and Δ_K for the quenched tunnel splitting. Instead of describing the quenched tunnel splitting by only two instanton paths, we are now in a position to specify it more as the destructive interference of many paths extracted from a perturbative approach. The destructive interference nature arises primarily from the alternating mixed paths Δ_{B_xK} (half-integer and even integer spins) or a combination of the pure path Δ_K and the mixed Δ_{B_xK} paths (odd integer spins). So far we expanded the two instanton path model through a detailed many path model with the corresponding important contributions to the quenched tunnel splitting.

In order to demonstrate that Eq.(5.3) and Eq.(5.4) also describe the negative K case correctly, we want to present this known behavior [54] in figure 5.2b. Figure 5.2b shows the situation where the transversal anisotropy K is negative. Here we see that no quenching of the tunnel splitting occurs, because the former alternating series Δ_{B_xK} in Eq.(5.3) and Eq.(5.4) is not alternating any more, due to the Hamiltonian in Eq.(5.1). The consequence is that

only positive contributions to the energy splitting are present, which makes it impossible to obtain a zero energy splitting.

5.5 Transversal magnetic field influence on integer spins

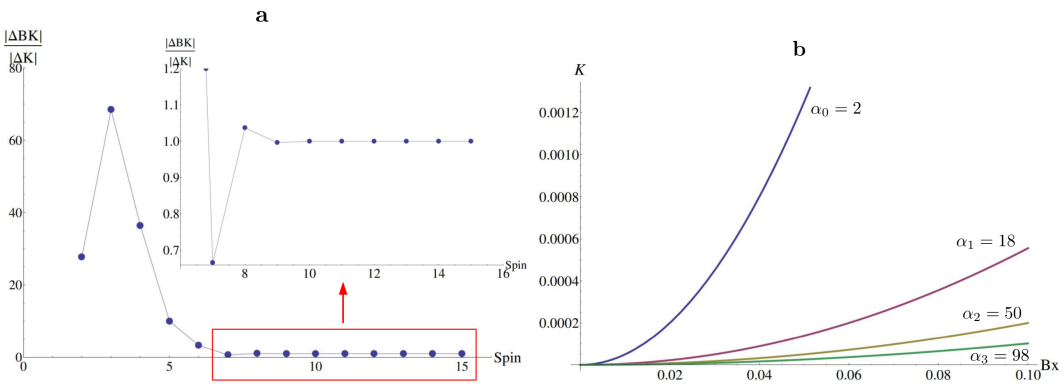

Figure 5.3: The evolution of the ratio Δ_{B_xK}/Δ_K for higher integer spins. **a.)** Here we show the evolution of the Δ_{B_xK}/Δ_K ratio for spin systems from $s = 2$ to $s = 15$. We see that for the same parameter set of B_x[meV], K[meV] and K_z[meV] the ratio increases to spins $s = 3$ until it decreases and oscillates asymptotically against one. Used parameters in figure 4a: $B_x = 0.1$ [meV] $K = 0.0002$ [meV] and $K_z = 1$ [meV]. **b.)** Here we show a plot of Eq.(5.16) ((blue, pink, yellow and red curves)), which defines the parameters B_x[meV] and K[meV] for $K_z = 1$[meV] where we obtain a $\Delta_{B_xK}/\Delta_K = 1$ ratio for higher integer spins. The curves separate areas, where we obtain $\Delta_{B_xK}/\Delta_K = 1$ ratios (curves) and where we obtain $\Delta_{B_xK}/\Delta_K \neq 1$ ratios (white areas between the curves).

The derivation of Eq.(5.3) and Eq.(5.4) enabled us to analyze the influence of the transversal magnetic field on the energy splitting of the ground doublet, for larger integer quantum spin systems, from another perspective. Our main concern related with Eq.(5.3) is to present conditions for obtaining a significant contribution of the transversal magnetic field to the quantum spin tunneling for integer spins. Figure 5.3a and 5.3b show an interesting property of the ratio Δ_{B_xK}/Δ_K for several integer spin quantum numbers and for a positive K. In

figure 5.3a, where we used a transversal magnetic field energy of $B_x = 0.1$[meV] ($H_x = 1.7$[T]) and a transversal anisotropy energy of $K = 0.0002$[meV] which is approximately three orders of magnitudes smaller than B_x, we see an increase of the ratio Δ_{B_xK}/Δ_K up to a spin of $s = 3$. After $s = 3$ the ratio decreases until it oscillates asymptotically against one ($\lim_{s\to\infty} = 1$). This behaviour is very fascinating because it indicates that for this set of parameters the contribution of the transversal magnetic field to the energy splitting is equal to the contribution of the transversal anisotropy. In figure 5.4 we show a situation,

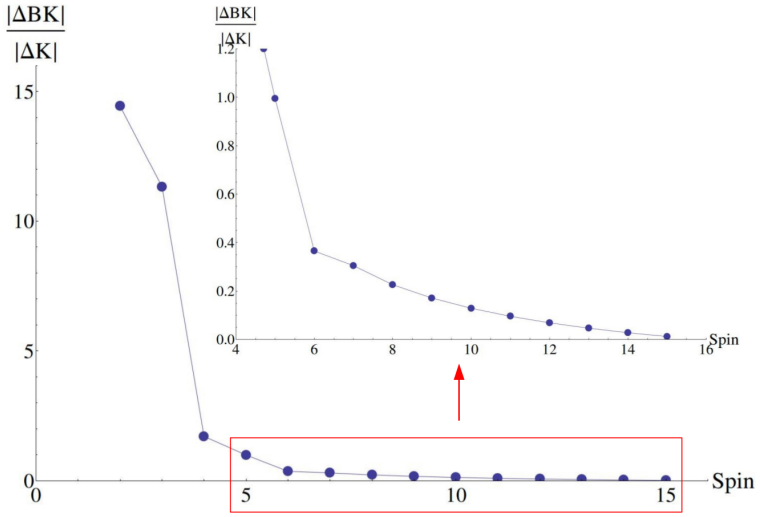

Figure 5.4: The evolution of the ratio Δ_{B_xK}/Δ_K for higher integer spins. Here we show the evolution of the Δ_{B_xK}/Δ_K ratio for spin systems from $s = 2$ to $s = 15$. In this figure we demonstrate the more prominent situation where for constant parameters B_x, K and K_z the ratio Δ_{B_xK}/Δ_K is decreasing with increasing quantum spin number s. Parameters used in figure C1: $B_x = 0.1$ [meV] ($H_x = 1.75$[T]), $K = 0.00077$ [meV] and $K_z = 1$ [meV].

which occurs for most parameters B_x, K, and K_z, where the ratio Δ_{B_xK}/Δ_K is decreasing with increasing spin quantum number until the influence of the transversal magnetic field (Δ_{B_xK}) on the energy splitting becomes negligible in contrast to that of transversal anisotropy (Δ_K).

5.5.1 Shared quenching points

Considering that for most parameters B_x, K and K_z within the perturbative regime the ratio Δ_{B_xK}/Δ_K is decreasing with increasing spin quantum number the question arises if the parameter set used in figure 5.3a is a unique one or whether it is a general behaviour for a group of parameters. In order to answer this question we permuted several parameters in Eq.(5.15) until we were able to create a value table of parameters with the property $\Delta_{B_xK}/\Delta_K = 1$ (in the limiting case of large quantum spins).

$$\frac{\Delta_{B_xK}}{\Delta_K} = \frac{\sum_{n=1}^{s-1} B_x^{\beta=2n} \cdot K^{\gamma=s-n} \cdot (-1)^{\gamma} 2^{\gamma} \sum_{j_1=1}^{\beta+1} \ldots \sum_{j_\gamma=j_{\gamma-1}+2}^{\beta+2\gamma-1} \prod_{i=1}^{\gamma} |(E_{s-j_i} - E_{-s})|}{(-1)^s 2^s K^s \prod_{j=1}^{s} |(E_{s-(2j-1)} - E_{-s})|} \tag{5.15}$$

From this value table we were able to set up the following equation, which reproduces the exact values of B_x, K and K_z to obtain a $\Delta_{B_xK}/\Delta_K = 1$ ratio in the limiting case of higher integer spins:

$$\frac{1}{\alpha_m K_z} \cdot B_x^2 = K \tag{5.16}$$

where

$$\begin{aligned} &\alpha_m = 2 + \sum_{n=0}^{m} 16n, \qquad m \in \mathbb{N}_0 \\ &\alpha_m \in [2, 18, 50, 98, 162, ...] \end{aligned} \tag{5.17}$$

The values which satisfy Eq.(5.16) lead to a situation where the contribution to the energy splitting of the mixed Δ_{B_xK} and the pure Δ_K paths are nearly equal in the limiting case of large quantum spins ($\Delta_{B_xK} = -\Delta_K$), as demonstrated in figure 5.3a. Since the pure Δ_{B_x} path is

$$\Delta_{B_x} = -(\Delta_{B_xK} - \Delta_K) \tag{5.18}$$

we obtain a situation where the energy splitting is zero, $\Delta E = 0$. This means that our formula in equation(5.16)generates parameters (B_x, K and K_z) where

we obtain shared quenching points ($\Delta E = 0$) for all quantum spin numbers. This is interesting, because up till now we were solely in the position to calculate quenching points for individual spins, which mostly differ from each other. But now we are able to estimate, the rarely, shared quenching points for all spins, within the huge parameter space of not shared quenching points.
In summary, we found parabolic expressions (Eq.(5.16)), which enable us to estimate values of the transversal magnetic field, the transversal anisotropy and the uniaxial anisotropy where we obtain shared quenching points ($\Delta E = 0$) for all quantum spin numbers.

5.5.2 Negative uniaxial anisotropy K

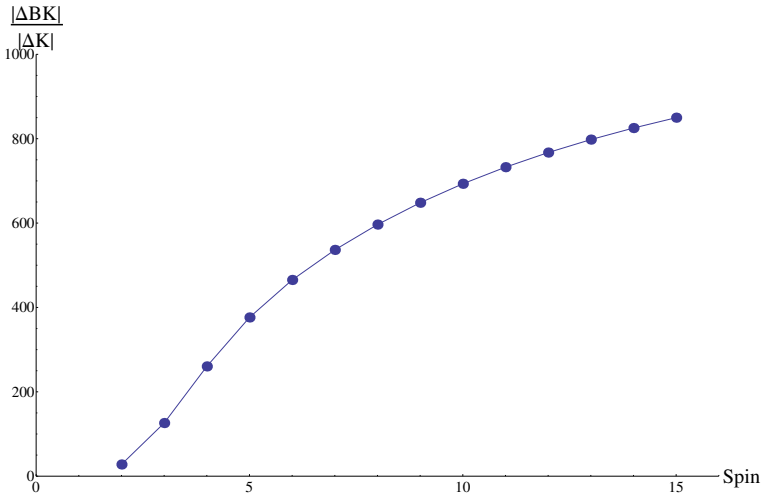

Figure 5.5: Here we show the evolution of the Δ_{B_xK}/Δ_K ratio for spin systems from $s = 2$ to $s = 15$. We see that for the same parameter set of B_x, K and K_z as in figure 5.3, with the sole difference that the transversal anisotropy K is negative, the ratio is constantly increasing with increasing spin quantum number. The asymptotic oscillation against one does not appear. Used parameters: $B_x = 0.1$ [meV] $K = -0.0002$ [meV] and $K_z = 1$ [meV].

The situation changes drastically when the transversal anisotropy energy K is negative (hard axis), because then the series Δ_{B_xK} does not alternate and there are no negative contributions to the energy splitting. The consequence is that the ratio Δ_{B_xK}/Δ_K does not converge to one, which means that the

contribution of the transversal magnetic field on the energy splitting can be orders of magnitude larger than all other contributions for higher integer spins. This is shown in figure 5.5.

5.6 Vanishing of mixed $\Delta_{B_x K}$ paths

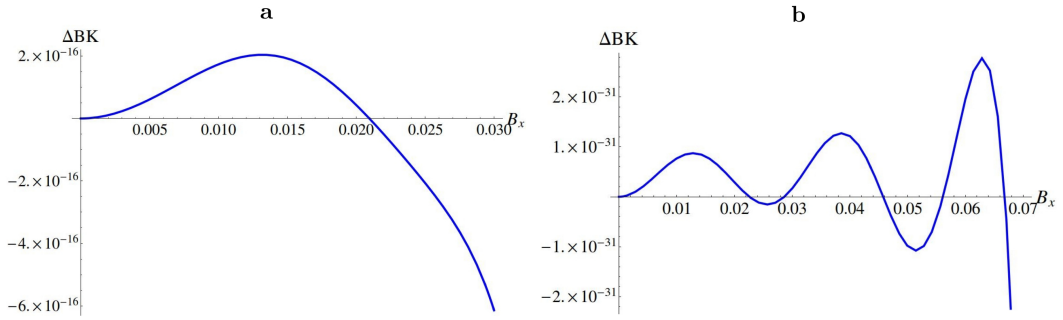

Figure 5.6: Vanishing of mixed $\Delta_{B_x K}$ paths under certain values of B_x. **a.)** Here we show a spin $s = 5$ system, which is the smallest possible system where the vanishing of the mixed $\Delta_{B_x K}$ paths appears. We see that for $B_x = 0.021$[arb.units] the value of $\Delta_{B_x K}$ is zero. Used parameters: spin $s = 5$, $K = 0.01$ [arb.units] and $K_z = 1$ [arb.units]. **b.)** Here we show a spin $s = 13$ system to illustrate the spin quantum number dependence for the number of the vanishing points. We see that the spin $s = 13$ system contains, in contrast to the spin $s = 5$ system, five vanishing points for B_x. Parameters for spin $s = 13$: $K_z = 1$ [arb.units], $K = 0.001$ [arb.units].

Here we want to introduce an effect, which is not described by the quenched tunnel splitting and which was made visible by our perturbative approach. This effect describes a unique situation where no mixing of tunneling paths occurs but instead only pure paths exist. By plotting the $\Delta_{B_x K}$ term against the transversal magnetic field demonstrated in figure 5.6a and 5.6b we see that the mixed $\Delta_{B_x K}$ paths are vanishing under certain values of B_x. In figure 5.6a we show a spin $s = 5$ system, which is the smallest possible system where this effect appears. We see that under the value of $B_x = 0.021$[arb.units], which depends on the parameters of K_z and K, the mixed $\Delta_{B_x K}$ paths are vanishing. The spin $s = 13$ system in figure 5.6b demonstrates that the number of these certain values of B_x, where the mixed $\Delta_{B_x K}$ paths are vanishing, depends on

the spin quantum number. It is important to mention that the number of these B_x values has the tendency to increase with increasing spin quantum number. Moreover, there seems not to be a systematic behind this increase. What we see is that for spin $s = 7$ there are three certain values of B_x, but for spin $s = 8$ only two.

This value differs for each spin and from the values of the quenched tunnel splitting, and leads to a linear combination of two pure paths Δ_{B_x} and Δ_K in Eq.(5.3) for integer spins and to the sole contribution Δ_{B_x} in Eq.(5.4) for the half-integer spins. This leads to the conclusion that in contrast to the quenched tunnel splitting, where the energy splitting is vanishing and so the quantum spin tunneling, here we have a situation where quantum spin tunneling occurs but the influence of the transversal magnetic field is drastically reduced, both for integer and half-integer spins. We can interpret this situation as the destructive interference of the Δ_{B_xK} paths, which occurs because of the alternating series structure for positive K.

5.7 Conclusion

In summary we derived an energy splitting formula of the ground doublet by using a perturbative approach with two perturbations for a Hamiltonian which contains a uniaxial anisotropy, a transversal magnetic field, and a transversal anisotropy. The formula we derived enables a detailed understanding of the quenched tunnel splitting and enables us to estimate exact parabolic equations in which the influence of the transversal magnetic field on the energy splitting is significant for integer spins and a positive K. The situation changes drastically for a negative K, where the contribution of the transversal magnetic field to the energy splitting can be orders of magnitude larger for higher integer spins than the contribution of the transversal anisotropy.

Chapter 6

Magnetisation behaviour of open and closed spin chains

6.1 Open spin chains

Nanomagnets, realized by antiferromagnetically exchange coupled Fe spin chains on a Cu(111) substrate, show in the regime of low external magnetic field B_z a magnetization behaviour, which cannot be explained by theoretical models, using an effective Hamiltonian for the thermodynamic equilibrium [57]. The purpose of this chapter is to analyse if Landau-Zener scenarios are responsible for this phenomenon and further to analyse if an external magnetic field dependence of the magnetic moments of the edge spins is the cause of the experimental observations. Before we explain our approaches we want to describe the system and its unexpected magnetization behaviour in more detail.

The effective Hamiltonian, which describes a system of three or more antiferromagnetically exchange coupled quantum spins on a substrate within an external magnetic field B_z, is:

$$\hat{H} = J \sum_{<i,j>}^{n} \hat{S}_i \otimes \hat{S}_j - B_z \sum_{i=1}^{n} \hat{S}_{z_i} - K_z \sum_{i=1}^{n} \hat{S}_{z_i}^2, \tag{6.1}$$

whereby the dimension of the components of the spin operator is equal to the dimension of the Kronecker product of the single-particle Hilbert spaces:

$$\dim(\hat{S}_x, \hat{S}_y, \hat{S}_z) = \dim(\hat{H}_1 \otimes ... \otimes \hat{H}_n). \tag{6.2}$$

The first term of the Hamiltonian in Eq.(6.1) describes the anti-ferromagnetic exchange interaction, the second term the interaction with the external magnetic field and the last term the uniaxial anisotropy. The competition between the first and the second term of Eq.(6.1) defines the magnetisation curve characteristics. The behaviour of a system described by the Hamiltonian in Eq.(6.1) (with equal magnetic moments) can be generalized as follows:

I.) Within the regime, where the Zeeman energy is dominating, all spins are oriented parallel to each other and are parallel relatively to the magnetic field (saturation).

II.) Reducing the magnetic field energy adiabatically, until the anti-ferromagnetic exchange interaction energy is dominant, leads to an anti-parallel orientation of the spins relative to each other. Due to the linear spin chain geometry, it is energetically favourable for the edge spins to have a parallel orientation relative to the magnetic field, which is obvious by considering the Hamiltonian in Eq.(6.1). The inner spins need to be oriented mostly anti-parallel to each other and relative to the edge spins. Since for spin chains with an even number of spins, the two edge spins cannot be both anti-parallel to the inner spins (if the inner spins should have an anti-parallel orientation to each other), a second configuration exists in order to avoid a preferable configuration. This is shown in figure 6.2b,d.

Now we want to demonstrate graphically what we described previously as the general adiabatic behaviour of a spin chain defined by the Hamiltonian in Eq.(6.1). Figure 6.1 shows a typical magnetisation curve for the Hamiltonian in Eq.(6.1) for a spin quantum number $s = 1/2$ where we used a three quantum spin chain for which we calculated the expectation values $\langle \hat{S}_z \rangle$ by using the stationary Schrödinger equation:

$$\hat{H}|\Psi\rangle = E|\Psi\rangle. \tag{6.3}$$

In order to obtain the eigenvalues and eigenstates we solved the stationary Schrödinger equation for the not explicit time-dependent Hamiltonian in Eq.(6.1) by using exact diagonalization. Hereby we changed the magnetic field B_z adiabatically for each diagonalization iteration. With the knowledge of the

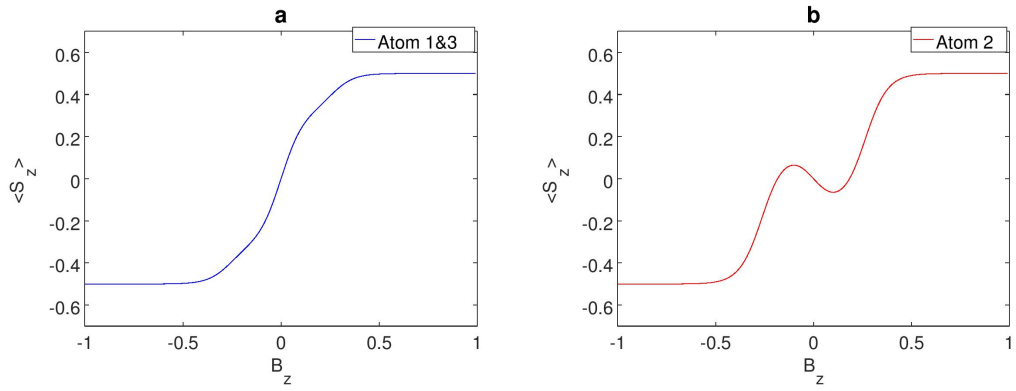

Figure 6.1: Here we show the typical Ising-like magnetization behaviour of a three spin 1/2 chain. **a.)** The magnetization curves for the edge spins are identical. **b.)**The inner spin shows the expected anti-parallel orientation for an antiferromagnetically coupled system.

eigenvalues and eigenstates, for each iteration, we calculated the thermodynamically weighted expectation values by using the Boltzmann statistics:

$$\langle S_{z_j} \rangle = \sum_{i}^{n} p_i \langle \psi_i | \hat{S}_{z_j} | \psi_i \rangle, \qquad p_i = \frac{e^{-E_i/k_B T}}{\sum_{i}^{n} e^{-E_i/k_B T}} \tag{6.4}$$

to obtain magnetisation curves for a system within the thermodynamic equilibrium. The curves in figure 6.1 are consistent with the results of the Ising model. What can be seen in figure 6.1 is that, in the regime of $B_z > 0.5$ [a.u], all three spins are aligned parallel to each other and parallel to the external magnetic field. By reducing the magnetic field adiabatically ($0.0 < B_z < 0.5$ [a.u]) the two edge spins, demonstrated through figure 6.1a, still tend to be oriented parallel to the magnetic field, but the middle spin in figure 6.1b tends to an anti-parallel orientation to the magnetic field and to the edge spins. This kind of behaviour is well known and should be expected in every experiment which is described by the Hamiltonian in Eq.(6.1) (within the thermodynamic equilibrium). So far we described the adiabatic magnetisation behaviour of a quantum spin chain defined by the Hamiltonian in Eq.(6.1). In contrast to this behaviour the results from experimental measurements performed on a Fe chain on a Cu(111) substrate show a different magnetisation behaviour, although the same Hamiltonian like in Eq.(6.1) was assumed. Figure 6.2 shows the measurements, which are inconsistent with the theory. The different behaviour occurs

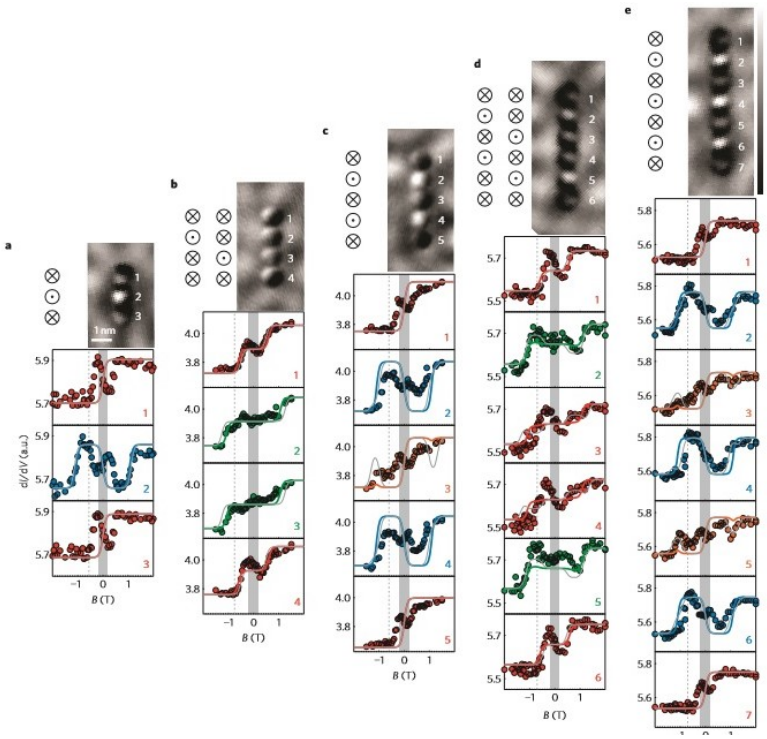

Figure 6.2: Reprinted by permission from nature publishing group (npg). This figure shows the experimental data[57] (dots), which does not fit with the associated Ising-model calculations (lines)

within the regimes of lower magnetic fields B_z, which are highlighted with grey areas in figure 6.2. Especially the three-spin chain system in figure 6.2a, in the regime of lower B_z fields, shows clearly the opposite behaviour to the magnetisation curves derived from theoretical calculations in figure 6.1. Now we want to describe this difference in detail by using the three spin chain example in figure 6.1 and in figure 6.2a. The main difference between the measurements and the theory, by assuming that the Hamiltonian in Eq.(6.1) is valid, is that the average orientation of the edge spins, within the experiment is anti-parallel to the external magnetic field B_z whereby the middle spin is parallel to the magnetic field in the regime of $B_z \approx 0.25$ [T], shown in figure 6.2a. The theory predicts the opposite behaviour, since it is thermodynamically preferable that the edge spins are on average parallel to the magnetic field B_z and the middle spin should be most of the time anti-parallel to the field B_z, if we assume that all magnetic moments within the spin chain are equal (figure 6.1). This circumstance forces us to make the following assumptions:

1.) If the measurements represent the thermodynamic equilibrium state, then it follows that the Hamiltonian in Eq.(6.1) is not complete and we are missing some kind of effect.

2.) If the measurements do not represent the thermodynamic equilibrium state, then we might be dealing with some kind of excited state behaviour, where the Hamiltonian in Eq.(6.1) could be complete or still could be incomplete .

6.1.1 Landau-Zener dynamics on open spin chains

Our first approach is to assume that the Hamiltonian in Eq.(6.1) is complete and that the measurements show some kind of excited magnetization behaviour. In order to model non-equilibrium behaviour in general, we need to decide by what kind of approach such an excited behaviour can be obtained. Since we choose a quantum mechanical description, by using the time-dependent Schroedinger equation, the Landau-Zener scenarios are a possibility to generate transitions from one eigenstate into another eigenstate by sweeping the external magnetic field diabatically. To observe diabatically transitions, within the experiment, two conditions are necessary:

1.) an environment of low temperature
2.) and of low damping.

These conditions are mandatory, because otherwise strong environment effects like a high damping would suppress diabatical transitions by nearly instantaneous relaxations into the "initial eigenstate". Since these conditions are fulfilled within the experiment, we can assume the Landau-Zener transitions as a realistic approach.

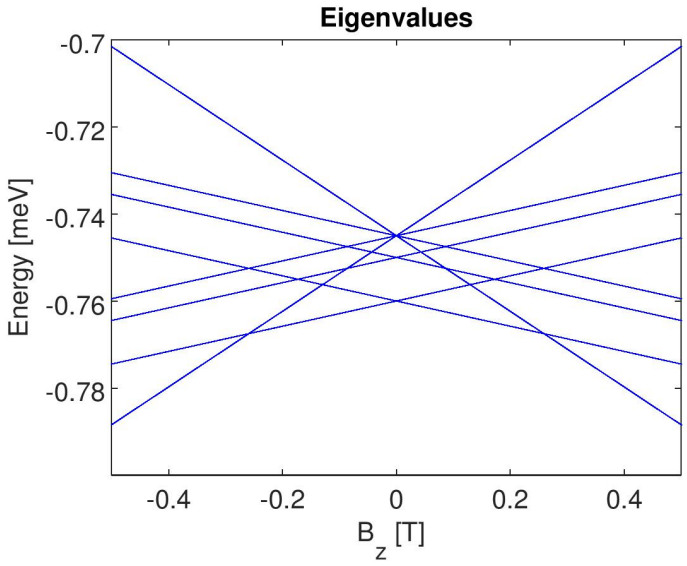

Figure 6.3: Eigenvalues of a three spin 1/2 chain.

6.1.2 Landau-Zener transitions on spin 1/2 chains

The simplest example to start with is an anti-ferromagnetically exchange coupled three spin 1/2 chain. Before we discuss our results we want to analyse the energy landscape of this system shown in figure 6.3. The energy landscape is important in order to locate all possible state transition points. Figure 6.3 shows the eigenvalues of the anti-ferromagnetically exchange coupled three spin 1/2 chain. Since all crossing points in figure 6.3 are not avoided, which means that the energy is degenerated at these locations, it is not possible to obtain diabatical state transitions. Within such a situation the system will not be able to leave the initial eigenstate. In order to obtain transitions from the initial eigenstate into another eigenstate it is necessary to generate avoided level crossing points by including off-diagonal elements in the Hamiltonian, which can be realised for example by a transversal magnetic field. The number and locations of the avoided level crossing points, which are determinated by the interaction term within the Hamiltonian, defines the degree of freedom which we have to generate diabatic eigenstate transitions.

Figure 6.4a shows a situation where a small B_x field is able to avoid the energy degeneration located at $B_z = 0$. To demonstrate an adiabatical case, at the avoided level crossing point at $B_z = 0$, we prepare the system in the initial diabatic state $| \uparrow\uparrow\uparrow \rangle$, which is the energetically lowest state at $B_z = 0.5$ [T].

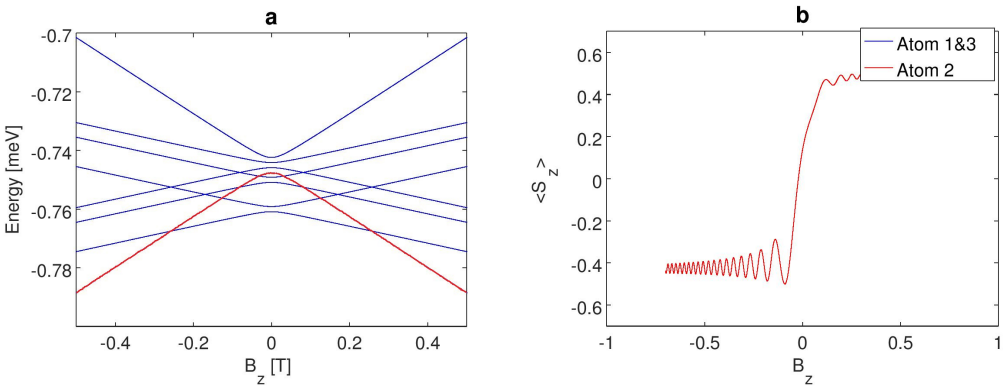

Figure 6.4: Simplest Landau-Zener scenario of an adiabatic behaviour of the three spin 1/2 chain. **a.)** Eigenvalues of the three spin 1/2 chain with an adiabatic passage (red eigenvalue). The system remains in the initial eigenstate. **b.)**The adiabatic passage leads to a spin flip, from $\left|1/2\right\rangle$ to $\left|-1/2\right\rangle$.

By changing the external magnetic field B_z adiabatically the system remains in its eigenstate and thus undergoes a transition of the initial spin orientations to the diabatic state $\left|\downarrow\downarrow\downarrow\right\rangle$, shown in figure 6.4b. Since the magnetization curves in figure 6.4b, calculated by solving the time-dependent Schroedinger equation with the classical Runge-Kutta method, does not look like the magnetization curves in figure 6.1, obtained by the Boltzmann statistics in Eq.(6.4), we can assume that the off-diagonal elements caused by the transversal magnetic field is not sufficient to create a situation like the theory predicted magnetisation curves in figure 6.1 nor the experimental measurements in figure 6.2a. It follows that we need to create additional avoided level crossing points, in order to obtain more diabatic state transition possibilities. An option to generate additional avoided level crossing points in figure 6.4a is to use an anisotropic exchange interaction. Figure 6.5a shows clearly that by applying an anisotropic exchange interaction, further avoided level crossing points occur.

Preparing the system in a $\left|\uparrow\uparrow\uparrow\right\rangle$ diabatic state and changing the external magnetic field B_z adiabatically, shown in figure 6.5b, leads to qualitative similar magnetization curves like in figure 6.1a,b (which are generated by applying the Boltzmann distribution on the expectation values). This result shows that we succeeded in creating conditions to generate a pure quantum mechanical magnetisation behaviour which is similar to the thermodynamic statistical one.

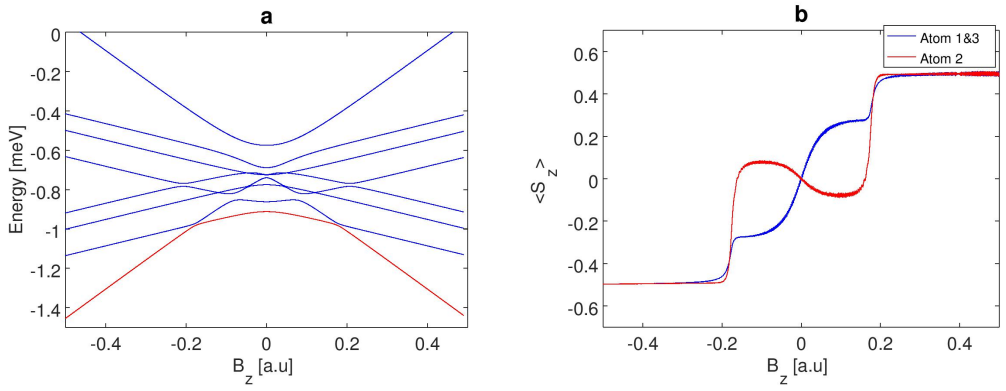

Figure 6.5: Adiabatic behaviour of the three spin 1/2 chain, with additional avoided level crossings. **a.)** Eigenvalues of the three spin 1/2 chain with an adiabatic passage (red eigenvalue). **b.)**The adiabatic passage leads to a magnetization behaviour similar to the behaviour of the Ising-like model calculation from the experimental data.

This justifies the efforts to manipulate the avoided crossing points further in order to approximate the magnetisation curves from the experiment, shown in figure 6.2.

Based on the energy landscape in figure 6.5a we modify the parameters until the first avoided level crossing gap is small enough that the system behaves diabatically at this region. This means that the system does not have enough time, during the magnetic field sweep, to remain in the initial eigenstate and execute a transition to another eigenstate, which is from a thermodynamical perspective unfavourable. Further we have to ensure that the second and third energy gap is wide enough for an adiabatic behaviour. Figure 6.6 shows a configuration where the system, at the first energy gap, behaves diabatically and at the second and third energy gab adiabatically relative to a certain magnetic field sweep time. The corresponding expectation values, for the red marked energy progression (energy path) from our dynamical calculations in figure 6.6, are shown in figure 6.7a and 6.7b. By comparing the curves from the experiment in figure 6.2a with the expectation values from figure 6.7a it is evident that the magnetization behaviour of the first and third spins (atoms) from our calculation is qualitatively similar to the first and third spins from the experiment, which is desirable. However, the second (middle) spin from

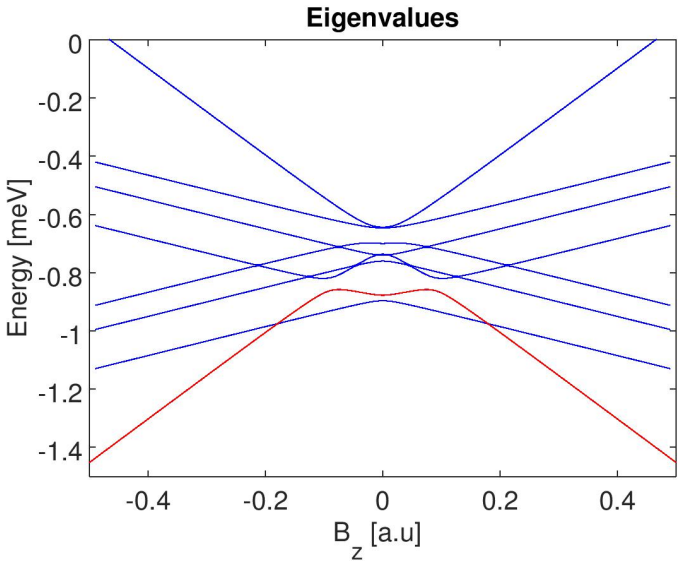

Figure 6.6: Eigenvalues of a three spin 1/2 chain, with a diabatic and adiabatic magnetization behaviour. During the first very small avoided level crossing the system undergoes a diabatic state transition, from the initial eigenstate to another eigenstate. At the next, much wider, avoided level crossing the system behaves adiabatically and remains in the new eigenstate. At the last small avoided level crossing the system undergoes again a diabatic state transition, but now from the new eigenstate back to the previous initial eigenstate (red eigenvalue).

the experiment and from our dynamical calculation shows a notably different magnetization behaviour.

Unfortunately, all other configurations which we tried out in order to generate new energy paths in figure 6.7a, like other initial eigenstates or by changing adiabatic and diabatic locations within the energy landscape, led to a disagreement between the experimental results and our calculations. Since we did not succeed in approximating the magnetization curves from the experiment with a spin 1/2 chain, we moved to a spin 3/2 system. A higher quantum spin number goes along with more degrees of freedom, especially for an interacting many-particle system. In our case we start with an antiferromagnetically exchange coupled three spin 3/2 chain, described by the Hamiltonian in Eq.(6.1). Compared to the 8 eigenstates from the previous spin 1/2 system, the spin 3/2

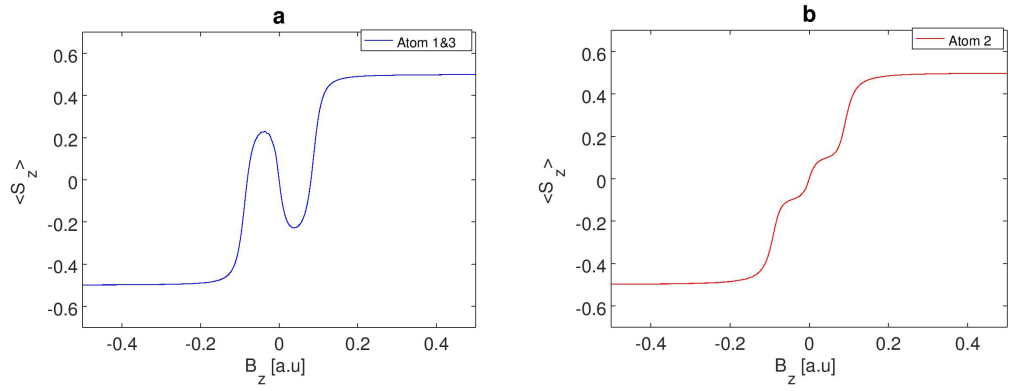

Figure 6.7: Diabatic and adiabatic magnetization behaviour of a three spin 1/2 chain, with eigenvalues shown in figure 6.6. **a.)** Here we see that the magnetization curves of the edge spins agree very good with the magnetization behaviour of the edge spins of the experimental data in figure 6.2a. **b.)** Unfortunately, the inner spin shows a completely different behaviour relative to the experimental behaviour.

chain possesses 64 eigenvalues and eigenstates which enables much more possibilities to generate several energy paths. Unfortunately, we see similar results like we obtained for the spin 1/2 case. The first spin and the last one of the three spin 3/2 chain system show a good agreement with the experimental results, but the middle spin shows a strongly divergent behaviour relative to the measurements, similar to the spin 1/2 case in figure 6.7. Spin 5/2 systems do not change the situation which we had for the spin 1/2 and spin 3/2 cases.

6.1.3 Conclusion

We show that the Landau-Zener scenario is not able to reproduce magnetizantion curves from the experimental data. We were able to reproduce the correct behaviour of the edge spins but not of the inner spins. Other approaches, for example the implementation of a DM-interaction, or a biquadratic exchange interaction in the Hamiltonian were not successful either.

6.1.4 External magnetic field dependent magnetic moments of the edge spins

Our second approach is related to the following assumption: If the measurements represent the thermodynamic equilibrium state, then it follows that the Hamiltonian in Eq.(6.1) is not complete and we are missing some kind of effect. Here, we assume an external magnetic field B_z dependence of the magnetic moments $\mu_s(B_z(t))$ of the edge spins:

$$\begin{aligned}\hat{H} &= \mu_s(B_z(t))J\hat{S}_1 \otimes \hat{S}_2 + \mu_s(B_z(t))J\hat{S}_{n-1} \otimes \hat{S}_n + J\Big(\sum_{<i+1,j+1>}^{n-1} \hat{S}_i \otimes \hat{S}_j\Big) \\ &- \mu_s(B_z(t))B_z\hat{S}_{z_1} - \mu_s(B_z(t))B_z\hat{S}_{z_n} - B_z\Big(\sum_{i=2}^{n-1}\hat{S}_{z_i}\Big) \\ &- \mu_s(B_z(t))K_z\hat{S}^2_{z_1} - \mu_s(B_z(t))K_z\hat{S}^2_{z_n} - K_z\Big(\sum_{i=2}^{n-1}\hat{S}^2_{z_i}\Big).\end{aligned} \tag{6.5}$$

The field B_z dependent magnetic moments $\mu_s(B_z)$ are given by

$$\mu_s(B_z(t)) = \mu_s - \frac{B_z(t)}{|B_z(t)|}\beta \cdot e^{\gamma\left(B_z - B_z(t)\frac{B_z(t)}{|B_z(t)|}\right)}, \tag{6.6}$$

where β and γ are tuning parameters. The indirect time-dependent magnetic

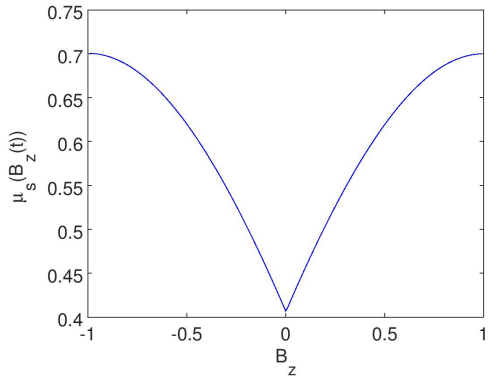

Figure 6.8: Evolution of the magnetic moments $\mu_s(B_z(t))$ of the edge spins for a three spin 1/2 chain.

moments $\mu_s(B_z(t))$ of the edge spins decrease with decreasing external magnetic field $B_z(t)$. The slope of the magnetic moment increases with decreasing

external magnetic field, which is shown in figure 6.8. The Boltzmann weighted expectation values of the eigenstates of the Hamiltonian in Eq.(6.5), for a three spin 1/2 chain, with a time-dependent external magnetic field $B_z(t)$ are shown in figure 6.9. We see that all three spins reproduce the experimental data well. Since we succeeded for a three spin 1/2 chain, we tested the same procedure

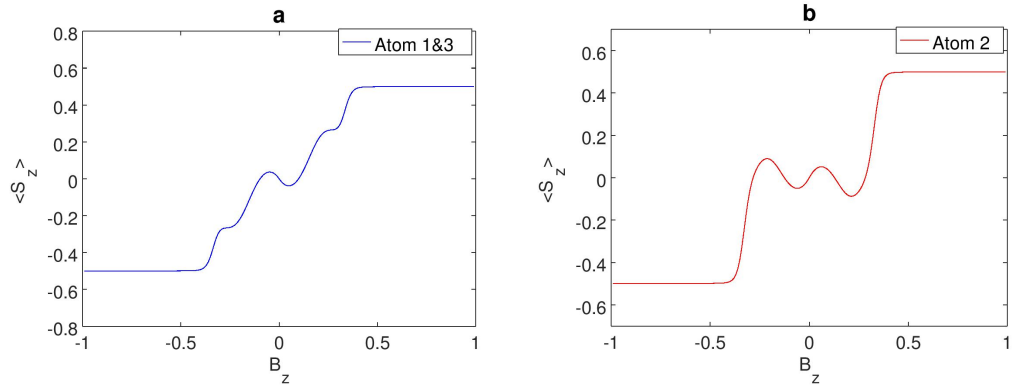

Figure 6.9: Magnetization curves created with magnetic field dependent magnetic moments $\mu_s(B_z(t))$ for a three spin 1/2 chain. **a.)** The magnetization behaviour of the edge spins are in good agreement with the experimental data. **b.)** The inner spin is in good agreement with the experimental data too.

for a four and five spin 1/2 chain, with results, which are in good agreement with the experimental data. The five spin 1/2 chain case is shown in figure 6.10. Similar to the three spin 1/2 chain case, we see in figure 6.10b,c,d a good agreement with the five spin chain from the experiment. In summary, we succeded to reproduce the experimental results for the spin 1/2 case (for three, four, and five spins) by reducing the magnetic moments, constantly with the external magnetic field, solely for the edge spins. Since we succeeded to reproduce the magnetization curves from the experiment, we tried the whole concept on a spin 3/2 system instead of the already good working spin 1/2 system. We found that the results from the spin 3/2 system reproduce the experimental results from figure 6.2 much better than the calculations with a spin 1/2 system. The very good agreement for the spin 3/2 case is shown in figure 6.11a,b for a system of three spin 3/2 chains. In figure 6.12 we show the corresponding evolution of the magnetic moments $\mu_s(B_z(t))$ of the edge spins. Up till now we were able to reproduce the magnetization curves from the experiment by assuming a magnetic field dependent magnetic moment $\mu_s(B_z(t))$

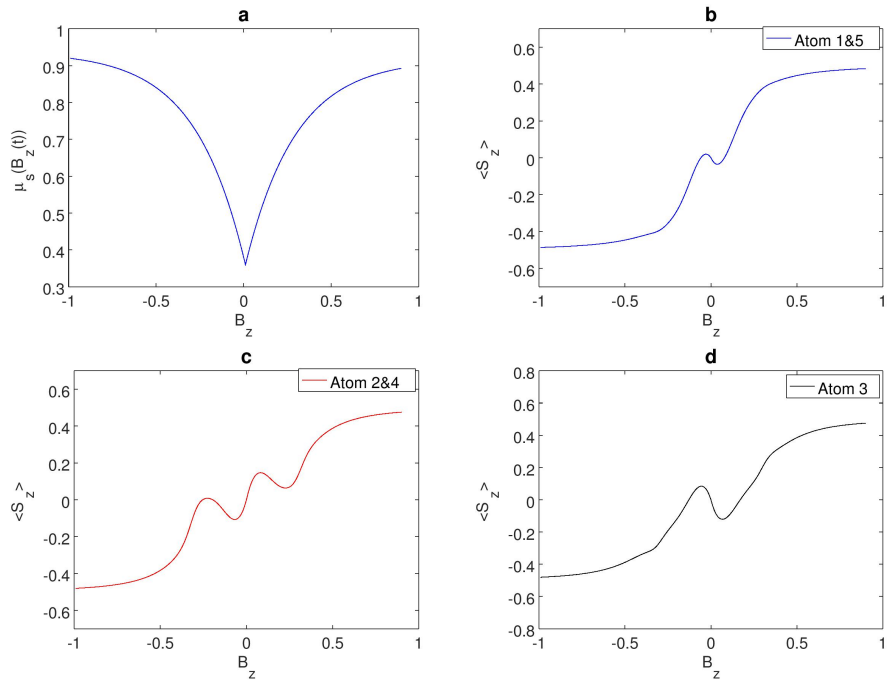

Figure 6.10: Magnetization curves created with magnetic field dependent magnetic moments $\mu_s(B_z(t))$ for a five spin 1/2 chain. **a.)** Evolution of the magnetic moments $\mu_s(B_z(t))$ of the edge spins for a five spin 1/2 chain. **b.)** The magnetization behaviour of the edge spins are in good agreement with the experimental data. **c.)** The inner spins are in good agreement with the experimental data too. **d.)** The middle spin is also in good agreement with the experimental data.

of the edge spins. Now the question arises what kind of physical effect can cause such a dependence. Unfortunately, we can only speculate now. Our idea is that the external magnetic field induces an opposing magnetic field within the substrate, which indeed should happen, because Cu(111) is diamagnetic. The opposing magnetic field is very low compared to the external field, and saturates already at a very weak external magnetic field. Our assumption is that this opposite magnetic field might shield the magnetic moments of the Fe spin chains, and since the edge spins are much more exposed to the surrounding Cu atoms, which generates the opposite magnetic field, the shielding should be stronger than for the inner spins. We further assume that the shielding of the magnetic moments depends on the strength of the external magnetic field, because we expect that for high external magnetic fields the opposite field

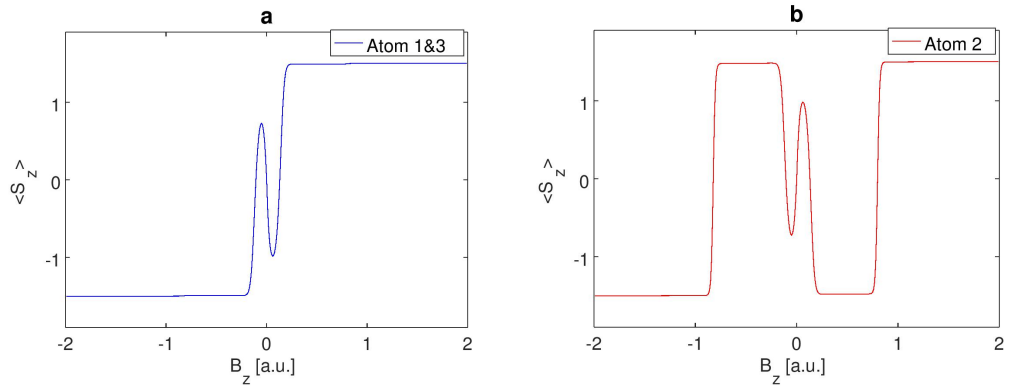

Figure 6.11: Magnetization curves created with magnetic field dependent magnetic moments $\mu_s(B_z(t))$ for a three spin 3/2 chain. **a.)** The magnetization behaviour of the edge spins are in a much better agreement with the experimental data than for the spin 1/2 calculations. **b.)** The inner spin also is in a better agreement with the experimental data.

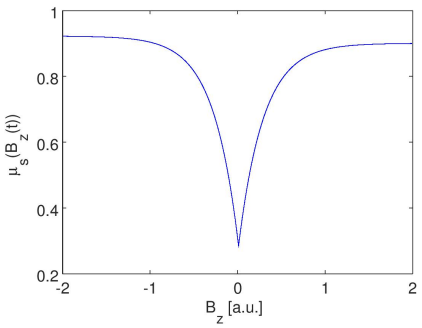

Figure 6.12: Evolution of the magnetic moments $\mu_s(B_z(t))$ of the edge spins for a three spin 3/2 chain.

is suppressed (stronger magnetic field lines tend to displace weaker magnetic field lines). Only when the external magnetic field is weak enough that it cannot suppress the opposite magnetic field (which at the same time needs to be strong enough in order to induce it to saturation) we can observe the decrease of the magnetic moments of the Fe atoms (especially the edge spins of the Fe chain) with a decrease of the external magnetic field. In order to model such a situation we chose a mathematical expression for the dependence, which is presented in Eq.(6.6). The decrease of the magnetic moments, in particular of the edge spins, leads to a point where it is energetically more favourable to inverse the spin configuration, relative to the configuration which is expected

for an Ising-like model which deals with constant magnetic moments.

6.1.5 Conclusion

We investigated the possibility of external magnetic field dependent magnetic moments of the edge spins in order to explain the experimental data. We analyse configurations of three, four, and five spin 1/2 chains and found good agreement with the magnetization behaviour from the experiment. Further, we analysed a three spin 3/2 configuration and found that this configuration reproduces the experimental data much better than the spin 1/2 counterpart.

6.2 Closed spin chains: Non-collinear metastable states

This chapter is an extract from the publication:

S. Castillo-Sepúlveda, R. A. Escobar, and D. Altbir, M. Krizanac, and E. Y. Vedmedenko, Phys. Rev. B **96** 024426 (2017).

Our main contributions are the chapters "Analytical calculation of the lowest excited states" and "Analytical calculation of the free energy".

6.2.1 Introduction

In addition to open linear chains [56, 57, 58], we studied stationary equilibrium magnetic configurations formed by effective magnetic moments of closed magnetic chains with uniaxial anisotropy coupled with antiferromagnetic exchange and dipolar interactions. Such ring structures with different anisotropy axes can be experimentally prepared [59, 60, 61, 62, 63, 64, 65, 66, 67]. The main objective is to identify which kind of magnetic states, different from the collinear ground states, can be stabilized. We show that there are many stable stationary states and that these states correspond to the non-collinear spin spirals for vanishing anisotropy or to kink solitons for high magnetic anisotropy. Particularly, the non-collinear Möbius magnetic state can be stabilized at finite temperatures in non-frustrated rings or other closed shapes with an even number of sites without the Dzyaloshinskii-Moriya interaction.

6.2.2 Analytical calculation of the ground state

We use an atomistic Heisenberg-like model in our calculations. Each atom is represented by a magnetic moment $\vec{\mu}_i = \mu_s \cdot \vec{S}_i$, with $\mu_s = 2.2\mu_B$, where $\vec{S}_i$ is the unit and dimensionless vector parallel to $\vec{\mu}_i$.

$$H = \sum_{i \neq j} \left(DE_{ij} - J_{ij} \vec{S}_i \cdot \vec{S}_j \right) - K \sum_i \left(\vec{S}_i \cdot \hat{z} \right)^2, \tag{6.7}$$

where E_{ij} is the dipolar energy given by

$$E_{ij} = \omega \frac{\vec{S}_i \cdot \vec{S}_j - 3(\hat{n}_{ij} \cdot \vec{S}_i)(\hat{n}_{ij} \cdot \vec{S}_j)}{r_{ij}^3}, \tag{6.8}$$

with $r_{ij} = |\vec{r}_i - \vec{r}_j|$, $\hat{n}_{ij} = (\vec{r}_j - \vec{r}_i)/r_{ij}$, and $\omega = \mu_0 \mu_s^2 / 4\pi$, with μ_0 the magnetic permeability in the vacuum. In these expressions D is a constant that allows to turn on or off the dipolar interaction by taking the values 1 or 0, and is dimensionless. The exchange interaction constant J_{ij} is defined solely for nearest-neighbour moments.

In the following S. Castillo-Sepúlveda, R. A. Escobar, and D. Altbir calculated energies of the pure antiferromagnetic (AFM) state, the antiferromagnetic spin spiral (AFSS) configuration, and the antiferromagnetic (AFM) domains with kink-like solitons (KS) in between (see Figure). By considering a closed chain with N magnetic moments, a KS contains M magnetic moments, whereby $M < N$. It follows that the AFM region is formed by $(N - M)$ magnetic moments. The internal energy is then given by contributions from the kink solitons and the antiferromagnetic domains.

The first case which S. Castillo-Sepúlveda, R. A. Escobar, and D. Altbir discussed is the situation with $M = N$. The spatial dependence of magnetization of such an AFSS configuration can be described as

$$\begin{aligned} \vec{S}(i, \Delta\theta_k^{(N)}) &= \vec{S}_x(i, \Delta\theta_k^{(N)}) + \vec{S}_z(i, \Delta\theta_k^{(N)}) \\ \vec{S}_x(i, \Delta\theta_k^{(N)}) &= \sin\big((i-1)\Delta\theta_k^{(N)}\big)\hat{x}, \\ \vec{S}_z(i, \Delta\theta_k^{(N)}) &= \cos\big((i-1)\Delta\theta_k^{(N)}\big)\hat{z}, \end{aligned} \tag{6.9}$$

where i defines the coordinate along the ring and $\Delta\theta_k^{(N)}$ is the angle between two neighbouring moments. In order to obtain periodic boundary conditions $\vec{S}(1, \Delta\theta_k^{(N)}) = \vec{S}(N+1, \Delta\theta_k^{(N)})$, it is necessary that $\Delta\theta_k^{(N)} = 2\pi k/N$, with k an integer value between 1 and $N - 1$. The energy of the system is defined by

$$E(\Delta\theta_k^{(N)}) = \sum_{i=1}^{N} \vec{S}(i, \Delta\theta_k^{(N)}) \cdot \vec{S}(i+1, \Delta\theta_k^{(N)}) - K \sum_{i=1}^{N} S_z^2. \tag{6.10}$$

By inserting Eq.(6.9) in Eq.(6.10) it follows

$$E(\Delta\theta_k^{(N)}) = -JN\cos(\Delta\theta_k^{(N)}) - K \sum_{i=1}^{N} \cos^2\big((i-1)\Delta\theta_k^{(N)}\big). \tag{6.11}$$

Minimizing Eq.(6.16) leads to

$$\frac{dE(\Delta\theta_k^{(N)})}{d\Delta\theta_k^{(N)}} = JN\sin(\Delta\theta_k^{(N)}) + 2K\sum_{i=1}^{N}\Big((i-1)\cos^2\big((i-1)\Delta\theta_k^{(N)}\big) \cdot \sin^2\big((i-1)\Delta\theta_k^{(N)}\big)\Big) = 0. \tag{6.12}$$

From the solutions of Eq.(6.12) S. Castillo-Sepúlveda, R. A. Escobar, and D. Altbir obtained energy expressions for even N and for odd N. For even N the energy is given by

$$E = -N(K-J), \tag{6.13}$$

and for odd N the minimum energy is

$$E = JN\cos(\pi/N) - K\sum_{i=1}^{N}\cos^2\big((i-1)\pi/N\big). \tag{6.14}$$

In figure 6.13 they plotted Eq.(6.13) and Eq.(6.14) for even and odd N.

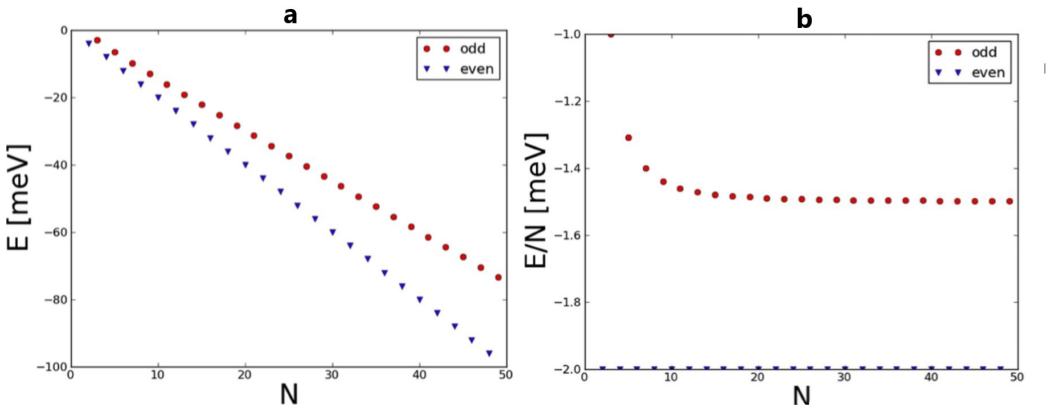

Figure 6.13: Reprinted by permission from APS physics. (a) Internal energy of a pure AFSS state for even and odd number of magnetic moments N when $K = -J = 1$ meV. When N is even, the AFSS state is identical to the AFM state. (b) Internal energy normalized by N for the same parameters used in (a). They observed that if N increases, the difference $|E_N/N - E_{N+1}/(N+1)|$ converges to 0.502 meV. We see that the AFSS state for odd number of magnetic moments is not the minimum of the energy.

We can conclude that for low anisotropies ($|K| < |J|$) and $D = 0$, the lowest

energy state for even N corresponds to an AFM configuration, which is equivalent to an AFSS with $\Delta\theta = \pi$. Any other kind of AFSS possesses higher energy. The total energy of an AFSS in a chain with an odd number of sites is always larger than that of the closest chain with an even number of moments. The larger the length of those two chains, the more pronounced the total energy difference despite the almost identical length (± 1) as seen in Fig. 6.13. This effect occurs due to the frustration inherent to odd chains. Thus, longer chains exhibit a higher degree of frustration, so it follows that their energy is larger as compared to a chain with an even number of spins.
In the next step, they calculated the difference ΔE_N between the energy of an AFSS state $[E(AFSS_M^N)]$ and a KS state $[E(KS_N)]$ as a function of kink soliton length M. By minimizing Eq.(6.16) for the AFSS state and for the KS state they obtained the following expression for the difference ΔE_N for the case of odd N (number of magnetic moments) and odd M (kink soliton length):

$$\begin{aligned} &\Delta E = \kappa(N) - \kappa(M) \\ &\kappa(x) = -Jx\big(1 - \cos(\pi/x)\big) - K\sum_{i=1}^{x} \cos^2\big((i-1)\pi/x\big) + Kx. \end{aligned} \tag{6.15}$$

If $\Delta E < 0$ then the lowest energy state is the AFSS, while if $\Delta E > 0$, the lower energy corresponds to a KS state. Figure 6.14 shows the results of Eq.(6.15) for several anisotropy K values. They observed that larger anisotropy values K are associated with smaller kink solitons.

The case for even N and even M as well as even N and odd M leads to an energy which is the same as for the full AFM state,

$$E = -N(K - J). \tag{6.16}$$

This leads to the conclusion that the ground state of rings with an even number of constituents is an AFM configuration, while that of rings consisting of an odd number of magnetic moments corresponds to the KS configuration. Herewith S. Castillo-Sepúlveda, R. A. Escobar, and D. Altbir have shown that in closed rings with an odd number of particles the KS is the stable magnetic

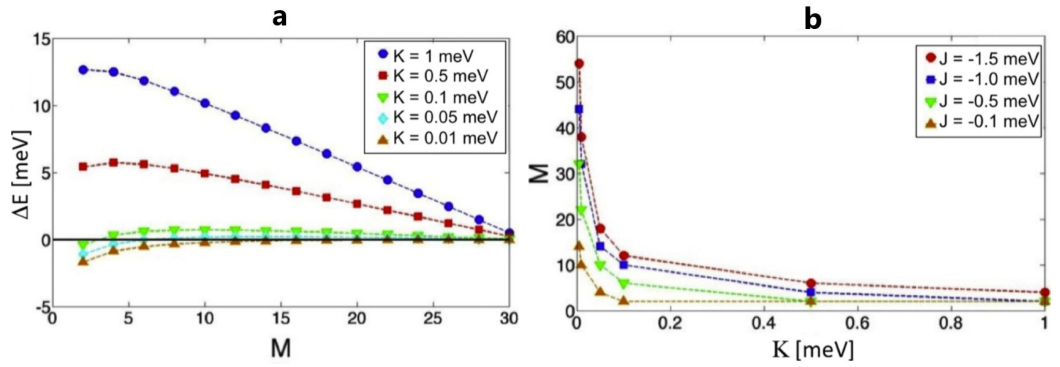

Figure 6.14: Reprinted by permission from APS physics. (a) Difference between the internal energies of the AFSS and KS states for $N = 31$, $J = 1$ meV, and different values for K. $\Delta E > 0$ indicates that a knot is present. (b) Size of a kink soliton (knot) as function of the anisotropy for $N = 31$.

configuration. The ground state of closed rings with an even number of spins is an ideal AFM configuration.

6.2.3 Analytical calculation of the lowest excited states

Here, we analyze the lowest excited configurations of rings, defined by Eq.(6.7) for $D = 0$, with an even number of spins. The lowest excited metastable configurations of non-collinear spin spirals can be observed in the phase space[68]. An example of such a phase space is given in Fig. 6.15a for a chain consisting of four magnetic moments subject to a uniaxial anisotropy and the exchange interaction $J < 0$. This example concerns the case of an AFSS with the angle $\Delta\theta \subset [0, \pi]$ between nearest-neighboring spins. Only the angle between the first and the last spins in a chain can differ from $\Delta\theta$ if $N\Delta\theta/\pi$ is not integer. The abscissa gives the polar spherical angle θ_1 of the first spin with respect to the z-axis. The spiral is two-dimensional, i.e., the four spins have the following S_z components: $\cos(\theta_1)$, $\cos(\theta_1 + \Delta\theta)$, $\cos(\theta_1 + 2\Delta\theta)$, and $\cos(\theta_1 + 3\Delta\theta)$. In this simplest possible case the three non-trivial periodic configurations correspond to $\Delta\theta = \pi/4$, $\pi/2$, $3\pi/4$ defining π, 2π, 3π magnetization rotations along a chain, respectively. For $|K| \gg |J|$, these configurations correspond to the band of low-energy saddle points as seen in Fig. 4(a). Additionally, there are 12 local energy minima [blue in Fig. 6.15a]. Six of them (dark blue) corre-

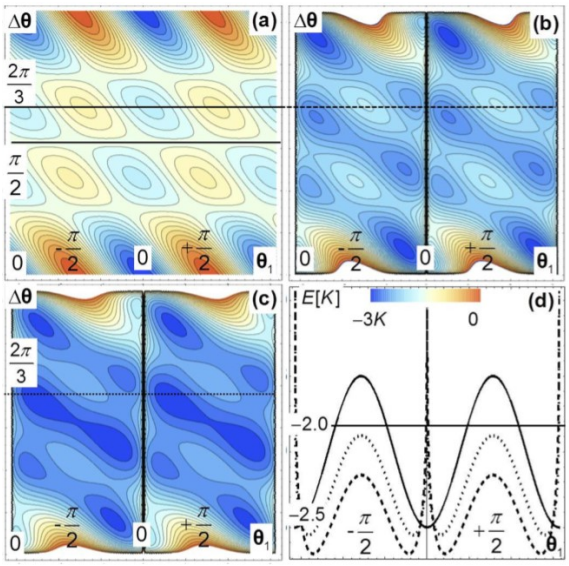

Figure 6.15: Reprinted by permission from APS physics. Analytical calculation of the internal (a) and Gibbs free energy (b)-(d) of the four effective magnetic moments coupled by nearest-neighbor exchange interaction J and subject to uniaxial anisotropy K for $|K| \gg |J|$. $\Delta\theta$ is the angle between the nearest-neighboring spins, while θ_1 is the absolute polar spherical angle of the first spin. The color scheme goes from dark blue (dark gray) for low energies to light (light gray) for high energies. Panel (a) shows the internal energy map in the $\theta_1 - \Delta\theta$ coordinates. (b), (c) Gibbs energy G of the same sample in the same phase space at $k_BT = 0.2$K and $k_BT = 0.35$K, respectively, with K the anisotropy constant (density of states $\rho = 100$). (d) Cross section of the maps (a)-(c) at $\Delta\theta = \pi/2$ and $\Delta\theta = 2\pi/3$. Cross-section line styles correspond to those in (a)-(c).

spond to collinear ground states, but the other six (light blue) to non-collinear metastable configurations with $\Delta\theta = \pi/3$ or $2\pi/3$. Hence, already a very short chain with an even number of magnetic moments at zero temperature can be frozen in a non-collinear state if the anisotropy is high enough. Inclusion of the dipolar coupling enhances this effect.

6.2.4 Analytical calculation of the free energy

In order to study the influence of the finite temperature on these local energy minima the free energy landscape has been calculated analytically. The free

energy can be defined as

$$G = E - TS = E - k_B T \cdot \ln(\Omega_E), \tag{6.17}$$

where E is the internal energy, k_B the Boltzmann constant, S the entropy, and Ω_E the number of states with energy E. For non-collinear states the number of states corresponds to the length of a circle made by the first spin on the surface of a unity sphere: $\Omega_E = \int_0^{2\pi} \rho \cdot \cos(\theta_1) d\theta_1 = 2\pi\rho \cdot \sin(\theta_1)$, where ρ is the number of states per unit radian. The first magnetic moment can have $2\pi\rho\sin(\theta_1)$ orientations, while orientations of other moments for a configuration of an energy E are fixed by the angle $\Delta\theta$ between them and the angle $\theta_1 + n\Delta\theta$ with respect to the z-axis. Figures 6.15b and 6.15c give $G(\theta_1, \Delta\theta)$ for two different temperatures, while Fig. 6.15d shows the cross sections of the energy landscape of Figs. 6.15a-6.15c for vanishing J. The two solid lines in Fig.6.15d correspond to the internal energy of Fig.6.15a. The straight solid line shows the band of saddle points at $\Delta\theta = \pi/2$, while the sine-shaped solid line corresponds to local energy minimum at $\Delta\theta = 2\pi/3$. The dashed and dotted lines correspond to the free energy for $\Delta\theta = 2\pi/3$ and $k_B T = 0.2$K and 0.35K, respectively. The density of states ρ influences the absolute value of the free energy but does not change either positions or shapes of minima and maxima. The total number of local energy minima is directly proportional to the number of sites in a chain. Particularly, the minima appear when $\Delta\theta = 2\pi m/(N-1)$ with integer $m \in [1, N-1]$. Therefore, there are nine local energy minima for the chain consisting of four effective magnetic moments, while their number increases to twelve for the chain of five moments, etc. The inclusion of the dipolar interaction enhances the anisotropy and, therefore, makes the local energy minima deeper. Thus, the number of non-collinear configurations increases for longer chains. The entropy changes the energy landscape significantly and particularly, the entropy of the internal energy minima corresponding to non-collinear configurations is much larger than that of collinear states. As a consequence, the local energy minima at $\theta_1 = 0$ split. The splitting increases with increasing temperature and corresponds to complicated non-collinear magnetic states. Hence, the local minima of the free energy in periodic chains might correspond to AFSS or KS and are very important for the determination of magnetization configurations at finite temperatures. This effect is particularly important if the lifetime of a

metastable state is comparable to or larger than the characteristic time of the measurement. Another interesting observation from Fig. 6.15 is that the local minima of the free energy correspond to the non-homogeneous spin spiral; that is, in one part of the spiral the rotation happens quicker than in another. One can regard such configurations as almost collinear antiferromagnetic domains with knotlike solitons between those described above. Among other things this finding explains why one finds domain walls in antiferromagnetic systems, where the domain walls are energetically unfavourable.

6.2.5 Monte Carlo simulations

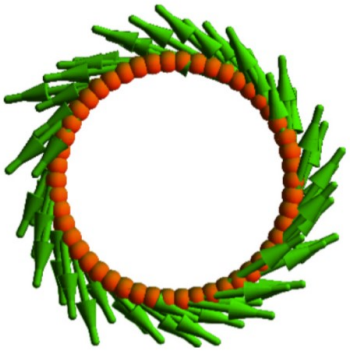

Figure 6.16: Reprinted by permission from APS physics. Equilibrium MC configuration of a chain consisting of 50 moments for $D = 1$, $J = 0$ meV and $K = 0$ meV.

In realistic systems one has to consider three-dimensional Heisenberg spins as well as dipolar interactions. This makes the phase space very complicated and inaccessible by analytical calculations. To check the stability of the described metastable solutions we have performed extended Monte Carlo (MC) simulations of finite magnetic chains of different lengths. Particular attention has been paid to the closed rings consisting of effective magnetic moments coupled by dipolar and antiferromagnetic exchange interactions as well as subject to the on-site uniaxial anisotropy, because in this case an additional aspect of spin parity becomes important. To study the magnetic states of these structures we carried out MC simulations with the Metropolis algorithm under local dynamics and the single spin flip method [69]. Technical aspects of the MC

procedure can be found in [69, 70]. The energy is given by Eq. (4). Since we consider an antiferromagnetic coupling between neighboring sites J values between -0.1 and -40 meV have been explored. This range of values includes systems reported by Savina et al. [71] and references therein. The simulations have been started with a random orientation of magnetic moments. The new orientation of each randomly chosen magnetic moment has been accepted with a Boltzmann probability $p = \min(1, \exp(\Delta E/k_B T))$. The rings were relaxed using a tempered annealing procedure until the equilibrium configuration has been achieved. Relatively low finite temperatures $k_B T \ll |J|$ have been used in the calculations. The number of Monte Carlo steps (MCS) considered in each relaxation process was $3 \cdot 10^7$. To distinguish between effects induced by different energy contributions we started looking for equilibrium states of the system considering the involved energies separately. To analyze the impact of the different variables S. Castillo-Sepúlveda, R. A. Escobar, and D. Altbir looked at the purely dipolar case, that is, $J = K = 0$. In this case, independently of the number of sites in the ring, the magnetic configuration at remanence is a closured-vortex-like state, as illustrated in Fig. 6.16. For $J = 0$ and $D = 0$ two cases can be distinguished: easy z-axis for $K > 0$ and easy xy-plane for $K < 0$. For $K = 0.1$ meV, magnetic moments align themselves parallel to the z-axis, while the orientation of each moment (up or down) is random, as shown in Fig.6.17a. When $K = -0.1$ meV, the ring exhibits an in-plane magnetization. Similarly to the previous case the orientation of each moment in the plane is random, as evidenced in Fig.6.17b. In the purely antiferromagnetic case, that is $K = 0$ and $D = 0$, differences appear when considering rings with odd and even numbers of sites, for example $N = 100$ and $N = 101$. For even N and with no anisotropy and dipolar interaction involved, a perfect antiferromagnetic ordering has been found as shown in Fig.6.18(a). When an additional particle is included, $N = 101$, a knot soliton appears due to geometrical frustration, as shown in Fig. 6.19(a). Hence, the local energy minima described in Fig. 6.17 do not survive in the Monte Carlo simulations, because their life-times are too short and the energy barriers can be easily overcome. Once the role of every contribution to the energy has been analyzed separately, S. Castillo-Sepúlveda, R. A. Escobar, and D. Altbir considered all of them together, that is, $D = 1$, $J = -40$ meV, and $K = \pm 0.4$ meV. For the

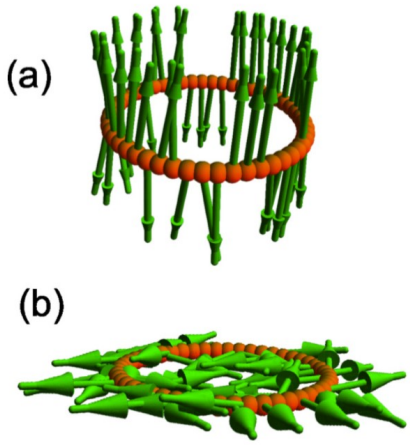

Figure 6.17: Reprinted by permission from APS physics. Equilibrium MC configuration of a chain consisting of 50 moments for $D = 0$, $J = 0$ meV and (a) $K = 0.4$ meV, (b) $K = -0.4$ meV.

sake of generality the chain length has been varied between 10 and 110 sites. Very short chains do not show any particularly surprising results. One finds a perfect AFM alignment for even N, while Möbius configurations for odd N. Depending on the direction of the easy axis two different orientations of KS can be found as shown in Figs. 6.19 and 6.20. These two different types of KS are labeled KN and KB due to the similarity they showed to Néel (see Fig. 6.19) and Bloch walls (see Fig. 6.20), respectively. For $K = 0$, both types of configurations, KB and KN, can be observed. The longer chains with anisotropy, however, show AFSS as equilibrium states for even N. S. Castillo-Sepúlveda, R. A. Escobar, and D. Altbir also observed a relation between the number of knots, number of sites, and anisotropy. For an odd number of sites all rings exhibit knots due to geometrical frustration. Most interestingly, however, they found the Möbius-like structure also in antiferromagnetic rings with an even number of effective moments. When they considered an even number of sites, they saw that larger values of K are needed to observe knots at a lower number of sites. For example, for vanishing K, 100 sites are needed in the ring to observe a first knot, while 80 sites are needed if $K = \pm 0.01J$, and 40 sites are needed for $K = \pm 0.1J$. This means that the local energy minimum becomes significantly populated only at large N. MC simulations have been performed to find the statistical averages by exploring the energy landscape. So, ideally

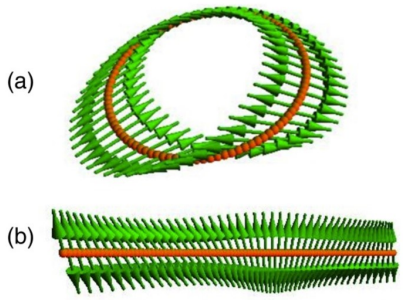

Figure 6.18: Reprinted by permission from APS physics. Equilibrium MC configuration of a chain consisting of 100 moments for $D = 0$, $K = 0$ meV, $J = -40$ meV: (a) closed AFM configuration and (b) the same shown with open ends for clarity.

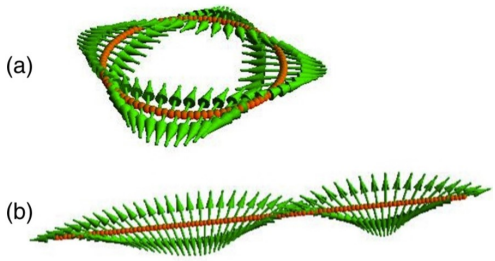

Figure 6.19: Reprinted by permission from APS physics. Equilibrium MC configuration of a chain consisting of 100 moments for $D = 1$, $K = -0.4$ meV, $J = -40$ meV: (a) closed KN configuration and (b) the same shown with open ends for clarity.

at the end of the simulation the averaging over the infinitely long time should result in the exact expectation values for the observables. At low temperatures and for large systems, however, the time scale of simulations is much smaller than the correlation times as S. Castillo-Sepúlveda, R. A. Escobar, and D. Altbir have shown recently [71]. For the reason of insufficient averaging and long lifetimes of the excited states the deepest local minima with the lowest number of knots can be observed in the MC simulations. A typical MC relaxation of a KB state is shown in Fig. 6.21. Monte Carlo steps do not correspond to real time steps and, hence, do not provide us with reliable information on the non-equilibrium dynamics or the real relaxation time. However, it is important to note that the lifetimes of the metastable non-collinear states described in this paper might be finite and, hence, lowest KB or KN configurations might be

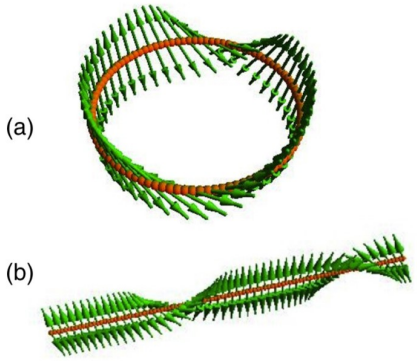

Figure 6.20: Reprinted by permission from APS physics. Equilibrium MC configuration of a chain consisting of 100 moments for $D = 1$, $K = 0.4$ meV ,$J = -40$ meV: (a) closed KB configuration and (b) the same shown with open ends for clarity.

detected experimentally. The investigation of the non-equilibrium dynamics of these metastable spin helices, therefore, would be of great interest. Because the strong anisotropy makes the local minima deeper, the non-collinear states are more easily found for higher anisotropy values. This nicely corresponds to the analytical considerations made above.

6.2.6 Conclusion

To conclude, in this paper we show analytically that closed chains coupled by antiferromagnetic exchange and subject to perpendicular magnetic anisotropy possess local energy minima corresponding to non-collinear topological spin spirals. Analytical analysis of the free energy at finite temperatures for chains with dominating anisotropy has shown that anisotropy increases the depth of the local energy minima. This makes the non-collinear configurations particularly stable for such chains ($|K| \gg |J|$). The large depth of the local energy minima results, in turn, in the increase of the activation energy needed for the relaxation towards the global energy minimum (collinear antiferromagnetic configuration). As the lifetimes of magnetic configurations exponentially depend on the activation energy ΔE ($\tau \propto \exp[\Delta E/k_B T]$) the lifetimes of the non-collinear configurations strongly increase with increasing anisotropy and decreasing temperature. Another important effect concerned with magnetic anisotropy is that with increasing anisotropy the extended spin spirals become

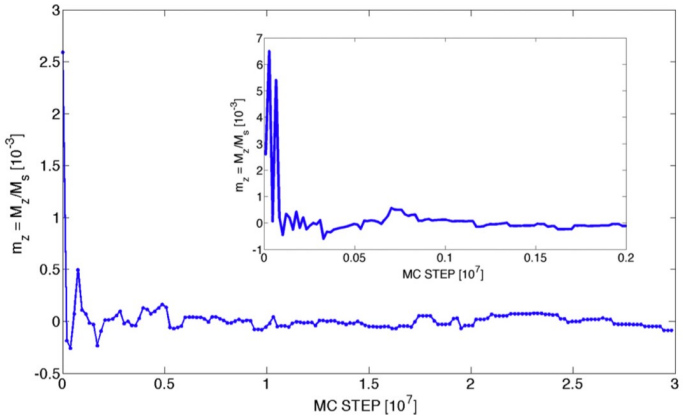

Figure 6.21: Reprinted by permission from APS physics. Typical MC relaxation of a chain consisting of 50 moments with $D = 1$, $K = 0.4$ meV, $J = -40$ meV at $T = 0.0001$K. The inset shows the fast part of the relaxation process. In this case, the magnetic configuration corresponds to the KB configuration.

energetically less favourable than localized kink solitons. Depending on the sign of the anisotropy constant two configurations for the kink soliton are possible: for $K > 0$, a Bloch-like KB soliton is stabilized, while for $K < 0$ a Néel-like KN soliton appears. A similar effect is observed when the dipolar interaction is introduced into the Hamiltonian: first, the dipolar interaction makes the local minima deeper because it induces magnetic anisotropy and, second, it might lead to a transformation of the spin spirals to kink solitons. The number of the local energy minima increases with the number of magnetic moments, because the angle between neighboring magnetic moments for a configuration corresponding to an energy minimum in a spiral equals $\Delta\theta = 2\pi m/(N-1)$. In a kink soliton this relation is more complicated but the tendency is similar. Therefore, increase of the chain length and the anisotropy leads to a complicated energy landscape with multiple local energy minima. Some of these minima are very deep and the lifetimes of corresponding states are large. For that reason the deepest local energy minima become populated also in the Monte Carlo simulations in long closed structures. Particularly interesting is the Möbius antiferromagnetic configurations with an even number of sites in closed chains. While the existence of such a configuration in chains with an odd number of sites has been reported, a similar configuration in chains with an even number of sites was unknown up to now. The non-collinear states can

be found in closed geometry of any shape. Although both methods, analytical calculations and numerical simulations, have been performed independently, they lead to consistent results and allowed us to validate the conclusions from different points of view.

Chapter 7

Summary

In the chapter "Quantum revivals and magnetization tunneling in effective spin systems" we analysed the correlation between the spin precession (quantum revival) and the magnetization tunneling. Particular attention has been given to the non-linear character of the uniaxial anisotropy, which leads to non-harmonic dynamics, when combined with a linear energy term in the Hamiltonian. Our analytical and numerical studies of the quantum dynamics of effective quantum spins have revealed that the quantum revival of expectation values and the total wave-function is identical for integer spin values, but very different for half-integer spins. It has been concluded that the quantum revival time (QRT) doesn't depend on the spin number but only on the spin statistics (integer or half-integer). According to the derived analytical expressions the expectation value revival time (EVRT) is shortest for integer field-anisotropy ratios. As the field can easily be tuned experimentally, and time-dependent measurements have become available in the last years, we hope that this finding will permit a highly precise measurement of magnetic anisotropies. An applied transverse field promotes the magnetization tunneling and it is shown that the EVRT is correlated with the magnetization tunneling.
In chapter "Perturbative calculations of quantum spin tunneling in effective spin systems with a transversal magnetic field and transversal anisotropy" the tunneling behaviour of any effective two-level system has been investigated with the aid of the time-dependent perturbation calculation. We derived an energy splitting formula of the ground doublet by using a perturbative approach with two perturbations for a Hamiltonian which contains a uniaxial

anisotropy, a transversal magnetic field, and a transversal anisotropy. The formula we derived enabled us to estimate an exact parabolic equation in which we obtain shared quenching points ($\Delta E = 0$) for all integer spins.
In chapter "Magnetisation behaviour of open and closed spin chains" we obtained the following results: For open spin chains we studied the magnetization behaviour of anti-ferromagnetically exchange-coupled effective quantum spins with the aim of reproducing experimental results that have been lacking a theoretical explanation so far. We show that the Landau-Zener scenario is not able to reproduce magnetizantion curves from the experimental data. We were able to reproduce the correct behaviour of the edge spins but not of the inner spins of the chains. Our studies on the external magnetic field B_z dependence of the magnetic moments $\mu_s(B_z(t))$ of the edge spins show good agreement with the experimental data and provide a possible explanation for this phenomenon.
For closed spin chains we show analytically that such chains coupled by antiferromagnetic exchange and subject to perpendicular magnetic anisotropy possess local energy minima corresponding to non-collinear topological spin spirals. Analytical analysis of the free energy at finite temperatures for chains with dominating anisotropy has shown that anisotropy increases the depth of the local energy minima. This makes the non-collinear configurations particularly stable for such chains ($|K| \gg |J|$). Another important effect concerned with magnetic anisotropy is that with increasing anisotropy the extended spin spirals become energetically less favourable than localized kink solitons. Depending on the sign of the anisotropy constant two configurations for the kink soliton are possible: for $K > 0$, a Bloch-like KB soliton is stabilized, while for $K < 0$ a Nel-like KN soliton appears. When the dipolar interaction is introduced into the Hamiltonian then: the local energy minima become deeper because it induces magnetic anisotropy. Furthermore, it might lead to a transformation of the spin spirals to kink solitons. Particularly interesting is the Möbius antiferromagnetic configuration with an even number of sites in closed chains. While the existence of such a configuration in chains with an odd number of sites has been reported, a similar configuration in chains with an even number of sites was unknown up to now.

Bibliography

[1] Eberly J H, Narozhny N B and Sanchez-Mondragon J J 1980 Phys. Rev. Lett. **44** 1323

[2] Seltzer S J, Meares P J and Romalis M V 2007 Phys. Rev. A **75** 051407R

[3] Robinett R W 2004 Phys. Rep. **392** 1

[4] Schmidt A G M, Azeredo A D and Gusso A 2008 Phys. Lett. A **372** 16

[5] Gora P F and Jedrzejek C 1993 Phys. Rev. A **48** 3291

[6] Narozhny N B, Sanchez-Mondragon J J and Eberly J H 1981 Phys. Rev. A **23** 236

[7] Fleischhauer M and Schleich W P 1993 Phys. Rev. A **47** 4258

[8] Bluhm R, Kostelecky A and Porter J 1996 Am. J. Phys. **64** 944

[9] Agarwal G S and Banerji J 1998 Phys. Rev. A **57** 3880

[10] Aronstein D L and Stroud C R 1997 Phys. Rev. A **55** 4526

[11] Aronstein D L and Stroud C R 2000 Phys. Rev. A **62** 022102

[12] Styer D F 2001 Am. J. Phys. **69** 56

[13] Wright E M, Walls D F and Garrison J C 1996 Phys. Rev. Lett. **77** 2158

[14] Villain P and Lewenstein M 2000 Phys. Rev. A **62** 043601

[15] Bocchieri P and Loinger A 1957 Phys. Rev. **107** 2

[16] Schulman L S 1978 Phys. Rev. A **18** 2379

[17] Chandrashekar C 2010 Cent. Eur. J. Phys. **8(6)** 979

[18] Bliss R S and Burgarth D 2014 Phys. Rev. A **89** 032309

[19] Wallace D 2015 J. Math. Phys. **56** 022105

[20] Gauyacq J P and Lorente N 2013 Phys. Rev. B **87** 195402

[21] Thiele S, Balestro F, Ballou R, Klyatskaya S and Ruben M 2014 Science **344** 1135

[22] Gatteschi D and Sessoli R 2003 Angew. Chem. Int. Ed. **42** 3

[23] Khajetoorians A A, Wiebe J, Chilian B, Lounis S, Blügel S and Wiesendanger R 2012 Nature Phys. **8** 497

[24] Zhou L, Wiebe J, Lounis S, Vedmedenko E Y, Meier F, Blügel S, Dederichs P H and Wiesendanger R 2010 Nature Phys. **6** 187

[25] Wieser R 2011 Phys. Rev. B **84** 054411

[26] Gauyacq J P and Lorente N 2014 Surf. Sci. **630** 325

[27] Them K, Stapelfeldt T, Vedmedenko E Y and Wiesendanger R 2013 New J. Phys. **15** 013009

[28] Neumann A, Altwein D, Thönnißen C, Wieser R, Berger A, Meyer A, Vedmedenko E Y and Oepen H P 2014 New J. Phys. **16** 083012

[29] Piquerel R, Gaier O, Bonet E, Thirion C and Wernsdorfer W 2014 Phys. Rev. Lett. **112** 117203

[30] Loth S, Etzkorn M, Lutz C P, Eigler D M and Heinrich A J 2010 Science **329** 1628

[31] Wernsdorfer W 2008 Comptes Rendus Chimie **11** 10

[32] Cheng-Wei Huang W and Batelaan H 2013 J. Comp. Meth. Phys. **2013** 308538

[33] Bullynck M 2009 Historia Mathematica **36** 1

[34] Gatland I R 1991 Am. J. Phys. **59** 155

[35] Zener C 1932 Proc. R. Soc. London Ser. A **137** 696

[36] Thorwart M, Grifoni M and Hänggi P 2000 Phys. Rev. Lett. **85** 860

[37] Wernsdorfer W, Chakov N E and Christou G 2005 Phys. Rev. Lett. **95** 037203

[38] Wernsdorfer W, Bhaduri S, Boskovic C, Christou G and Hendrickson D N 2002 Phys. Rev. B **65** 180403

[39] Garg A 1993 Europhys. Lett. **22** 205

[40] Klauder J R 1978 Phys. Rev. D **19** 2349

[41] Schilling R and Enz M 1986 Phys. Rev. C **19** L711

[42] Garanin D A 1991 J.Phys. A: Math. Gen **24** L61

[43] Hartmann-Boutron F 1995 J.Phys. I France **5** 1281

[44] Ulyanov V V and Zaslavskii O B 1999 Phys. Rev. B **60** 6212

[45] Garanin D A and Chudnovsky E M 1999 Phys. Rev. B **59** 3671

[46] Yoo S K and Park C S 2005 Phys. Rev. B **71** 012409

[47] Zhou B, Shen S Q and Liang J Q 2004 Eur. Phys. J. B **40** 87

[48] Loss D, DiVincenzo D P and Grinstein G 1992 Phys. Rev. Lett. **69** 037203

[49] Tejada J, Zhang X X, Barco E, Chudnovsky E M and Hernandez J M 1997 Phys. Rev. Lett. **79** 1754

[50] Friedman J R, Sarachik M P, Tejada J and Ziolo R 1996 Phys. Rev. Lett. **76** 3830

[51] Thomas L et al. 1996 Nature (London) **383** 145

[52] Sangregorio C, Ohm T, Paulsen C, Sessoli R and Gatteschi D 1997 Phys. Rev. Lett. **78** 4645

[53] Caneschi A et al. 1999 J. Magn. Magn. Mater. **200** 182

[54] Wernsdorfer W, Sessoli R 1999 Science **284** 133

[55] Gatteschi D, Sessoli R and Villain J 2011 Molecular nanomagnets (Oxford: Oxford Univ. Press) 199

[56] E. Y. Vedmedenko and D. Altwein, Phys. Rev. Lett. **112**, 017206 (2014)

[57] A. A. Khajetoorians, J. Wiebe, B. Chilian, S. Lounis, S. BlÃ$\frac{1}{4}$gel, and R. Wiesendanger, Nat. Phys. **8**, 497 (2012).

[58]] Y. T. Millev, E. Vedmedenko, and H. P. Oepen, J. Phys. D: Appl. Phys. **36**, 2945 (2003).

[59] L. Zhou, J. Wiebe, S. Lounis, E. Y. Vedmedenko, F. Meier, S. Blügel ,P .H. Dederichs, and R. Wiesendanger, Nat. Phys. **6**, 187 (2010).

[60] M .Haque, V. R. Chandra, and J. N. Bandyopadhyay, Phys. Rev. A **79**, 042317 (2009).

[61] J. R. Friedman, M. P. Sarachik, J. Tejada, and R. Ziolo, Phys. Rev. Lett. **76**, 3830 (1996).

[62] B. Behin-Aein, D. Datta, S. Salahuddin, and S. Datta, Nat. Nanotechnol. **5**, 266 (2010).

[63] J. P. Morgan, A. Stein, S. Langridge, and C. H. Marrows, Nat. Phys. **7**, 75 (2011).

[64] A. Schumann, P. Szary, E. Y. Vedmedenko, and H. Zabel, New J. Phys. **14**, 035015 (2012).

[65] O. Cador, D. Gatteschi, R. Sessoli, A.-L. Barra, G. A. Timcoc, and R. E. P. Winpenny, J. Magn. Magn. Mater. **290-291**, 55 (2005).

[66] K. Bernot, L. Bogani, A. Caneschi, D. Gatteschi, and R. Sessoli, J. Am. Chem. Soc. **128**, 7947 (2006).

[67] W. Wernsdorfer, Nat. Mater. **6**, 174 (2007).

[68] L. M. Sandratskii, J. Phys.: Condens. Matter **3**, 8565 (1991).

[69] K. Binder and D. W. Heerman, Monte Carlo Simulation in Statistical Physics (Springer, New York, 2002).

[70] E. Y. Vedmedenko, Phys. Status Solidi B **244**, 1133 (2007).

[71] Y. Savina, O. Bludov, V. Pashchenko, S. L. Gnatchenko, P. Lemmens, and H. Berger, Phys. Rev. B**84**, 104447 (2011).

[72] W. Nolting ISBN:978-3-642-25402-4 (2013)

[73] W. Nolting ISBN:978-3-642-24420-9 (2012)

[74] L.D. Landau, E. M.Lifschitz ISBN: 3-05-500067-6 (1979)

[75] D. Gatteschi, R. Sessoli, and J. Villain ISBN: 3-05-500067-6 (1979)

[76] J. Bartolome, F. Luis, and J. F. Fernandez ISBN 0â19â856753â7 (2006)

[77] A. Garg, New J. Phys. **19** 088001 (2017)

Publications

M. Krizanac, D. Altwein, E. Y. Vedmedenko, and R. Wiesendanger. Quantum revivals and magnetization tunneling in effective spin systems. New J. Phys. **18** 033029 (2016).

M. Krizanac, E. Y. Vedmedenko, and R. Wiesendanger. Perturbative calculations of quantum spin tunneling in effective spin systems with a transversal magnetic field and transversal anisotropy. New J. Phys. **19** 013032 (2017).

M. Krizanac, E. Y. Vedmedenko, and R. Wiesendanger. Reply to Comment on Perturbative calculations of quantum spin tunneling in effective spin systems with a transversal magnetic field and transversal anisotropy. New J. Phys. **19** 078001 (2017).

S. Castillo-Sepúlveda, R. A. Escobar, and D. Altbir, M. Krizanac, and E. Y. Vedmedenko. Magnetic Möbius stripe without frustration: Noncollinear metastable states. Phys. Rev. B **96** 024426 (2017).

Acknowledgements

Finally, I gladly thank the people who contributed to this Ph.D. thesis with their support.

• Prof. Dr. R. Wiesendanger for his great advice and the opportunity to work in an excellent research team.

• Dr. E. Vedmedenko for her support and advice.

• Julian Hagemeister and David Altwein for many nice discussions and for the great support.

• My parents Ivan and Ruza for their love and moral support.

• My wife Helene for her love, patience and encouragement.

Eidesstattliche Versicherung
Declaration on oath

Hiermit erkläre ich an Eides statt, dass ich die vorliegende Dissertationsschrift selbst verfasst und keine anderen als die angegebenen Quellen und Hilfsmittel benutzt habe.
I hereby declare, on oath, that I have written the present dissertation by my own and have not used other than the acknowledged resources and aids.

Hamburg, den 27.12.2017
Mario Krizanac